

Reproduced by

ed Services Technical Information Agency  
**DOCUMENT SERVICE CENTER**

KNOTT BUILDING, DAYTON, 2, OHIO

**AD -**



**126000**

**UNCLASSIFIED**

AD No. 12 600

ASTIA FILE COPY

TECHNICAL REPORT

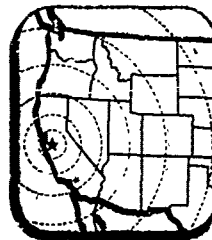
RADIO INTERFERENCE FROM CORONA  
DISCHARGES

*by*

R. L. Tanner

Technical Report No. 37, SRI Project No. 591  
Air Force Contract No. AF 19 (604)—266

April, 1953



**STANFORD RESEARCH INSTITUTE**

*Applied Research Center of the West*

**STANFORD, CALIFORNIA**

# STANFORD RESEARCH INSTITUTE

STANFORD, CALIFORNIA

April 1953

Technical Report No. 37, SRI Project No. 591  
Air Force Contract No. AF 19(604)-266

## RADIO INTERFERENCE FROM CORONA DISCHARGES

by

R. L. Tanner

Aircraft Radiation Systems Laboratory

Approved:

*J. T. Bolger*  
*for* J. V. N. Granger, Assistant Chairman  
Engineering Department

*T. H. Morrin*

T. H. Morrin,  
Director of Engineering Research

Copy No. 90

## ABSTRACT

Corona discharges are studied, with special attention given to the mechanisms by which they produce electromagnetic disturbances which cause interference with radio reception. The means by which these disturbances are coupled into the receiver, and the nature of the dependence of this coupling upon the geometrical configuration of the body on which the discharge occurs, are examined. The theory thus developed is applied to the problem of precipitation static as it occurs in aircraft.

## TABLE OF CONTENTS

	Page
ABSTRACT . . . . .	i
TABLE OF CONTENTS . . . . .	ii
LIST OF FIGURES . . . . .	iv
<b>I INTRODUCTION . . . . .</b>	<b>1</b>
A. History . . . . .	1
B. Experience During World War II . . . . .	3
C. Basic Phenomena Contributing to Precipitation Static . . . . .	3
D. Scope of Present Investigation . . . . .	6
<b>II AN EXTENSION OF THE LORENTZ RECIPROCITY THEOREM . . . . .</b>	<b>9</b>
A. General Considerations . . . . .	9
B. Derivation . . . . .	9
C. Interpretation . . . . .	12
<b>III THE NATURE OF NEGATIVE POINT CORONA DISCHARGES . . . . .</b>	<b>13</b>
A. Scope of Experimental Investigation . . . . .	13
B. Time Structure of Pulses . . . . .	13
C. Effect of Tip Radius and Pressure . . . . .	15
D. Effect of Applied Voltage . . . . .	18
E. Laplace Transform of Corona Pulse . . . . .	19
F. Dependence of Measured Currents on Coupling Between Discharge and Terminals . . . . .	20
G. Spatial Distribution of Currents in the Discharge . . . . .	22
<b>IV RESPONSE OF THE RECEIVER TO CORONA PULSES . . . . .</b>	<b>30</b>
A. The Coupling Function . . . . .	30
B. The Fixed Wire Antenna . . . . .	32
C. The Prolate Spheroidal Antenna . . . . .	35
<b>V THE CYLINDRICAL DIPOLE ANTENNA . . . . .</b>	<b>39</b>
A. General Considerations . . . . .	39
B. Relation of Coupling Function to Antenna Impedance . . . . .	39
C. The Symmetric Dipole . . . . .	43
D. Effect of Terminating Impedance . . . . .	44
E. The Asymmetric Dipole . . . . .	46
F. Coupling from Discharge at End of Short Element . . . . .	47
G. Coupling from Discharge at End of Long Element . . . . .	49

TABLE OF CONTENTS (Cont'd)

	Page
VI CONCLUSIONS AND RECOMMENDATIONS . . . . .	52
A. General Considerations for an Ideal Discharger. . . . .	52
B. Evaluation of Common Anti-Precipitation Static Devices . . . . .	54
C. Suggestions for Additional Research . . . . .	55
ACKNOWLEDGMENT . . . . .	57
APPENDIX A . . . . .	58
APPENDIX B . . . . .	63
LIST OF REFERENCES . . . . .	67

## LIST OF ILLUSTRATIONS

Figure		Following Page
1	Illustrating the Coupling from a Discharge on a Conducting Body . . . . .	9
2	Experimental Setup for Obtaining Time Structure of Corona Pulses . . . . .	13
3	Gate Circuit for Trigger Amplifier . . . . .	14
4	Effect of Tip Radius and Pressure on Negative Point Corona Pulses . . . . .	15
5	Dependence of Pulse Decay Time on Pressure . . . . .	15
6	Dependence of Pulse Rise Time on Pressure . . . . .	15
7	Dependence of Pulse Amplitude on Pressure and Tip Radius . . . . .	18
8	Effect of Applied Field on Corona Pulses . . . . .	19
9	Exponential Approximations to Corona Pulse . . . . .	19
10	Fourier Spectre of Approximations of Corona Pulse . . . . .	20
11	Effect of Altitude on Idealized Corona Pulse . . . . .	20
12	Illustrating the Application of the Coupling Theorem to the Analysis of Corona Pulses . . . . .	21
13	Setup for Finding Spatial Extent of Corona Currents . . . . .	22
14	Schematic Diagram of Setup for Finding Spatial Extent of Corona Currents . . . . .	22
15	Effect on Measured Pulse Amplitude of Varying $\epsilon$ . . . . .	24
16	Effect on Measured Pulse Amplitude of Varying $\frac{c}{r}$ . . . . .	24
17	Dependence of Measured Pulse Magnitude on $E_0$ . . . . .	24
18	Concentration of Field at Tip of Prolate Spheroid . . . . .	25
19	Spheroidal Coordinates Near Tip and Comparison with Actual Discharge Points . . . . .	26
20	Comparison of Fields at Tip of Discharge Point for Two Values of $\frac{c}{r}$ . . . . .	28
21	Model for Analysis of Fixed Wire Antenna . . . . .	32
22	The Function $\gamma$ , which Relates $\psi_1$ and $Y_1$ . . . . .	37
23	Coupling Function $\psi$ for Spheroid of $\frac{L}{D} = 70.7$ . . . . .	38

## LIST OF ILLUSTRATIONS (Cont'd)

Figure		Following Page
24	Coupling Function $\psi_1$ for Spheroid of $\frac{L}{D} = 7.05$ . . . . .	38
25	Illustrating Application of Impedance Analysis to Coupling Function for Cylindrical Dipole . . . . .	39
26	Impedance of Cylindrical Dipole for Thickness Factor $\Omega = 10$ , Compared with Rational Function Approximation . . . . .	43
27	Positions of Singularities Characterizing $Z_{11}$ . . . . .	43
28	Behavior of Coupling Function for Symmetric Dipole . . . . .	44
29	Terminal Voltage vs Frequency for Small Resistance Termination . . . . .	45
30	Open Circuit Terminal Voltage vs Frequency . . . . .	45
31	Thevenin's Equivalent Circuit for Obtaining Antenna Response with Arbitrary Terminating Impedance . . . . .	45
32	Asymmetric Dipole Impedance . . . . .	47
33	Frequency Behavior of Coupling from Short Element of Asymmetric Dipole . . . . .	48
34	Frequency Behavior of Coupling from Long Element of Asymmetric Dipole . . . . .	50
35	Illustrating Reduction in Generated Noise by Reduction in Pulse Size . . . . .	52
36	Discharge Scheme in which Discharge Points are Decoupled from Aircraft . . . . .	53
37	Low Noise Discharge Scheme . . . . .	54
A1	Comparison of Actual Discharge Point with Two Possible Mathematical Models . . . . .	58
A2	The Prolate Spheroidal Coordinate System . . . . .	58
A3	Ratio of Tip Field to Base Voltage for Idealized Discharge Electrode . . . . .	61
B1	Idealized Electrode Geometry . . . . .	63

# RADIO INTERFERENCE FROM CORONA DISCHARGES

April 1953

## CHAPTER I

### INTRODUCTION

#### A. History

The type of interference with radio reception now known as precipitation static has been experienced for many years.<sup>1,2,3\*</sup> Initial contact with this phenomenon was experienced in the operation of ground based receivers, where its occurrence was an inconvenience but not a hazard. By 1934, however, all commercial transport aircraft had been equipped with radio communication and navigation equipment.<sup>3</sup> Pilots began to depend upon these devices, and since precipitation static occurred with much greater frequency and intensity in aircraft than at ground stations, a serious hazard was created. Therefore it began receiving attention from most engineers concerned with the development and operation of radio equipment in aircraft.

Several attempts to explain the phenomenon were made. The one which received greatest acceptance was made in 1914 by Curtis.<sup>4</sup> Curtis contended that the static was generated by charged particles striking the antenna. Huckle reports several attempts to overcome the interference which were based on this conception.<sup>3</sup> None of them proved very successful, however.

---

\* Numbers refer to references listed at the end of this report.

The first progress to be made in the effort to overcome the effects of precipitation static occurred in 1935 with the introduction of the shielded loop antenna.<sup>2</sup> This antenna offered considerable improvement over the open-wire antenna which had been used until that time. Loop antennas were tested in the years 1935 and 1936 by two airlines. The improvement effected by their use was sufficiently great that the Department of Commerce ordered all air transport lines to equip their planes with loop antennas by October 1937.

A paper by Morgan in 1936 ascribes the success of the shielded loop antenna to the fact that it "prevents the charged particles from striking the antenna structure."<sup>2</sup> Additional experience with loop antennas indicated, however, that in spite of the very considerable improvement that resulted from their use, periods of very high precipitation static would occur in which all radio equipment was inoperative for 30 minutes or more.<sup>3</sup>

In an attempt to obtain more satisfactory solutions a program of flight investigation was set up in November 1936, and continued until June 1937. Scientists from Reed College, Purdue University, Oregon State College, Bendix Radio Corporation, and Bell Telephone Laboratories were involved in the program. United Airlines furnished the pilots, flight engineers, and a meteorologist. The results of this program are reported by Huckle.<sup>3</sup> The conclusion of greatest significance to come from the investigation was that precipitation static was due not to charged particles striking the antenna, but rather to corona discharges from the antenna itself or from other extremities of the aircraft which produced noise that coupled into the antenna. Although Huckle lists seven possible ways in his paper in which aircraft can acquire charge, he appears to give most weight to the theory that the aircraft is charged by the transfer of charge from charged particles which impinge upon it in flight. It is significant that his list does not contain any mention of triboelectric charging, which is now accepted as the principal cause.

## B. Experience During World War II

In spite of the improvement which resulted from the use of shielded loop antennas and the trailing wire dischargers which grew out of the investigation reported by Hucke, precipitation static was still a serious problem when the United States entered World War II. It is estimated that during World War II precipitation static was responsible for the loss each year of 1% of all aircraft based in certain areas of the United States.<sup>5</sup> The seriousness of the problem led to the establishment of the joint Army-Navy precipitation static project which was organized in May 1943. A large part of the work of the project was carried out at Minneapolis under the direction of Ross Gunn. Work was also done at the General Electric Company Laboratories in Schenectady, New York, under the direction of Irving Langmuir, at Oregon State College, at Washington State College, at Purdue University, and at the Naval Research Laboratory in Washington. In the course of these investigations much was learned about many of the phenomena involved in precipitation static, and several means for overcoming precipitation static were suggested. These include the dielectric-coated wire antenna and wick discharger which has now become standard equipment on aircraft,<sup>5</sup> the block and squirter discharger,<sup>6</sup> and the receiver blanking system.<sup>7</sup>

## C. Basic Phenomena Contributing to Precipitation Static

The conclusion reached in 1937 by Hucke and his co-workers that corona discharges were responsible for precipitation static has been abundantly substantiated since that time.<sup>5,8</sup> His explanations concerning the methods by which static charge is deposited on the aircraft have, however, been rejected. The charging effect is presently explained as a triboelectric phenomenon.<sup>5,9</sup> Precipitation particles striking the aircraft rub against it and glance off, leaving a charge in the same manner that a charge is left on an ebony rod when rubbed with fur. Langmuir,

Tanis and others have succeeded in reproducing these effects under laboratory conditions, and Langmuir and Tanis have investigated the charging effect as a function of particle and surface composition, angle of incidence, velocity of incidence, and particle size.<sup>9</sup> They have succeeded in fitting a large number of particle and surface substances into a triboelectric series which is in agreement with Coehn's rule that substances of high dielectric constant acquire a positive charge when rubbed against substances having a lower dielectric constant.

On the basis of the triboelectric charging mechanism, it is possible to explain the high charging rate which occurs in aircraft. Aircraft are known to charge at a much higher rate than can be justified on the basis of the charge measured on precipitation particles and the speed with which the aircraft flies through them. Langmuir even reports one instance in which the aircraft acquired a negative charge while flying through positively charged precipitation.<sup>10</sup> The triboelectric theory also explains qualitatively the observed effect of temperature on charging rate and the fact that aircraft consistently charge negatively. On the basis of Langmuir's investigation an effort was made to overcome the precipitation static problem by finding surface coatings for aircraft which would either take a positive charge or a reduced charge.<sup>5</sup> The effort proved unsuccessful, however.

The triboelectric charging which occurs when the aircraft enters precipitation soon raises the aircraft to extremely high voltages; voltages in the neighborhood of 1,000,000 volts have been shown to occur.<sup>5</sup> As the aircraft charges, a concentrated electric field is produced at sharp points and extremities. Eventually the field at these points becomes sufficiently great to cause the points to go into negative burst pulse corona. This type of corona discharge was first investigated by Trichel in 1938, and has been the subject of much investigation since that time.<sup>11,12,13,14,15</sup> It is known that the discharge pulses are of short duration, have a short rise time, and occur at a nearly periodic rate whose frequency depends upon the radius

of the discharge tip and the applied voltage. These discharge pulse when they occur at an audio frequency rate and couple electromagnetically into the radio receiver, account for the singing or semi-musical character which precipitation static is frequently observed to have.

Another phenomenon which frequently contributes to the production of precipitation static is cross field charging.<sup>5</sup> This is the effect which occurs when the aircraft flies between oppositely charged cloud masses and the electric field which exists between the clouds induces high field concentrations on points of the aircraft. Such a field produces corona discharges in the same manner as the field produced by triboelectric charging. Cross-field charging seldom, if ever, occurs except in conjunction with triboelectric charging, and then only for brief periods of time. Thus this effect is of secondary importance.

Another effect which is properly classified as a precipitation static phenomenon is that due to the charging of dielectric surfaces on the aircraft.<sup>16</sup> Surfaces such as glass windshields or plastic canopies, which are good insulators, are charged triboelectrically until a large voltage difference appears between these surfaces and the adjacent metal sections of the aircraft. When this voltage becomes sufficiently great, a spark discharge occurs between adjacent dielectric regions of differing potential or between the metal and the isolated dielectric section. The discharge produces electrical noise which may be coupled into the receiver. Recent work indicates that this type of interference is effectively eliminated by coating the dielectric surfaces with high resistance conductive films.<sup>17</sup>

Interest has recently been revived in the effect of charged precipitation particles striking the antenna. As mentioned earlier, this was the first explanation advanced for precipitation static. It was later rejected in favor of corona discharges as the noise-producing mechanism but concern has lately been expressed that this may be a contributing factor. The problem was recently investigated by Newman and Rondeau.<sup>18</sup> They reached the conclusion that charged rain drops striking an antenna can cause

significant noise voltages at the lower communication frequencies, although these are much less important than noise resulting from corona discharge. The noise produced in this manner depends upon the radius of curvature of the surface which the particle strikes. Larger voltages are produced by smaller radii.

#### D. Scope of Present Investigation

Review of previous work on precipitation static indicates two areas of the problem which have been inadequately explored and which should prove fruitful fields for investigation. The first of these concerns the fundamental physical nature of the negative point corona pulses which are the sources of precipitation static noise. These discharges have been subjected to much investigation, but many important questions remain unanswered. One aspect of the nature of the pulses which is of utmost importance in the production of precipitation static is their time structure or transient character. Many attempts to obtain oscillographic records of the pulses have been made, beginning with the work of Trichel<sup>11</sup> who was the first to observe that the discharge occurred as discrete pulses. The most recent attempt which has been reported is that of English.<sup>14</sup> In all these investigations the workers were hampered by the inadequacy of their equipment. Their results have therefore been erroneous, although this fact has not always been recognized.

In a very careful and thorough piece of work, Huggins investigated the character of positive point streamer pulses.<sup>8</sup> His method was essentially to determine the magnitude of the Fourier transform of the pulses through an investigation of the frequency spectrum of the noise voltages. He then postulated on the basis of physical reasoning a pulse form with a Fourier transform corresponding to that measured for the actual pulses. In this fashion he arrived at a much more accurate picture of the pulse form than later investigators who have attempted to obtain the shape of the

pulses by direct oscillographic methods. Unfortunately, Huggins was not able to employ this method in the investigation of negative point corona pulses because of his inability to control the repetition frequency of the pulses.

Another aspect of the discharge pulses which has received practically no attention, and one that is of paramount importance for a theory which adequately explains the mechanism of precipitation static, is the spatial extent of the discharges. It is well known that, in the course of the discharge, the charge leaves the point as free electrons which have very high mobility. As the electrons move out of the high field which immediately surrounds the point, they lose energy, slow down, and are captured by oxygen molecules to form negative ions.<sup>12</sup> The mobility of these ions is so much less than that of the electrons that, in terms of the time intervals of importance in the present study, the electrons can be considered to have come to rest when they become attached. It will presently be shown that the quantity of importance in determining the strength of the noise signals excited on the structure is not the actual value of the current flow in the discharge, but the dipole moment of the discharge, which is proportional to the product of the current flow and the distance over which the current flow takes place. The importance of knowing the spatial extent of the discharge becomes evident in the light of this fact.

The second area of the problem which appears to have been neglected in previous work is an investigation, in terms of fundamental electromagnetic theory, of the mechanism of coupling between the corona pulse and the receiver terminals. Previous investigations have either ignored the problem altogether, or have assumed that coupling was reduced in proportion to the distance between the point at which the discharge occurs and the terminals of the receiver. This assumption is not valid, in general, as will be shown in later sections.

The foregoing discussion has indicated some of the questions concerning precipitation static phenomena which remain to be answered. The present

investigation undertakes to answer some of the questions in both of the foregoing areas. In Chapter II a fundamental coupling theorem, based directly on Maxwell's field equations, is developed. The theorem is of considerable generality. It can be applied in discussing the noise signals coupled into the receiver from a discharge occurring at some remote corner of the aircraft. On the other hand, it can be applied to the converse situation; the dipole moment of the discharge can be inferred from the current pulse measured at the base of a discharge point and from certain supplemental electric field investigations for the discharge electrode system.

Chapter III is devoted to an account of a rather extensive experimental investigation of the transient nature of negative point corona pulses. The investigation was carried out with the aid of an oscilloscope of recent development which is capable of defining pulses having rise times of 7  $\mu$ s. The coupling theory developed in Chapter II is applied to infer from the oscillographic data the effective dipole moments of the discharges.

In Chapters IV and V the results of Chapters II and III are applied to antenna configurations which are of practical or theoretical interest. In Chapter VI devices presently in use for the suppression of precipitation static are discussed in the light of the theory developed, and suggestions for additional research are offered.

## CHAPTER II

## AN EXTENSION OF THE LORENTZ RECIPROCITY THEOREM

A. General Considerations

The coupling between the noise-producing discharge and the terminals of the receiver is of fundamental importance in a theory of precipitation static interference. A successful solution to the precipitation static problem for example, might lie in a device which forces the discharge to occur at a point on the aircraft from which its coupling to the receiver will be very small. Since the problem is an electromagnetic one, it can be approached through the use of Maxwell's field equations.

B. Derivation

Let us consider a conducting body of arbitrary shape as shown in Fig. 1. Two regions of particular interest are indicated. The first of these,  $T_1$ , represents a volume which has been removed from the original conducting body to form the antenna terminals. The second region,  $T_2$ , is external to the body and is defined by the volume in which charge moves during a discharge. Quantities defined for the terminals, region  $T_1$ , will be indicated by the subscript 1.

We now postulate two independent situations characterized by independent solutions to the field equations. The field quantities which correspond to the two situations will be designated by superscripts (1) and (2). For each of the situations indicated it is possible to write Maxwell's curl equations relating the field quantities  $\mathbf{E}$ ,  $\mathbf{H}$ , and  $\mathbf{J}$ . These equations, in their Fourier transformed form, are shown below

$$\nabla \times \mathbf{E} = -j\omega\mu\mathbf{H}, \quad (1)$$

T<sub>2</sub> REGION IN WHICH  
DISCHARGE OCCURS

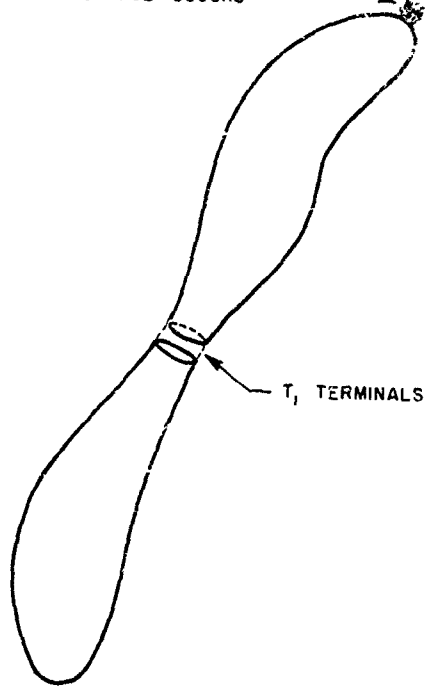


FIG. 1

ILLUSTRATING THE COUPLING FROM A  
DISCHARGE ON A CONDUCTING BODY

A-591-TR57-210

$$\nabla \times \mathbf{H} = j\omega\epsilon\mathbf{E} + \mathbf{J}. \quad (2)$$

We now form the vector quantity

$$\mathbf{E}^{(1)} \times \mathbf{H}^{(2)} - \mathbf{E}^{(2)} \times \mathbf{H}^{(1)}$$

to which we apply Gauss's divergence theorem:

$$\oint (\mathbf{E}^{(1)} \times \mathbf{H}^{(2)} - \mathbf{E}^{(2)} \times \mathbf{H}^{(1)}) \cdot d\mathbf{S} = \int \nabla \cdot (\mathbf{E}^{(1)} \times \mathbf{H}^{(2)} - \mathbf{E}^{(2)} \times \mathbf{H}^{(1)}) dv. \quad (3)$$

By applying the vector identity

$$\nabla \cdot \mathbf{A} \times \mathbf{B} = \mathbf{B} \cdot \nabla \times \mathbf{A} - \mathbf{A} \cdot \nabla \times \mathbf{B}$$

to the right side of Eq. (3) and substituting from Eqs. (1) and (2), several terms on the right are observed to cancel, and Eq. (3) becomes

$$\oint (\mathbf{E}^{(1)} \times \mathbf{H}^{(2)} - \mathbf{E}^{(2)} \times \mathbf{H}^{(1)}) \cdot d\mathbf{S} = \int (\mathbf{E}^{(2)} \cdot \mathbf{J}^{(1)} - \mathbf{E}^{(1)} \cdot \mathbf{J}^{(2)}) dv. \quad (4)$$

The volume included in the volume integral on the right is bounded by the surface of the surface integral on the left. For the situation under consideration, the volume with which we are concerned is all space external to the conductors of Fig. 1, including the regions  $T_1$  and  $T_2$ . The surface is therefore the surface of the conductors and the surface at infinity.

The radiation condition of Sommerfeld insures that the contribution to the surface integral over the surface at infinity vanishes.<sup>19</sup> The boundary conditions at the surface of a perfect conductor guarantee that any vector  $\mathbf{E} \times \mathbf{H}$  lies in a plane tangent to the surface, whereas the element vector  $d\mathbf{S}$  is normal to the surface. The vectors  $\mathbf{E} \times \mathbf{H}$  and  $d\mathbf{S}$  are therefore orthogonal and the surface integral is identically zero. Equation (4) can thus be written as

$$\int \mathbf{E}^{(2)} \cdot \mathbf{J}^{(1)} dv = \int \mathbf{E}^{(1)} \cdot \mathbf{J}^{(2)} dv, \quad (5)$$

where we are free to specify what conditions shall apply in situations (1) and (2) provided only that the conditions that are specified are consistent with Maxwell's equations. The conditions obtaining in situations (1) and (2) are as follows.

Situation (1). A voltage  $V_1^{(1)}$  is applied to the antenna terminals, the current density  $J^{(1)}$  has a finite value in region  $T_1$  and is zero elsewhere. The integrand of the integral on the left side of Eq. (5) is therefore non-zero only in region  $T_1$ .

Situation (2). A discharge occurs in region  $T_2$ ,  $J^{(2)}$ , and therefore the integrand of the right side of Eq. (5) is non-zero only in region  $T_2$ .

As a result of the specified conditions, Eq. (5) becomes

$$\int_{T_1} \mathbf{E}^{(2)} \cdot \mathbf{J}^{(1)} dv = \int_{T_2} \mathbf{E}^{(1)} \cdot \mathbf{J}^{(2)} dv. \quad (6)$$

We now define the integral on the left of Eq. (6) as the product  $V_1^{(2)} I_1^{(1)}$ , and rearrange the equation into the form

$$V_1^{(2)} = \frac{1}{I_1^{(1)}} \int_{T_2} \mathbf{E}^{(1)} \cdot \mathbf{J}^{(2)} dv. \quad (7)$$

Equation (7) is one form of the basic coupling theorem in which we are interested. A more convenient form is obtained by dividing both sides of the equation by the antenna terminal impedance  $Z_{11}$ . The left side of Eq. (7) then becomes  $\frac{V_1^{(2)}}{Z_{11}}$  which is the open circuit voltage produced at the antenna terminals by the discharge divided by the impedance seen looking into these terminals. According to Thevenin's theorem the quantity thus obtained is the short circuit current produced at the terminals by the discharge. We shall label this current  $I_1^{(2)}$ . It is quite evident that the

product  $I_1^{(1)} Z_{11}$  which occurs in the denominator of the right side is the voltage  $V_1^{(1)}$ . Equation (7) can therefore be written

$$I_1^{(2)} = \frac{1}{V_1^{(1)}} \int_{T_2} \mathbf{E}^{(1)} \cdot \mathbf{J}^{(2)} dv. \quad (8)$$

### C. Interpretation

Equation (8) represents the coupling theorem in its most useful form. If the space and time distribution of the current density during the discharge is known, and if the electric field produced in the region of the discharge by a voltage applied to the antenna terminals can be determined, then it is possible to calculate the short circuit current produced at the antenna terminals by the discharge. With this information, Thevenin's theorem, and conventional circuit theory, the response of a radio receiver connected to the antenna terminals can then be calculated.

A converse interpretation of Eq. (8) can be made. If we know the short circuit current  $i_1^{(2)}$  produced by the discharge, and the electric field  $\mathbf{E}^{(1)}$  produced by the voltage  $V_1^{(1)}$ , then Eq. (8) can be regarded as an integral equation for the discharge current distribution  $\mathbf{J}^{(2)}$ . It is not difficult to show that solutions to the integral equation are not unique; several different distributions of  $\mathbf{J}^{(2)}$  might produce the same response  $I_1^{(2)}$ . By making use of supplementary information, however, it is possible to deduce considerable information concerning the nature of the discharge from Eq. (8). In the following chapters both interpretations of the equation will be employed.

## CHAPTER III

### THE NATURE OF NEGATIVE POINT CORONA DISCHARGES

#### A. Scope of Experimental Investigation

The experimental program was divided into two phases. In phase 1 the currents at the base of several discharge points of known geometry were studied by means of a high speed oscillograph. The transient character of the base current was obtained as a function of point radius, pressure, and electric field. Phase 2 of the study provided auxiliary oscillographic information from which the spatial distribution of the discharges studied in phase 1 could be determined.

#### B. Time Structure of Pulses

The schematic diagram of Fig. 2 shows the experimental setup used for obtaining oscillograms of the corona pulses. The high positive voltage applied to the spherical electrode in the bell jar induces negative point corona pulses at the discharge point. The point is connected through a pressurized coaxial connector to a coaxial cable leading to the oscilloscope. Signals from the discharge pulses travel down the cable and are absorbed in the terminating resistor, thus producing a voltage at the oscilloscope terminals.

A Tektronix Model 517 Oscilloscope, which has distributed vertical deflection and trigger amplifiers, was used in this phase of the investigation. The vertical amplifier has a bandwidth of approximately 70 Mc (down 8 db at 100 Mc), and is capable of defining pulses having rise time of 0.007  $\mu$ s with a deflection sensitivity of 0.1 v/cm. An ultra high speed sweep circuit provides sweep rates as high as 0.010  $\mu$ s/cm. The sweep rate

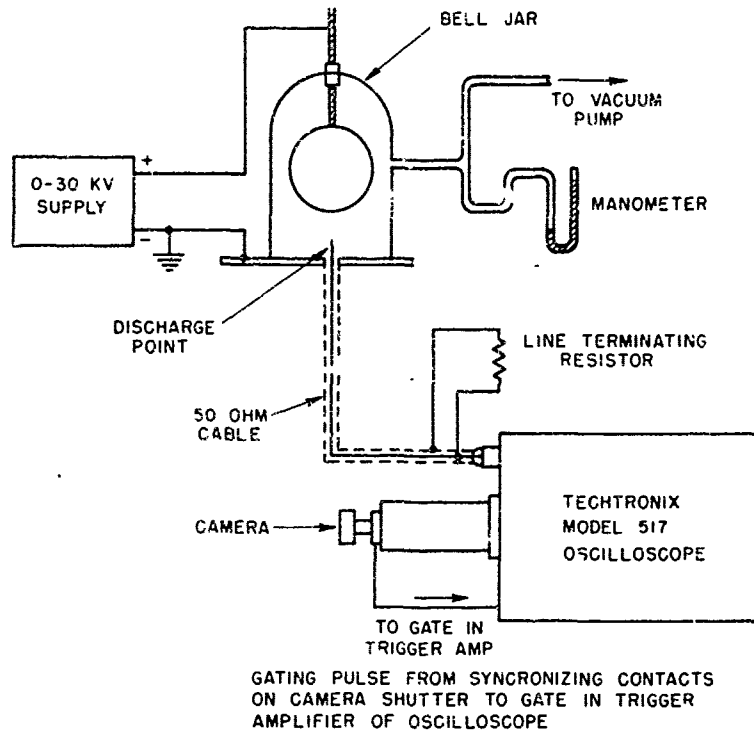


FIG. 2

EXPERIMENTAL SETUP FOR OBTAINING TIME  
STRUCTURE OF CORONA PULSES

A-591-TR37-212

calibration was checked by applying a 100 Mc voltage to the vertical amplifier. It was found to differ inappreciably from the indicated value.

The oscilloscope was modified to incorporate a gate in the trigger amplifier circuit, which was actuated by a pulse from the synchronizing contacts on the camera shutter. The purpose of the gate was to permit the photographing of single corona pulses, even though the pulses were re-occurring at a rapid rate. By this means better definition of the pulse shapes was obtained. A schematic of the gate circuit is shown in Fig. 3. Its operation is as follows: The plate of the final tube of the trigger pulse amplifier is normally shorted out by a balanced diode bridge so that the unblanking and sweep circuits of the scope are not operated by incoming pulses, although the pulses are applied to the vertical deflection plates. When the shutter of the camera arrives at the fully open position, the synchronizing contacts on the shutter close. This initiates a biasing pulse which travels down the transmission line and is applied to the diode bridge, effectively removing the short from the plate. Consequently, the first pulse to arrive after the camera is open trips the sweep and unblanking circuits of the scope and is thus photographed. The width of the gate pulse can be narrowed by reducing the size of C in Fig. 3. By determining the gate width necessary to include only one pulse, an approximate measure of the repetition rate of the pulses is obtained. The repetition rates obtained in this way are in agreement with those obtained by other investigators and will not be included in this report. The balanced feature of the gate bridge is necessary since otherwise the gating pulse from the camera shutter would trip the sweep and unblanking circuits prematurely.

The discharge points used in the investigation were hemispherically capped cylinders. The points were made by lapping hemispherical tips on small diameter tungsten rods. Four values of tip radius were used 0.005, 0.0075, 0.010 and 0.015 in. For each value of tip radius, oscillograms were taken at pressures ranging from 100 mm Hg to atmospheric, and for several values of applied electric field. Pulse rates and magnitudes were

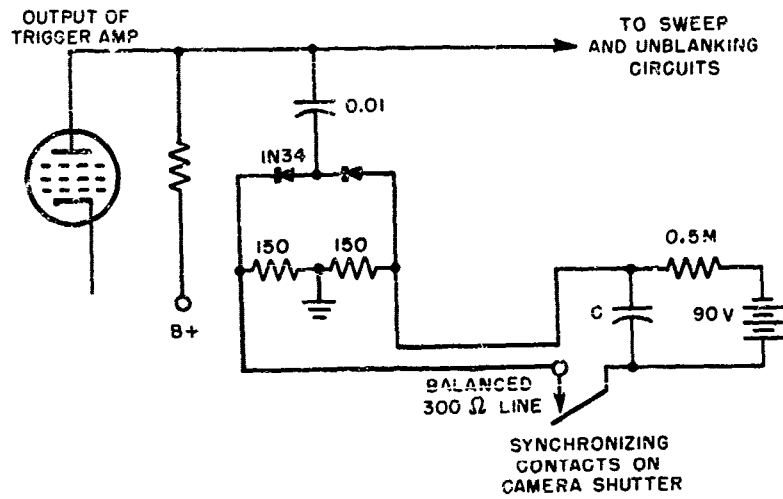


FIG. 3  
GATE CIRCUIT FOR TRIGGER AMPLIFIER

A-591-TR37-209

found to depend heavily upon tip radius and pressure. The dependence of pulse time structure upon applied field was found to be less important, although some effect was observed.

### C. Effect of Tip Radius and Pressure

The effects of tip radius and pressure on pulse shape are best studied by comparing pulses for different radii and different pressures at a value of applied electric field just sufficient to produce a discharge. Although the actual field values required to produce the discharge vary widely with pressure and tip radius the basic physical processes involved in the discharge are probably comparable at a value of applied field which just exceeds the critical field.

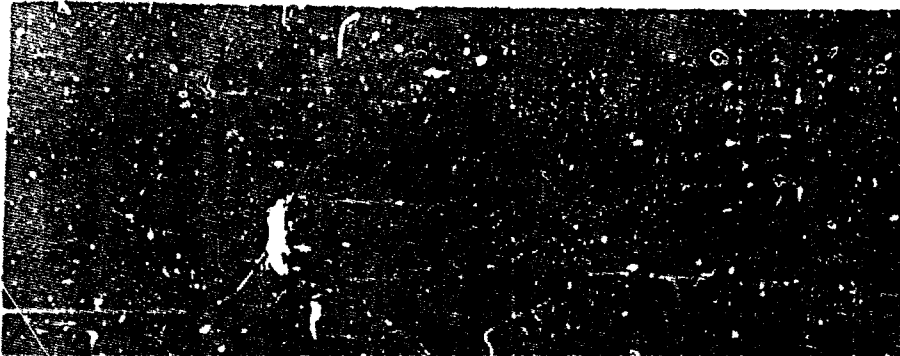
The oscillograms of Fig. 4 show the effect on the pulse shape of varying tip radius and pressure. It is evident that the pulses preserve a remarkable similarity of form for changes of the variables. All of the pulses shown can be quite well defined by the three parameters  $a$ ,  $t_1$ , and  $t_2$  illustrated by the sketch at the lower right of the figure. It is apparent that to a good approximation the parameters  $t_1$  and  $t_2$  which define the pulse shape are independent of tip radius, and depend only on pressure. The nature of the pressure dependence is illustrated by the graph of Fig. 5. It is seen from this graph that  $t_2$  is approximately inversely proportional to pressure.

The graph of Fig. 6 illustrates the dependence of the rise time  $t_1$  upon pressure. It is obvious that the measured value of  $t_1$  is limited at the higher pressures by the response of the oscilloscope. Examination of the pulses recorded at the higher pressures reveals that the recorded rise times for all of them is very nearly  $0.007 \mu s$  between the 10% and the 90% points of the leading edge. This is precisely the limit of rise time response for the oscilloscope. It is therefore likely that the true rise times are also approximately inversely proportional to pressure as is

GROUP A

TIP RADIUS = 0.005 IN. (0.0127 CM)

$$\frac{V_1^{(1)}}{E_t} = 0.0254 \text{ CM}$$



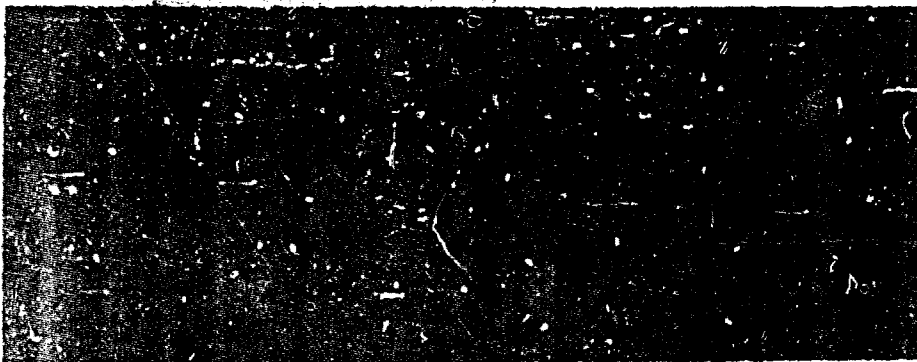
P = 760 MM

$\sigma = 2.6 \text{ MA}$

$t_1 = 0.010 \mu \text{ SEC.}$

$t_2 = 0.024 \mu \text{ SEC.}$

$M_{pk} = 0.066 \text{ MA-CM}$



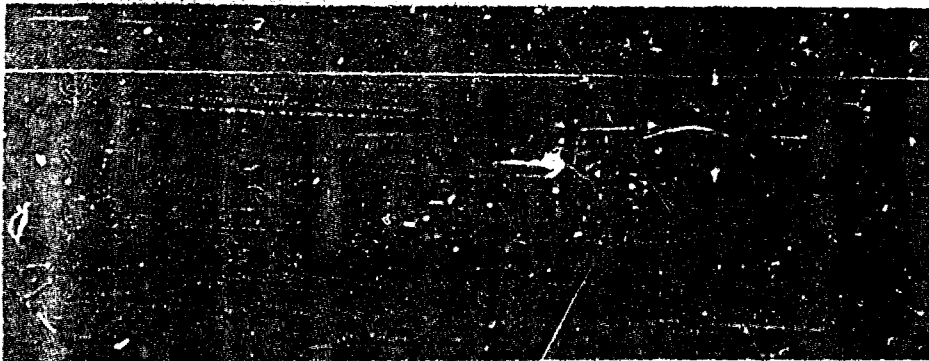
P = 400 MM

$\sigma = 1.0 \text{ MA}$

$t_1 = 0.014 \mu \text{ SEC.}$

$t_2 = 0.038 \mu \text{ SEC.}$

$M_{pk} = 0.0254 \text{ MA-CM}$



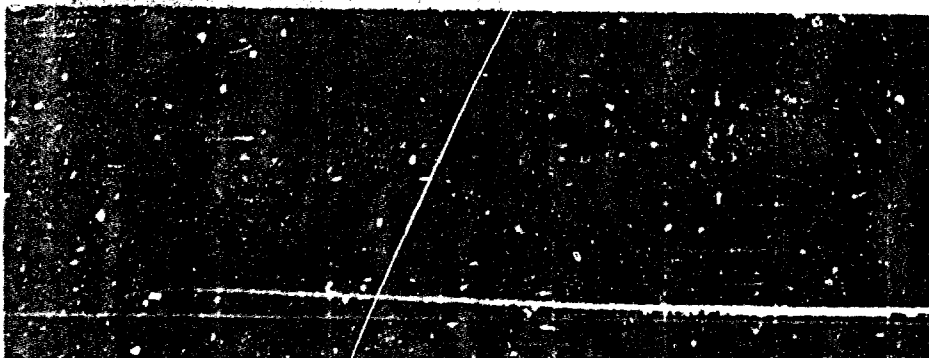
P = 200 MM

$\sigma = 0.8 \text{ MA}$

$t_1 = 0.020 \mu \text{ SEC.}$

$t_2 = 0.10 \mu \text{ SEC.}$

$M_{pk} = 0.0204 \text{ MA-CM}$



P = 100 MM

$\sigma = 0.3 \text{ MA}$

$t_1 = \text{---}$

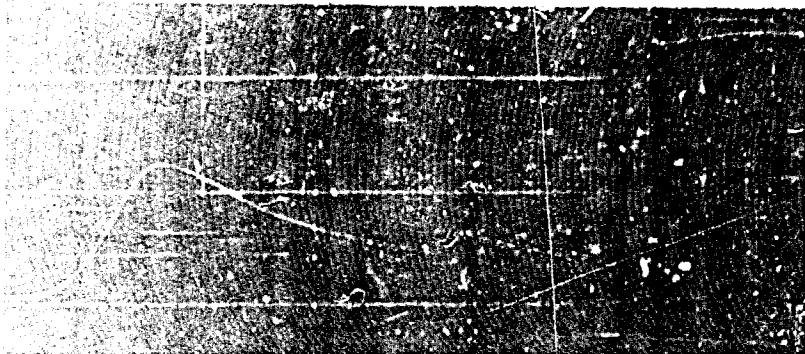
$t_2 = 0.18 \mu \text{ SEC.}$

$M_{pk} = 0.0076 \text{ MA-CM}$

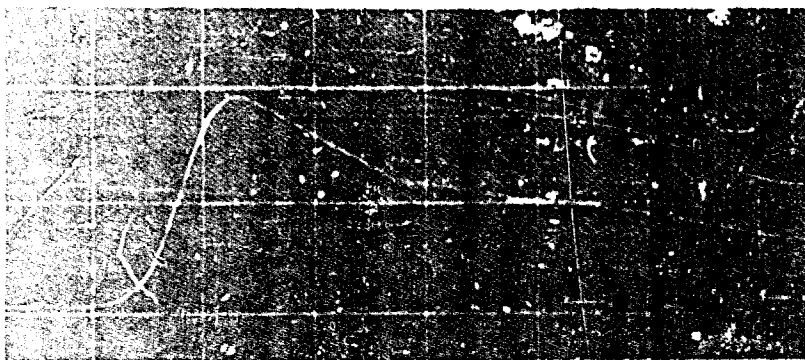
GROUP B

TIP RADIUS = 0.0075 IN. (0.0190 CM)

$$\frac{V_1^{(1)}}{E_1} = 0.036 \text{ CM}$$



$P = 760 \text{ MM}$   
 $\alpha = 9.0 \text{ MA}$   
 $t_1 = 0.011 \mu \text{ SEC}$   
 $t_2 = 0.028 \mu \text{ SEC.}$   
 $M_{pk} = 0.324 \text{ MA-CM}$



$P = 400 \text{ MM}$   
 $\alpha = 3.8 \text{ MA}$   
 $t_1 = 0.012 \mu \text{ SEC}$   
 $t_2 = 0.045 \mu \text{ SEC.}$   
 $M_{pk} = 0.137 \text{ MA-CM}$

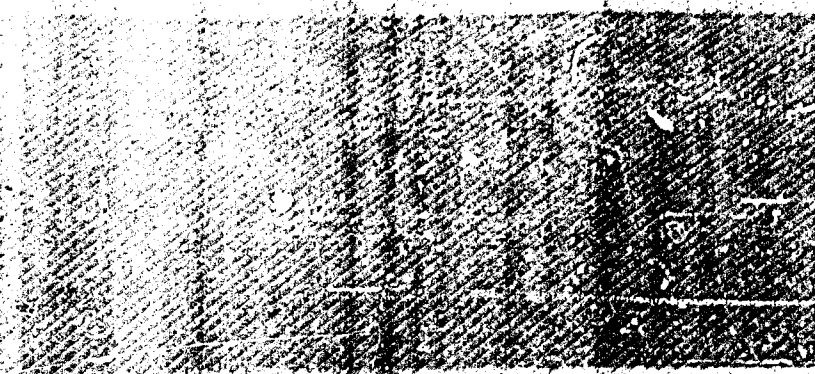


$P = 200 \text{ MM}$   
 $\alpha = 1.1 \text{ MA}$   
 $t_1 = 0.020 \mu \text{ SEC.}$   
 $t_2 = 0.093 \mu \text{ SEC.}$   
 $M_{pk} = 0.040 \text{ MA-CM}$

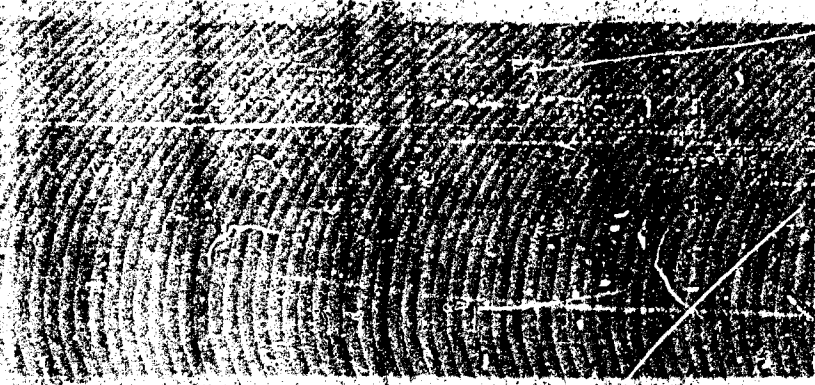


$P = 100 \text{ MM}$   
 $\alpha = 0.8 \text{ MA}$   
 $t_1 = 0.034 \mu \text{ SEC.}$   
 $t_2 = 0.130 \mu \text{ SEC.}$   
 $M_{pk} = 0.029 \text{ MA-CM}$

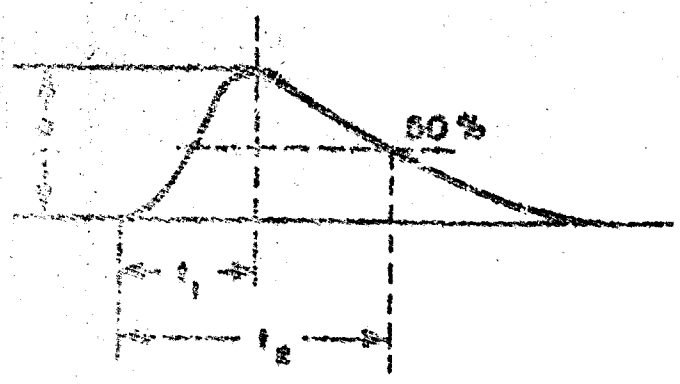
101 P 2  
 10.0234 CM  
 10.0234 CM



$P = 750 \text{ MM}$   
 $\phi = 10.0 \text{ MA}$   
 $t_1 = 0.011 \mu \text{ SEC.}$   
 $t_2 = 0.028 \mu \text{ SEC.}$   
 $M_{PR} = 0.480 \text{ MA-CM}$



$P = 400 \text{ MM}$   
 $\phi = 4.0 \text{ MA}$   
 $t_1 = 0.014 \mu \text{ SEC.}$   
 $t_2 = 0.048 \mu \text{ SEC.}$   
 $M_{PR} = 0.180 \text{ MA-CM}$



Best Available C



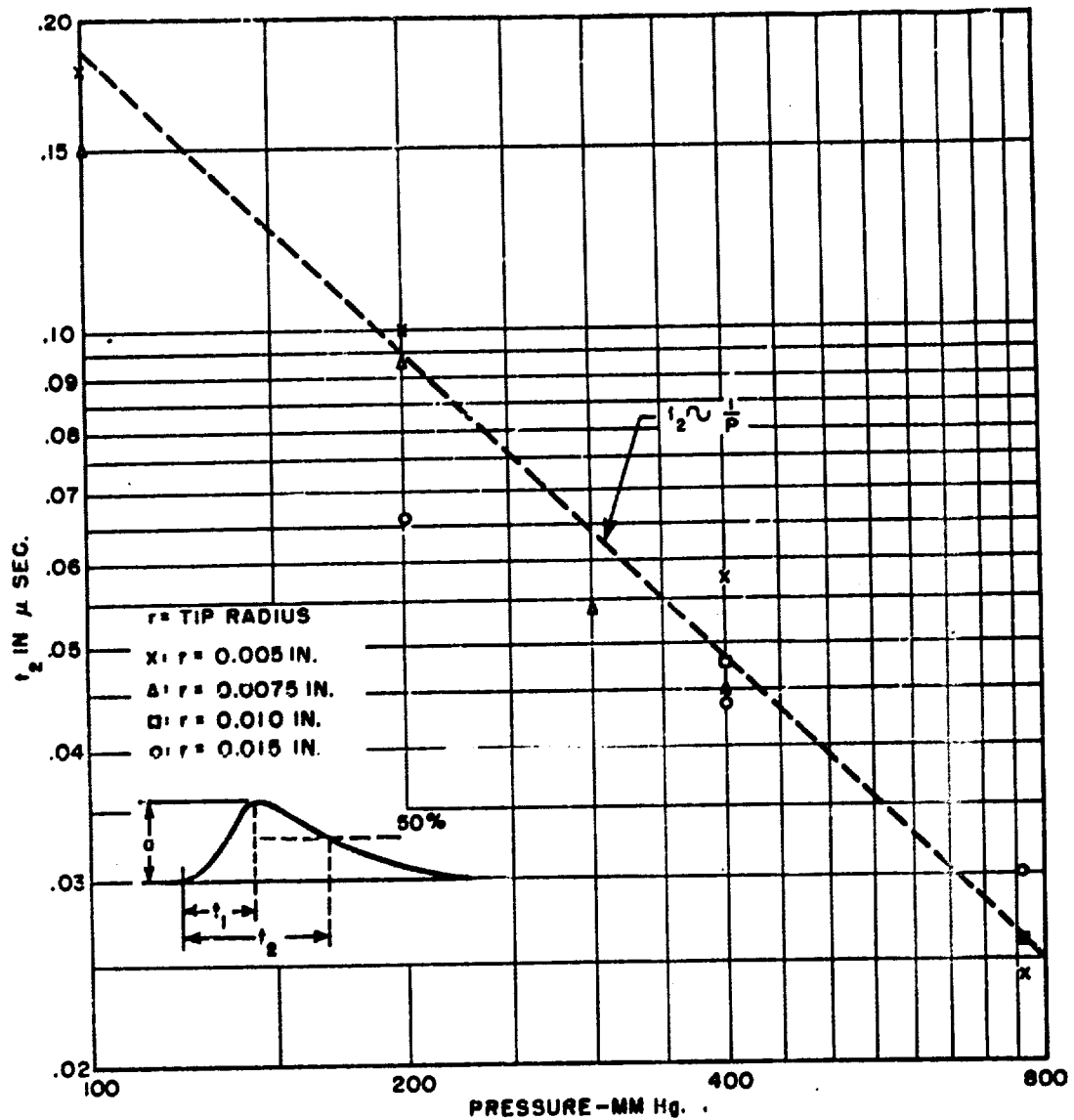
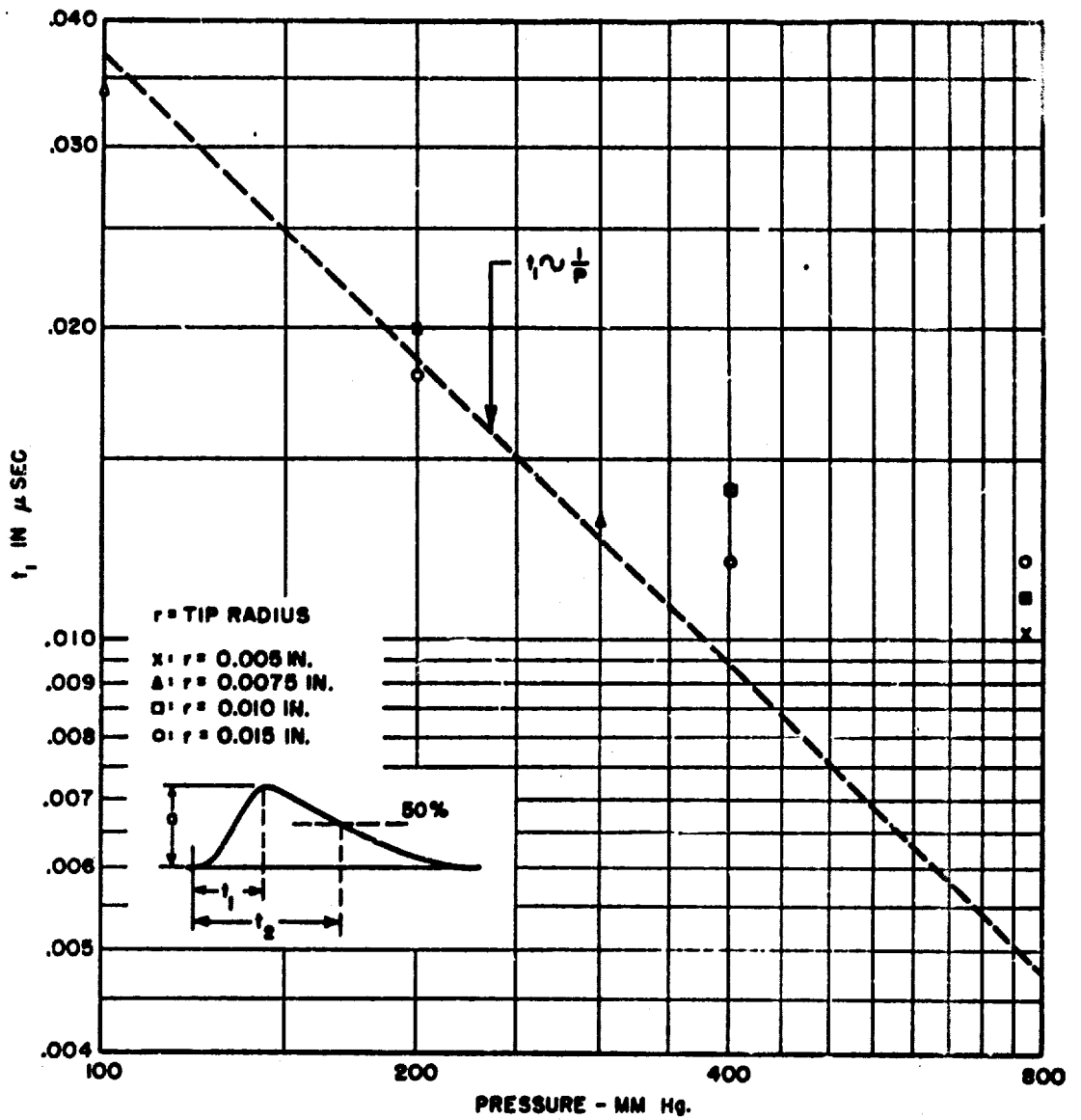


FIG. 5

DEPENDENCE OF PULSE DECAY TIME ON PRESSURE

A-591-TR37-237



**FIG. 6**  
**DEPENDENCE OF PULSE RISE TIME ON PRESSURE**

indicated by the data at the lower pressures. If inverse proportional pressure dependence is accepted, extrapolation from lower pressures indicates a value of approximately  $0.005 \mu\text{s}$  for the rise time at atmospheric pressure.

A consideration of the fundamental processes involved in the electrical breakdown of air during a corona impulse lends support to the conclusion that rise and decay times are inversely proportional to pressure. Let us assume first that the discharge is confined to a space sufficiently small that the field in the region of the discharge is approximately constant, and consider the field condition which makes the discharge possible. This condition is that a free electron which is created by some chance ionizing effect has a high probability of acquiring ionizing energy between collisions. The energy acquired between collisions is proportional to the product of the electric field and the distance traveled by the electron in the direction of the field. Since the distance between collisions is inversely proportional to pressure, and the ionizing energy is constant, breakdown voltage is proportional to pressure under conditions which make the mean free path small compared to the radius of curvature of the electrodes. This well-known relationship was observed to hold in the present experiments.

Now let us consider the motion of any charged particle involved in the discharge. The distance which the particle moves between collisions is inversely proportional to pressure, or

$$d = \frac{k_1}{P} . \quad (9)$$

In addition, for the present experiments, the relation between the critical field and pressure is given by

$$E = k_2 P . \quad (10)$$

Now, if we consider only motion due to the electric field, we have for the distance

$$d = \frac{1}{2} \frac{Ee}{m} t^2, \quad (11)$$

or

$$t = \sqrt{\frac{2dm}{Ee}}.$$

where  $\frac{e}{m}$  is the charge to mass ratio of the electron. Substituting Eqs. (9) and (10) in (11) we find that

$$t = \frac{k_3}{P}. \quad (12)$$

Equation (12) states that the time between collisions for any charged particle involved in the discharge is inversely proportional to the pressure. In deriving it we have neglected effects which are probably of some importance such as the modification of the field by space charge during the course of the discharge. The fields contributed by space charge are given by

$$E_{s.p.c.h.} = \nabla \int \frac{\rho}{\epsilon_0 r} dv. \quad (13)$$

Since all distances involved in the production of a particular element of the space charge are in inverse proportion to the pressure, the  $r$  in the denominator of the integrand in Eq. (13) is inversely proportional to pressure. Therefore, the component of the field contributed by the space charge is also directly proportional to pressure in accordance with Eq. (10). Now if, as Eq. (12) states, the time required to complete all corresponding individual motions is increased in inverse proportion to pressure, the time required to complete the discharge as a whole will be in inverse proportion to the pressure.

In deriving Eq. (12) we depend upon the assumption that all motions of charged particles which contribute to the external effect of the discharge occur in regions of nearly constant field near the discharge point. The fact that Eq. (12) actually appears to be obeyed by the discharges indicates that the regions of large transient current flow are confined close to the discharge point. This view is supported by other evidence, as will be shown in a later section.

Figure 7 gives the dependence of pulse amplitude on pressure and tip radius. The data are so scattered that it is improper to conclude from them that the pulse amplitudes obey any regular mathematical relation to the variables. There is some indication, however, that the amplitudes might be directly proportional to the pressure, as evidenced by their scatter about the lines having slopes of unity on the log-log plot of Fig. 7. The direct proportionality might also hold for variations in tip radius if other factors, particularly the applied field, were more carefully controlled.

D. Effect of Applied Voltage

The most prominent effect of variations in the applied voltage is an increase in pulse repetition frequency with increasing voltage. This effect has been reported by many investigators and was confirmed by the writer. It is discussed in detail elsewhere,<sup>12,20</sup> and will not be included in the present discussion. Next to the effect on repetition frequency, the most noticeable effect of applied voltage is on the pulse amplitude. At a value of applied field just exceeding the critical value required for the production of corona, the pulses are stable in amplitude. With a very slight increase in voltage the pulses appear to grow in amplitude, attaining peak values which exceed by at least 50% the initial value. They also become somewhat erratic in amplitude; succeeding pulses some times differ in size by more than 50%. This effect may be due to some

ve for the  
  
(11)  
  
g Eqs. (9)  
  
(12)  
  
r charged  
e pressure.  
e impor  
the  
re given  
  
(13)  
  
ment of  
in the  
to  
space  
Eq. (10).  
spounding  
the time  
oportion

l mot.  
the  
arge  
charge  
onfir  
viden  
  
e and  
de fr  
ation  
itude  
their  
st of  
is in  
re ca  
  
ge is  
This  
by th  
e in  
on fr  
pulse  
al va  
plit  
in an  
ial v  
some  
some

motions  
 he dis  
 ge point.  
 arges  
 nfinid  
 idence  
  
 and tip  
 e from  
 tion to  
 tudes  
 heir  
 t of  
 s in tip  
 e care

ge is an  
 This  
 oy the  
 in  
 on fre  
 lse  
 l value  
 plitude.  
 n ampli  
 al value.  
 some  
 some

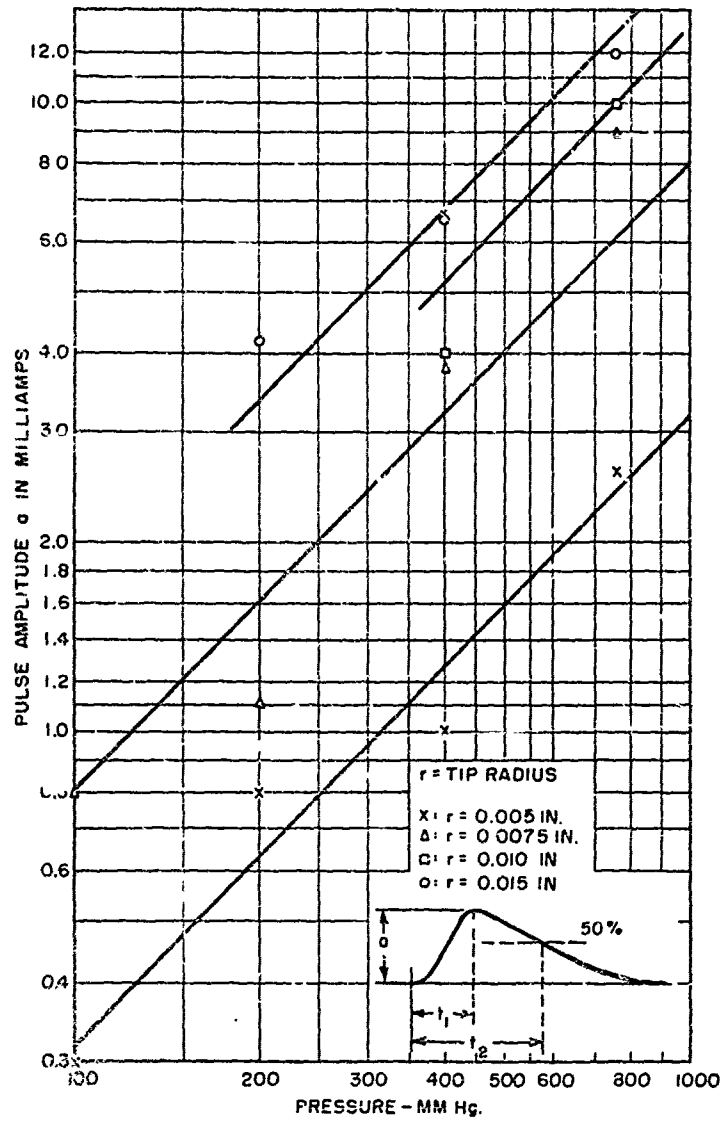


FIG. 7  
 DEPENDENCE OF PULSE AMPLITUDE  
 ON PRESSURE AND TIP RADIUS  
 A-591-TR37-239

irregularity in the microscopic geometry of the point. It probably accounts for the scatter of the data in Fig. 7 since it was discovered that the high voltage power supply used in obtaining these data had a slight hum component in the output voltage. At the time the data were obtained the critical dependence of pulse amplitude on the voltage was not fully appreciated.

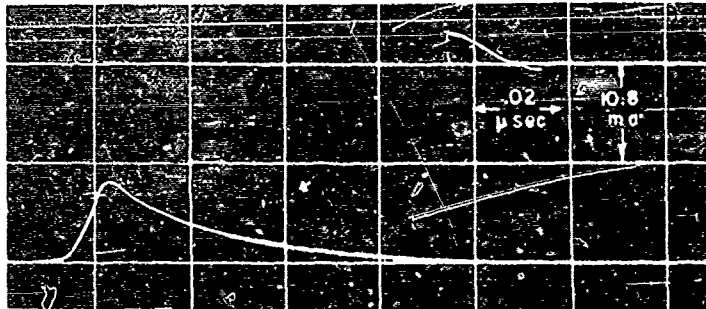
As the voltage is increased beyond a few percent of the critical value the amplitude of the pulses diminishes with increasing voltage. This effect is illustrated by the sequence of oscillograms in Fig. 8, which cover a range of applied voltages of nearly 2 to 1. The oscillograms of Fig. 8 also make it evident that the effect of voltage on the time structure of the individual pulses is slight. Although there is some lengthening of the pulses at higher voltages, this effect can to a good approximation be neglected.

#### E. Laplace Transform of Corona Pulse

If at a later time the transient response of antenna receiver systems to corona pulses were to be considered, it would be necessary to have the Laplace transforms of the pulses. On the basis of the time structure data just presented it is possible to define an idealized pulse shape which closely resembles the actual pulses and which can be expressed as a sum of decaying exponential functions. The Laplace transform of such a pulse is easily determined.

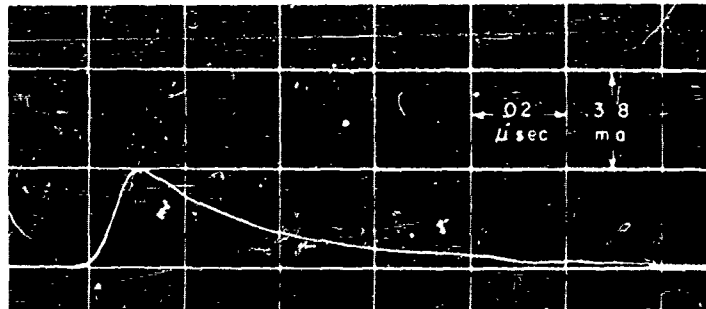
Figure 9 shows a corona pulse replotted from an actual oscillogram together with two approximations to the pulse. The oscillogram used was taken at a pressure of 200 mm Hg since at this pressure the oscillograph is capable of resolving the pulse. On the basis of the observed dependence of pulse forms on pressure, the pulse shape at higher pressures can be obtained by compressing the time scale of Fig. 9 in inverse proportion to the pressure.

y accounts  
 at the  
 ht hum  
 ned the  
 ly  
 ical value  
 This ef  
 ch cover  
 Fig. 8  
 ure of  
 ng of the  
 be  
 systems  
 ave the  
 ure data  
 hich  
 a sum of  
 else is  
 ogram  
 ed was  
 ograph  
 ependence  
 be ob  
 n to the

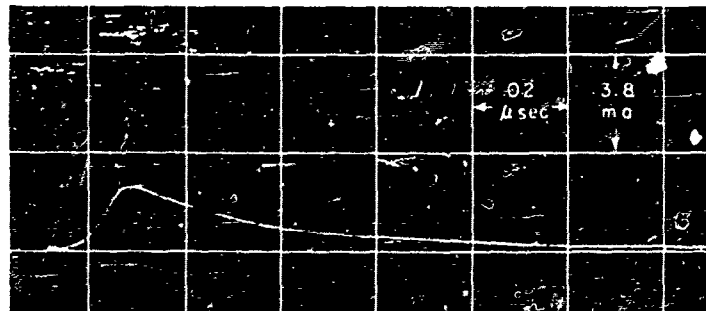


$E_{ot}$  = FIELD APPLIED AT TIP

$i = 9 \text{ MA}$   
 $t_1 = 0.012$   
 $t_2 = 0.028$   
 $E_{ot} \approx 100 \text{ KV/CM}$



$i = 3.8 \text{ MA}$   
 $t_1 = 0.012$   
 $t_2 = 0.032$   
 $E_{ot} \approx 150 \text{ KV/CM}$



$i = 2.4 \text{ MA}$   
 $t_1 = 0.012$   
 $t_2 = 0.036$   
 $E_{ot} \approx 185 \text{ KV/CM}$

FIG. 8  
 EFFECT OF APPLIED FIELD ON CORONA  
 PULSES FROM POINT OF 0.015 IN.  
 RADIUS AT ATMOSPHERIC PRESSURE

A-581-T437-203

APPLIED

/CM

/CM

/CM

— CORONA PULSE REPLOTED FROM OSCILLOGRAM P = 200 MMHg

- - -  $i_1 = 1.140e^{-0.091t}$

- - -  $i_2 = 1.140e^{-0.091t} - 1.560e^{-0.117t}$  CGS(129t - 0375)

(t IN MILLIMICROSECONDS)

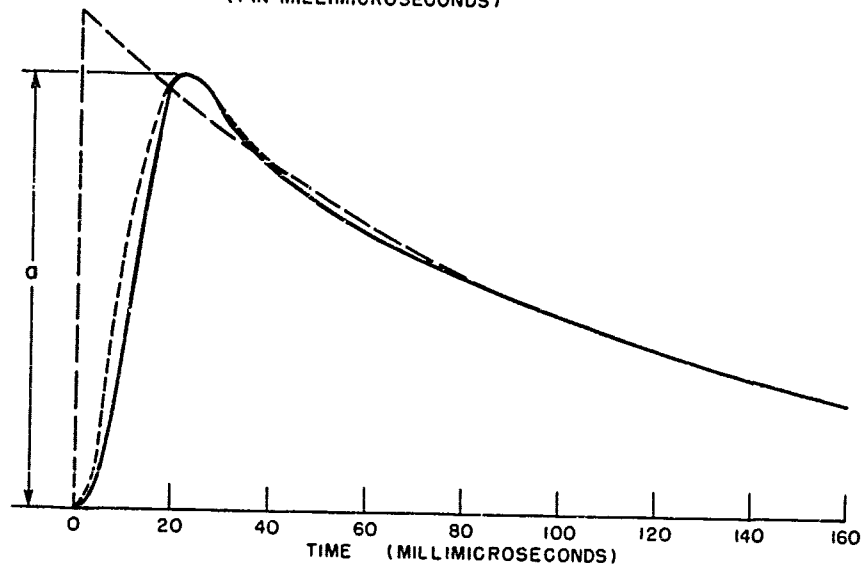


FIG. 9  
EXPONENTIAL APPROXIMATIONS TO CORONA PULSE

A-591-TR57-221

Either of the approximations shown in Fig. 9 is a reasonably good representation, the second being remarkably similar to the actual pulse. A quantitative idea of how well the approximations represent the pulse can be gained by comparing the Fourier spectra of the two approximations. The Laplace transforms of the approximating pulses are found to be

$$L_1(p) = \frac{1.14a}{10^9} \frac{1}{.0091 + p} \quad (14)$$

$$L_2(p) = \frac{1.14a}{10^9} \left\{ \frac{1}{.0091 + p} - 1.37 \left[ \cos 43^\circ \frac{.117 + p}{(.117 + p)^2 + (.129)^2} + \sin 43^\circ \frac{.129}{(.117 + p)^2 + (.129)^2} \right] \right\} \quad (15)$$

where  $L_1$  is the transform of the first approximation and  $L_2$  is the transform of the second. The Fourier transforms are found from the Laplace transforms by setting  $p$  equal to  $j\omega$ . These have been calculated, and are shown in the graphs of Fig. 10. It is apparent from these graphs that the only difference between the spectra of the two pulse models is at the very high frequencies, where the contribution of the leading edge becomes important. Even here, however, the difference is small. There seems little purpose, therefore, in using the more complicated model.

Because of the dependence of pulse time structure upon pressure, the spectra of the pulses are affected by altitude. Fig. 11 shows the spectra of the idealized pulse at two altitudes.

#### F. Dependence of Measured Currents on Coupling Between Discharge and Terminals

As indicated previously, an adequate model of the discharge pulse must include information both on the currents which flow during the pulse and on

v good  
pulse.  
pulse  
imations.  
be

(14)

(15)

e trans-  
place  
and are  
that the  
the very  
nes im-  
ms little

ire, the  
spectra

ulse must  
se and on

591 37

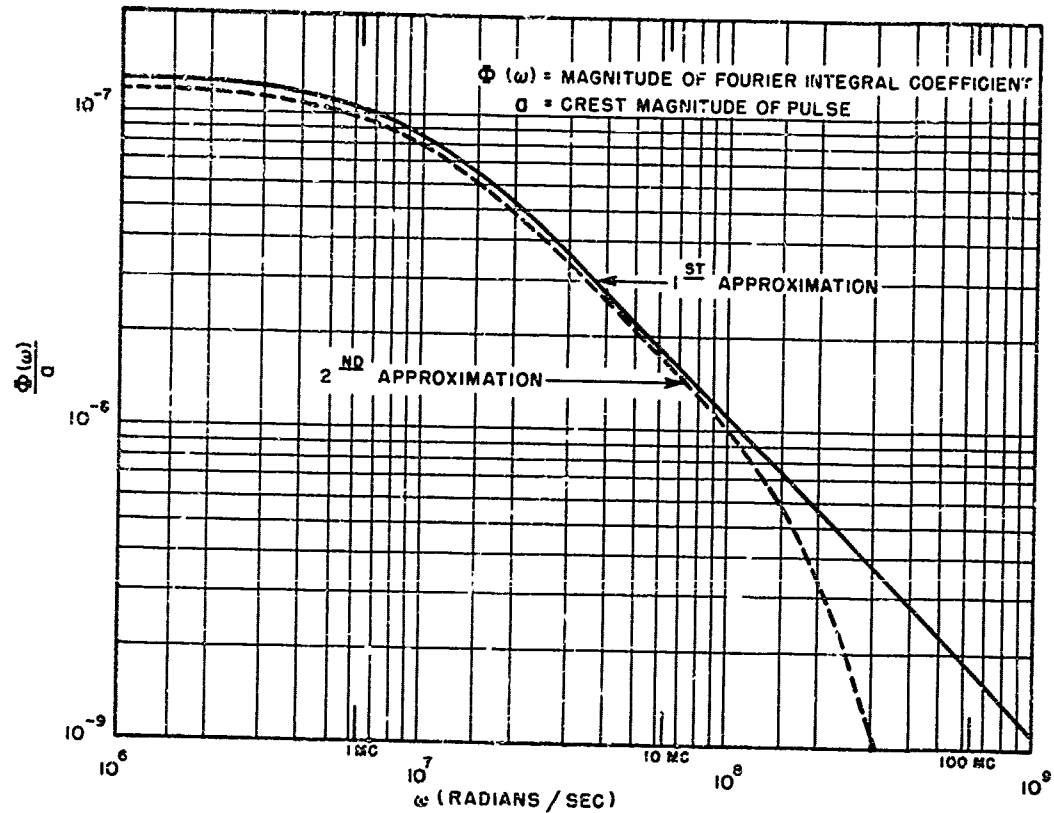


FIG. 10  
FOURIER SPECTRA OF APPROXIMATIONS OF CORONA PULSE  
(P=200 MM Hg)

A-591-TR37-23

TR37-23

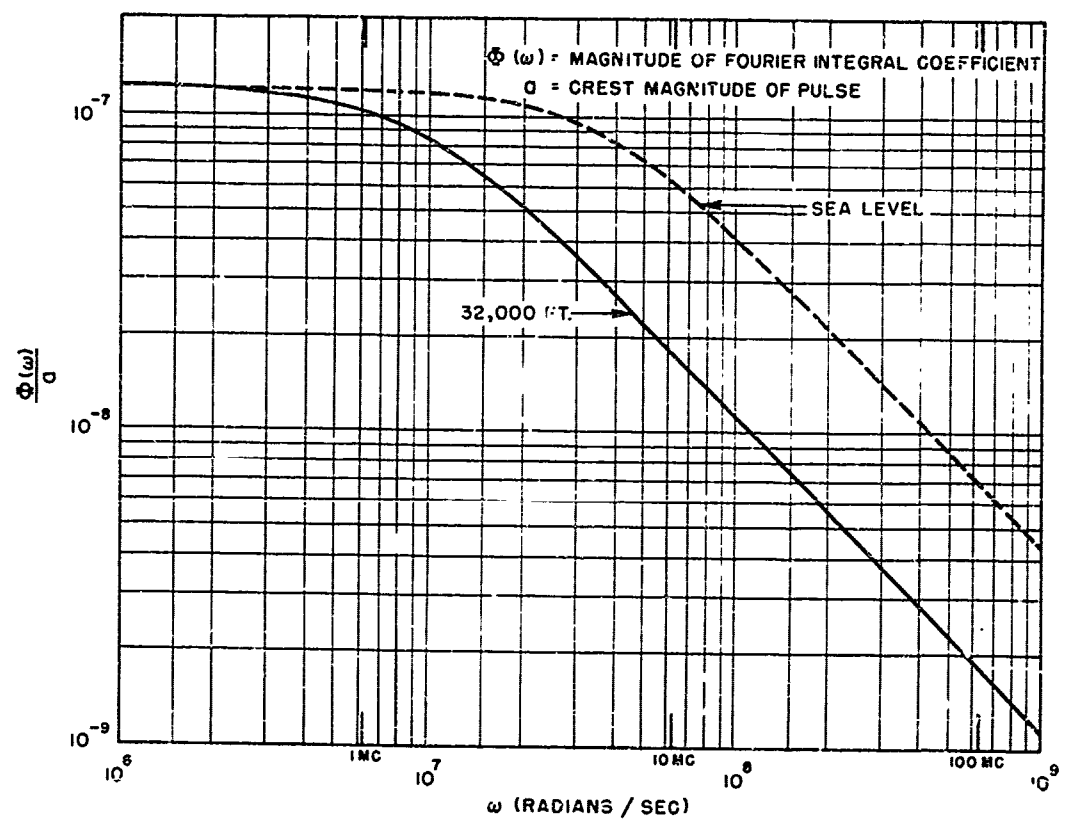


FIG. 11  
 EFFECT OF ALTITUDE ON IDEALIZED CORONA PULSE

A-591-TR37-236

CIENT

10<sup>8</sup>

10<sup>9</sup>

10<sup>6</sup>

10<sup>7</sup>

10<sup>8</sup>

10<sup>9</sup>

1 MC

10 MC

100 MC

TR37-233

FFICIE

10<sup>8</sup>

10<sup>9</sup>

10<sup>6</sup>

10<sup>7</sup>

10<sup>8</sup>

10<sup>9</sup>

1 MC

10 MC

100 MC

TR37-

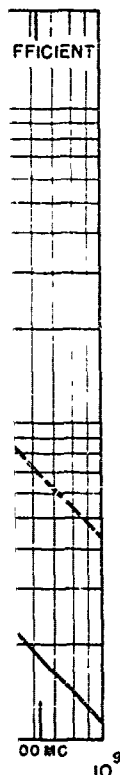
the spatial extent of these currents. Previous investigations have assumed that the current which was measured at the base of the discharge point was the current flowing in the discharge itself. No evidence concerning the extent of the current flow other than photographs is available, and these give no quantitative information. It will be shown in the present section that although the base current provides a measure of the actual discharge current, the two are by no means identical.

Let us apply the reasoning of Chapter II to the discharge situation illustrated by the schematic diagrams of Fig. 12. According to Eq. (8) the short circuit current  $I_1^{(2)}$  is given by

$$I_1^{(2)} = \frac{1}{V_1^{(1)}} \int_{T_2} E^{(1)} \cdot J^{(2)} dv. \quad (8)$$

Now the currents which are shown in the oscillograms of Fig. 4 are not the short circuit currents, but the currents through a 50-Ω resistance. It will be remembered however, that to derive the expression for  $I_1^{(2)}$  we divided the open circuit voltage  $V_1^{(2)}$  by  $Z_{11}$ , the impedance looking into terminals 1. For the geometry of Fig. 12,  $Z_{11}$  is the capacitive reactance of the short length of conductor (1.3 cm for the oscillograms of Fig. 4) which forms the discharge point. This reactance is many thousand ohms at the highest frequencies involved in the pulses. The 50-Ω resistance can therefore be neglected by comparison, making it apparent that the measured current pulses are inappreciably different from the actual short circuit currents.

Equation (8) makes it evident that  $I_1^{(2)}$ , the current measured, depends not only on the actual discharge currents, but on the coupling between the point of the discharge and the measuring terminals, a fact which has been overlooked by other investigators. This coupling is indicated in Eq. (8) by the ratio  $\frac{E^{(1)}}{V_1^{(1)}}$ . It is only for the limiting case, in which the current flow extends beyond the region in which the field  $E^{(1)}$  has appreciable values that the current measured is identical with the actual discharge



II-TR37-236

ave as  
 charge  
 nce con  
 available  
 the  
 of the  
 tuation  
 q. (8)  
 (8)  
 e not the  
 e. It will  
 divided  
 terminals l.  
 he short  
 forms the  
 hest fre  
 re be  
 rent pulses  
 s.  
 l. depends  
 etween the  
 as been  
 Eq. (8)  
 ne current  
 able  
 scharge

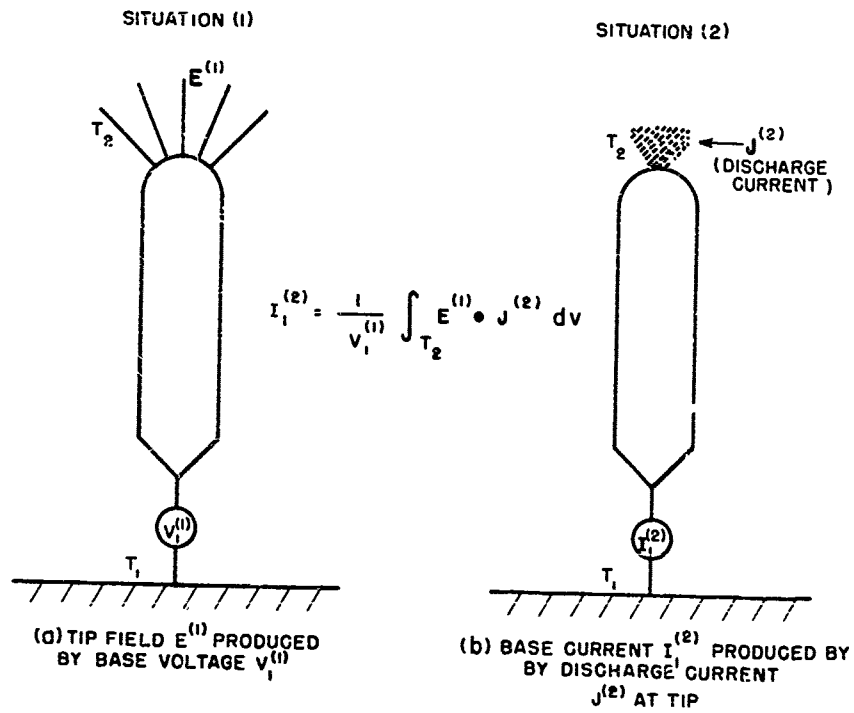


FIG. 12  
 ILLUSTRATING THE APPLICATION OF THE COUPLING THEOREM  
 TO THE ANALYSIS OF CCRONA PULSES

A-591-TR37-223

currents. As has been previously suggested, the actual currents are confined to much smaller regions than this.

It is possible, by means of Eq. (8) and a knowledge of the field quantity  $\frac{E^{(1)}}{V_1}$  for the electrode geometry, to deduce the dipole moments of the discharges, provided we know their spatial extent. The data of Fig. 4 do not provide this information, however, and it is necessary to devise other experiments which will do so.

#### G. Spatial Distribution of Currents in the Discharge

The basic coupling relation of Eq. (8) provides a clue to an experimental procedure which will give information on the spatial extent of the discharges. Examination of the equation indicates that if we devise an electrode geometry which will enable us to vary the quantity  $\frac{E^{(1)}}{V_1}$  while at the same time holding fixed the field which produces the discharge, we can infer from the resulting variations in  $I_1^{(2)}$  information concerning the volume occupied by the discharge currents. The electrode arrangement shown in the photograph of Fig. 13 and illustrated schematically in Fig. 14 was designed to accomplish this purpose. Electrodes A and B are flat circular discs. The diameters of these discs are sufficiently large to insure uniform fields in the vicinity of the discharge point when a voltage difference exists between the discs. The field about the discharge point can then be analyzed as the field about such a point when placed in an otherwise uniform field. The fields about the points are discussed in detail in Appendix A.

The applied d c field  $E_0$  which produces the discharge is quite evidently of the form indicated. The assertion that the field  $E^{(1)}$  of Eq. (8) is also of this form requires some justification. The field  $E^{(1)}$ , as given in the equation is a dynamic field. It is a function both of coordinates and frequency. Since the electrodes are small compared to the wavelengths of the highest frequencies in the spectrum of the impulse, however a

re con

eld

ents of

f Fig. 4

evise

xperi

of the

re an

while at

we can

the

nt shown

14 was

ircular

re uni

iffer

can

other

etail

evi

Eq. (8)

as given

dinates

lengths

a

591 37

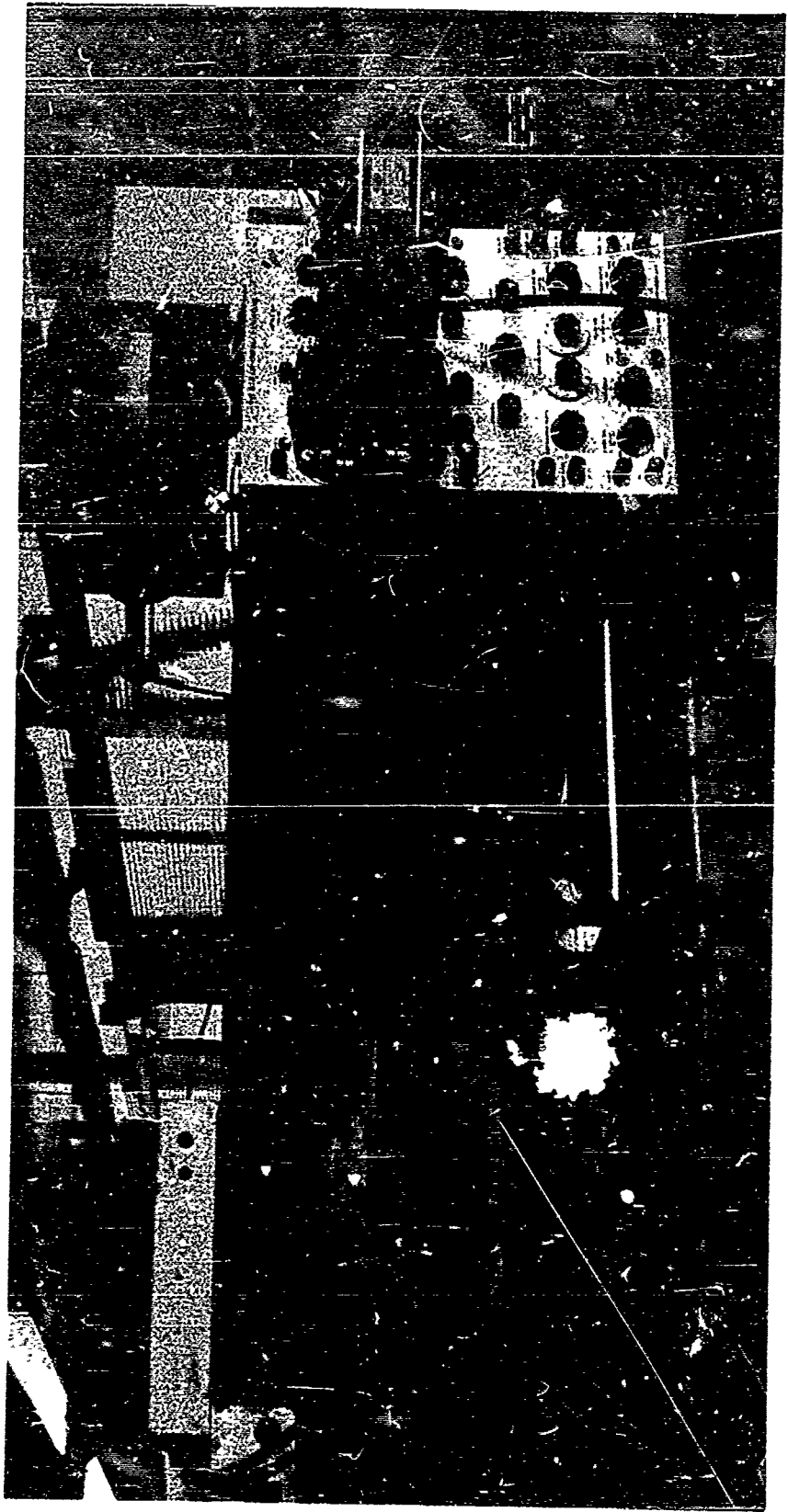


FIG. 13  
SETUP FOR FINDING SPATIAL EXTENT OF CORONA CURRENTS

FIG. 13

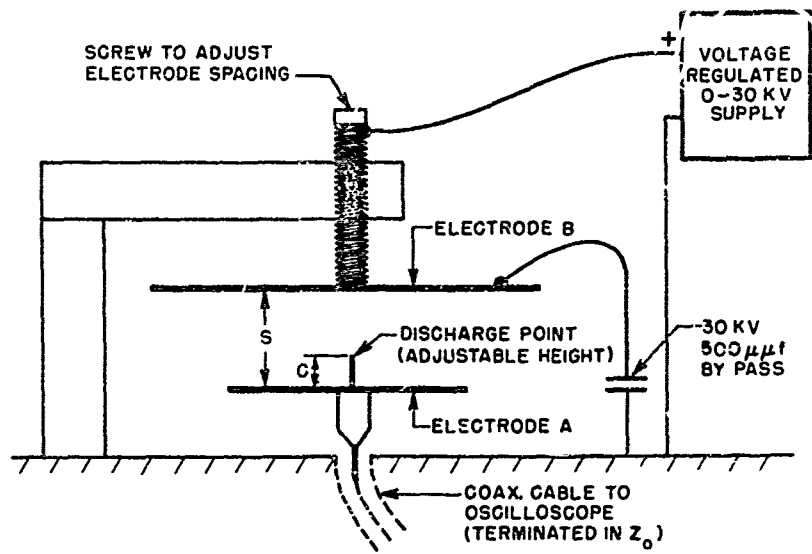


FIG. 14  
SCHEMATIC DIAGRAM OF SETUP FOR FINDING  
SPATIAL EXTENT OF CORONA CURRENTS

A-591-TR37-213

quasistatic analysis applies. The 500  $\mu\mu\text{f}$  bypass capacitor connected between electrode B and Fig. 14 is large compared to the capacitance between electrodes A and B, and therefore insures that electrode B can be considered as being at ground potential when computing  $E^{(1)}$ .

It is apparent from the foregoing discussion that the setup shown permits the quantity  $\frac{E^{(1)}}{V_1^{(1)}}$  to be varied in either of two ways. By varying the spacing  $s$  between electrodes A and B, the field between them (for a given voltage between A and ground) is varied. If the height of the discharge point is held constant while  $s$  is varied, the magnitude of  $E^{(1)}$  is varied while the geometry of  $E^{(1)}$  is unchanged. By maintaining  $s$  constant, however, and varying the height of the point, both the geometry and the magnitude of  $E^{(1)}$  are varied for a given value of  $V_1^{(1)}$ .

As before, the quantity recorded in the oscillograms is the current through a 50- $\Omega$  resistance rather than the short circuit current. In the present instance the impedance  $Z_{11}$  is the reactance due to the capacitance of electrode A. This capacitance has a maximum value at minimum spacing of slightly under 6  $\mu\mu\text{f}$ . The frequency at which the reactance of a 6  $\mu\mu\text{f}$  capacitor becomes 50 ohms is 53 Mc. Since the bandwidth of the Techtronix 513 Oscilloscope used in this phase of the experimental study is only 16 Mc, it is evident that the observed pulses are again negligibly affected by the finite value of the resistance between terminals.

The oscilloscope used in the present study has considerably less time resolution than the Model 517 Oscilloscope used to obtain the data of Fig. 4. This is not of great importance, however, because an accurate definition of the time structure of the pulses is of no value. The experiments described in this section were intended to obtain accurate information concerning the pulse amplitudes, and since the linear range of the vertical amplifier in the 513 Oscilloscope is greater than that of the 517 Oscilloscope, it is better for this purpose.

The high voltage power supply used in the experiments of this section was much better regulated and filtered than the one used for the

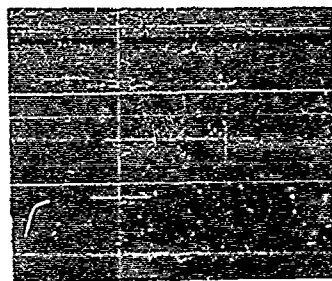
experiments of the previous section. As a result the pulses at applied fields just exceeding the critical value were so stable in amplitude and form that succeeding traces on the oscilloscope exactly superposed, and it was possible to obtain multiple trace oscillograms.

The oscillograms of Figs. 15 and 16 show the results of varying the ratio  $\frac{E^{(1)}}{V_1^{(1)}}$  by the two methods outlined above. Figure 15 shows the effect of varying the spacing  $S$  with the tip height  $C$  held constant at 0.672 cm. The electric field at the surface of disc A in the absence of the discharge point is found analytically in Appendix B. This field is uniform over a region of extent considerably greater than the dimensions of the discharge point so that  $E^{(1)}$ , the actual field near the discharge point produced by the voltage  $V_1^{(1)}$ , is the field calculated in Appendix B times the concentration factor which is introduced by the discharge point itself. (Appendix A.) The field calculated in Appendix B will be called  $E_0^{(1)}$ , while the field at the extreme tip of the discharge point will be called  $E_t^{(1)}$ .

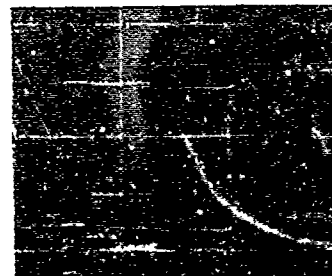
From the foregoing analysis it is clear that if the current flow is confined to a relatively small region near the discharge point, the measured magnitudes of the pulses should vary with  $S$  in the same way as does  $E_0^{(1)}$ . In the graph of Fig 17 the field quantity  $\frac{E_0^{(1)}}{V_1^{(1)}}$  and the pulse magnitudes as obtained from the oscillograms of Fig. 15 are both plotted as functions of  $S$ . The scale of pulse magnitudes is arbitrarily adjusted to make the pulse magnitude at minimum spacing coincide with the curve of  $\frac{E_0^{(1)}}{V_1^{(1)}}$  at that spacing. The close agreement of the other points with the curve can be regarded as a verification of the general coupling theorem as applied to corona pulses, and as proof that the transient currents in the pulses do not extend from the points to distances which are of the same order of magnitude as the minimum distance between the tip of the point and electrode B.

The result of Fig. 17 yields one other conclusion concerning corona pulses. The data of that figure together with Fig. 15 show that the

applied  
 tube and  
 d, and it  
 ing the  
 e effect  
 672 cm.  
 discharge  
 over a  
 discharge  
 oduced by  
 concen  
 (Appen  
 hile the  
 ).  
 low is  
 e  
 ay as  
 e pulse  
 lotted as  
 sted to  
 e of  
 h the  
 eorem as  
 in the  
 same  
 point



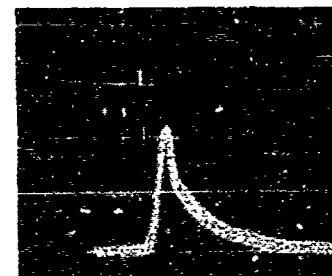
$\alpha = 3.8 \text{ MA}$   
 $S = 1.69 \text{ CM}$   
 $\frac{E_0^{(1)}}{V_i^{(1)}} = 2.39$



$\alpha = 3.2 \text{ MA}$   
 $S = 2.0 \text{ CM}$   
 $\frac{E_0^{(1)}}{V_i^{(1)}} = 2.04$



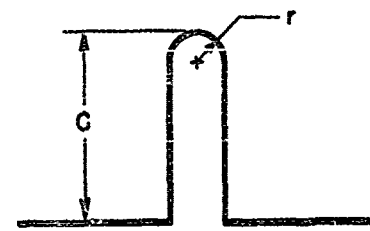
$\alpha = 2.4 \text{ MA}$   
 $S = 2.94 \text{ CM}$   
 $\frac{E_0^{(1)}}{V_i^{(1)}} = 1.48$



$\alpha = 2.0 \text{ MA}$   
 $S = 4.0 \text{ CM}$   
 $\frac{E_0^{(1)}}{V_i^{(1)}} = 1.22$



$\alpha = 1.7 \text{ MA}$   
 $S = 5.0 \text{ CM}$   
 $\frac{E_0^{(1)}}{V_i^{(1)}} = 1.11$



FOR ALL OSCILLOGRAMS:

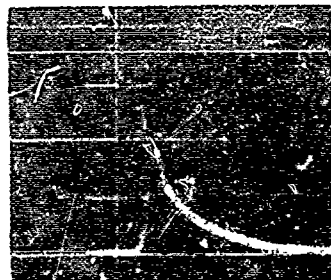
$c = 0.672 \text{ CM}$   
 $r = 0.038 \text{ CM}$   
 $\frac{E_1}{E_0} = 14.6$

HORIZ. SCALE = 0.10  $\mu\text{SEC./DIV.}$   
 VERT. SCALE = 2 MA / DIV.

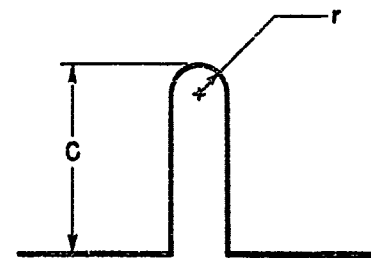
$\mu\text{SEC.}$   
 $/\text{DIV.}$

FIG. 15

EFFECT ON MEASURED PULSE  
 AMPLITUDE OF VARYING S  
 (SEE FIG. 14)



$a = 1.7 \text{ MA}$   
 $c = 0.36 \text{ CM}$   
 $\frac{c}{r} = 9.4$

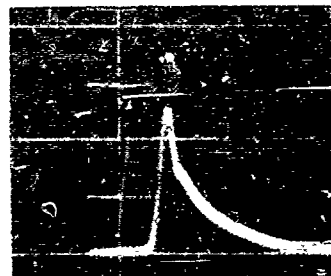


FOR ALL OSCILLOGRAMS:

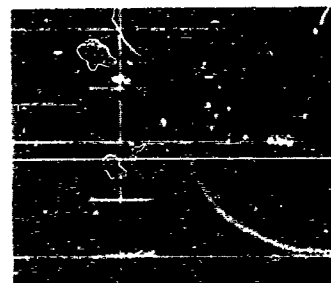
$c = 0.672 \text{ CM}$   
 $r = 0.038 \text{ CM}$

$\frac{E_t}{E_0} = 14.6$

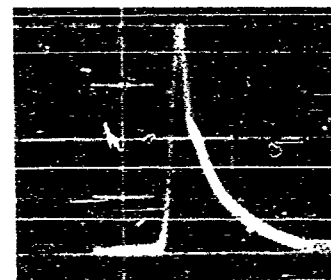
HORIZ. SCALE =  $0.10 \mu\text{SEC.} / \text{DIV.}$   
 VERT. SCALE =  $2 \text{ MA} / \text{DIV.}$



$a = 2.5 \text{ MA}$   
 $c = 0.674 \text{ CM}$   
 $\frac{c}{r} = 17.7$



$a = 3.1 \text{ MA}$   
 $c = 1.03 \text{ CM}$   
 $\frac{c}{r} = 27.1$



$a = 4.0 \text{ MA}$   
 $c = 1.35 \text{ CM}$   
 $\frac{c}{r} = 35.4$

FIG. 16

EFFECT ON MEASURED PULSE  
AMPLITUDE OF VARYING  $\frac{c}{r}$

C-591-TR37-204

$\mu\text{SEC.} / \text{DIV.}$   
 $/ \text{DIV.}$

SEC./ DIV.  
DIV.

ELECTRODE ARRANGEMENT  
(SEE FIG. 14)

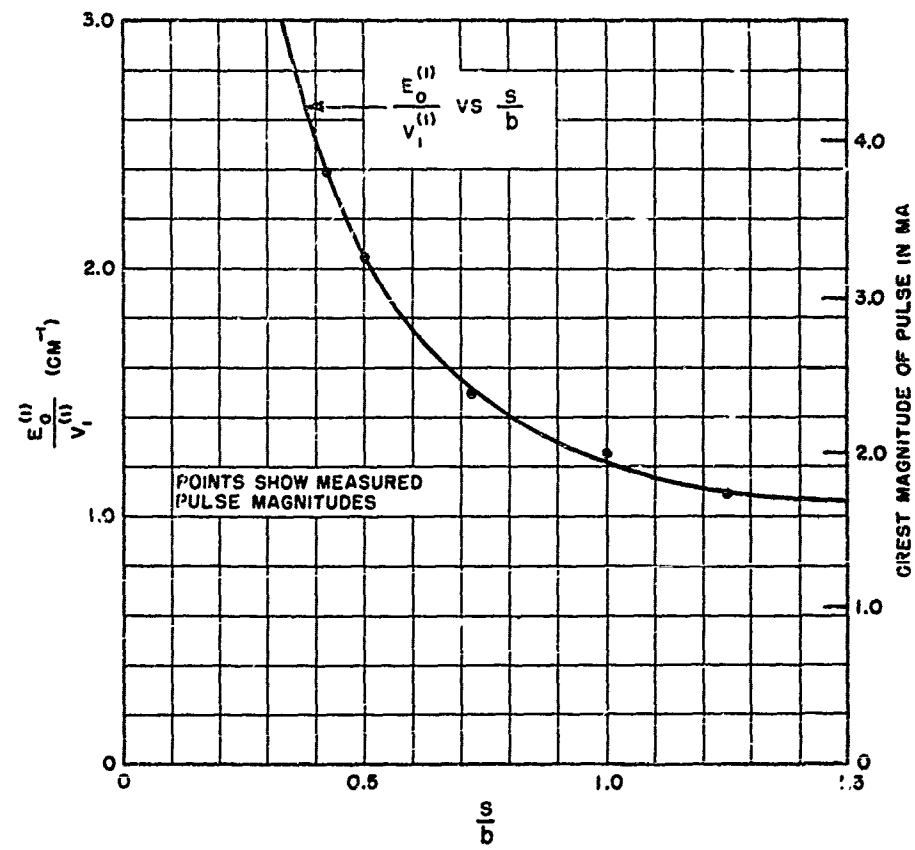
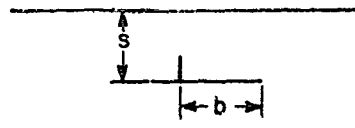


FIG. 17

DEPENDENCE OF MEASURED PULSE MAGNITUDE ON  $E_0^{(1)}$

A-591-TR57-215

discharges are independent in form and magnitude of the fields of dynamic reaction which are excited by the discharge. Such a result would be expected from physical reasoning. The impressed d-c fields which produce the discharge are of the order of 100,000 v/cm, while the reaction fields are probably never more than 100 v/cm and cannot, therefore, appreciably influence the discharge processes. The fact that the discharge currents are independent of the reaction fields is an important property of the discharge since it enables us to validly state that the  $J$  term in Eq. (2) is independent of the other field quantities.

The oscillograms of Fig. 15 establish nothing concerning the dimensions of the volume occupied by the discharge currents other than that it is smaller than the minimum value of  $S$ . More definite information is provided, however, by the oscillograms of Fig. 16. To obtain the oscillograms in this figure, the spacing  $S$  was held at a constant value of 2.94 cm and the height of the point varied in four steps from 0.36 cm to 1.35 cm. With the tip radius held constant the variation in point height produces a variation in the ratio  $\frac{E_t^{(1)}}{V_0^{(1)}}$ . The dependence of this ratio upon tip height is analyzed in Appendix A. In the curve of Fig. 18  $\frac{E_t^{(1)}}{E_0^{(1)}}$  is plotted as a function of the ratio  $\frac{c}{r}$ . The four indicated points are the magnitude data from the oscillograms of Fig. 16 plotted to an arbitrary scale which makes the point for the greatest value of  $\frac{c}{r}$  coincide with the curve of  $\frac{E_t^{(1)}}{E_0^{(1)}}$ . The close coincidence of the other points shows that the measured current depends almost entirely upon the field in the near vicinity of the tip of the discharge point.

Let us next investigate what quantitative information concerning the spatial extent of the pulses can be inferred from the data of Fig. 16 in conjunction with the basic coupling theorem Eq. (8) which is rewritten below:

$$I_i^{(2)} = \frac{1}{V_1^{(1)}} \int E^{(1)} \cdot J^{(2)} dv, \quad (8)$$

GREST MAGNITUDE OF PULSE IN MA

0.0

0

0

0

215

of dynamic  
 and be ex-  
 produce  
 on fields  
 appreciably  
 currents  
 of the  
 in Eq. (2)  
 the dimen-  
 that it  
 on is pro-  
 scillograms  
 4 cm and  
 cm. With  
 es a vari-  
 height is  
 as a  
 itude data  
 ich makes  
 $\frac{E_t^{(1)}}{E_0^{(1)}}$ . The  
 $E_0$   
 rent de-  
 tip of the  
  
 ing the  
 . 16 in  
 .tten  
  
 (8)

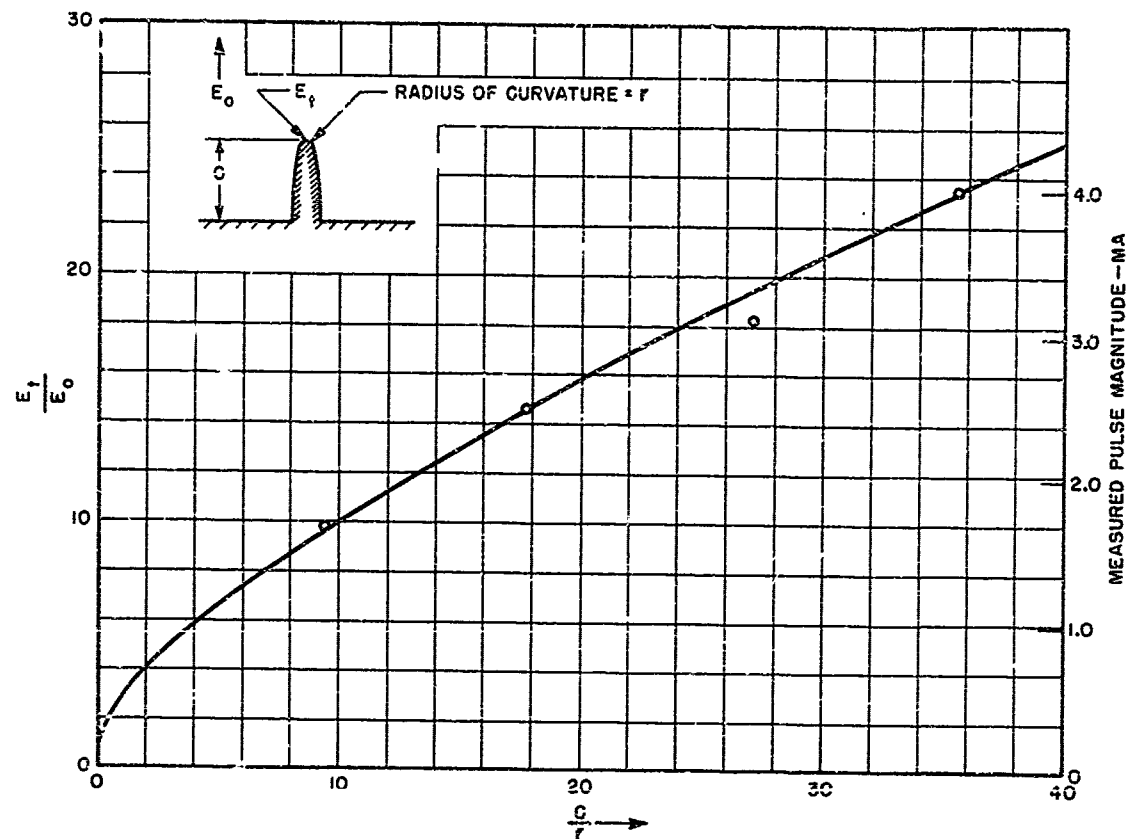


FIG. 18  
 CONCENTRATION OF FIELD AT TIP OF PROLATE SPHEROID  
 (COMPARISON WITH MEASURED PULSE MAGNITUDES)

A-591-1937-2 4

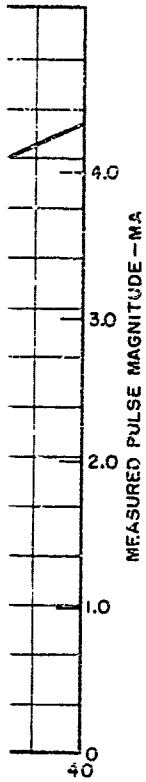
We first assume that the current flow is sufficiently parallel to the field lines that the cosine of the angle between  $E^{(1)}$  and  $J$  is not appreciably different from unity. We further assume that the current flow is near the axis, i.e., that it is confined to values of  $\eta$  for which the electric field is nearly constant. Examination of the field expressions in Appendix A and Fig. 19, which shows the relation of tip sizes to coordinates, indicates that this condition holds for an area on the tip of radius as large as the radius of the tip. Photographs taken by Loeb indicate that the radial extent of the discharge is considerably smaller than this.<sup>15</sup>

In view of the assumptions concerning the field, it is possible to replace the integrand quantity  $(E^{(1)} \cdot J^{(2)} dv)$  by  $(E_z^{(1)} I_d^{(2)} h_\xi d\xi)$ , where  $I_d^{(2)}$  is the discharge current, which can be considered as being confined to a filament along the axis,  $E_z^{(1)}$  is the field on the axis, and  $h_\xi d\xi$  is the space differential along the axis. The current  $I_d^{(2)}$  is a function of  $\xi$  only. To determine the effective extent of the discharge currents we assume that  $I_d^{(2)}$  has a constant value between the surface of the discharge point at  $\xi_0$  and some arbitrary value of  $\xi$ , which we shall call  $\xi_a$ , and that it is zero for values of  $\xi$  larger than  $\xi_a$ . We then investigate the terminal response of such a current and compare it with the results obtained from the oscillograms of Fig. 16. For the conditions outlined, Eq. (8) becomes

$$I_1^{(2)} = \frac{V_d^{(2)}}{V_1^{(1)}} \int_{\xi_0}^{\xi_a} E_z^{(1)} h_\xi d\xi \quad (15)$$

We recognize the integral in Eq. (14) to be the difference in potential between the surface of the discharge point and the point on the axis defined by the coordinate  $\xi_a$ .

One special case for the value of the integral is of interest. If we assume that the current flow extends to electrode B, the value of the integral quite apparently becomes  $V_1^{(1)}$ , and



the field  
 appreciably  
 near the  
 electric field  
 Appendix A and  
 indicates  
 as the  
 radial  
  
 ble to  
 ( $\xi$ ), where  
 confined  
 $h_\xi d\xi$  is  
 action of  
 nts we  
 discharge  
 , and that  
 he termi-  
 tained  
 p. (8)

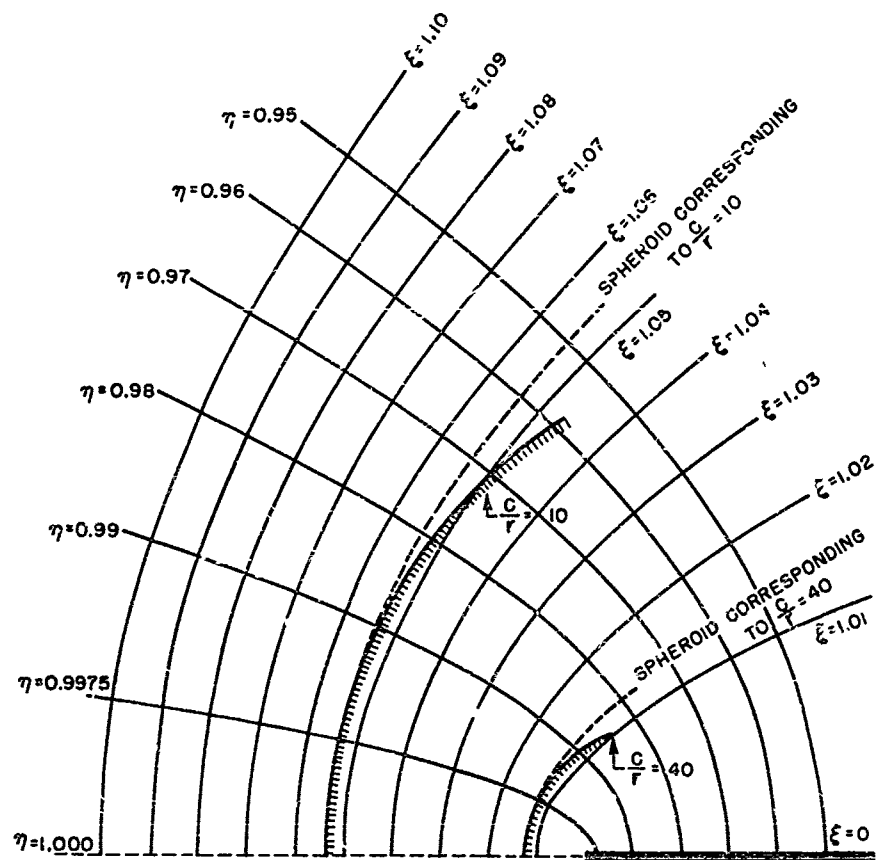


FIG. 19  
 SPHEROIDAL COORDINATES NEAR TIP AND  
 COMPARISON WITH ACTUAL DISCHARGE POINT

A-591-TR37-222

(16)

ential be  
 defined  
  
 . If we  
 the

$$I_i^{(2)} = I_d^{(2)},$$

or the measured current is the same as the discharge current. For such a circumstance all the oscillograms of both Fig. 15 and Fig. 16 would have the same magnitude. That they do not is conclusive proof that the discharge currents are greater than the measured response, and that the extent of the discharges is less than the spacing between electrodes.

The potential expression which is defined by the integral of Eq. (16) is derived by Smythe<sup>21</sup> and given in Appendix A. However, since from Fig. 16 the observed pulse magnitudes are proportional to  $E_t^{(1)}$ , a more significant quantity for the present investigation is the ratio of that integral to the field at the surface of the tip. The quantity thus defined is given by Eq. (17) below:

$$\frac{\int_{\xi_0}^{\xi_a} E_z^{(1)} h_\xi d\xi}{E_t^{(1)}} = c \frac{\xi_a}{\xi_0} \frac{\left(1 - \frac{\coth^{-1} \xi_a - \frac{1}{\xi_a}}{\coth^{-1} \xi_0 - \frac{1}{\xi_0}}\right)}{\left(1 - \frac{\coth^{-1} \xi_a - \frac{1}{\xi_a}}{\coth^{-1} \xi_0 - \frac{1}{\xi_0}}\right)} \quad (17)$$

If we plot the quantity of Eq. (17) versus distance from the tip for different values of  $\frac{c}{r}$ , we determine how far the current  $I_d^{(2)}$  can extend and still preserve the proportionality between  $I_i^{(2)}$  and  $E_t^{(1)}$ . Let us call  $z'$  the distance from the tip normalized with respect to the tip radius (held constant in the present experiments). It can then be shown that

$$z' = \frac{\xi_a - \xi_0}{\xi_0} \frac{c}{r}.$$

Figure 20 shows a plot of the quantity defined in Eq. (17) versus  $z'$  for values of  $\frac{c}{r}$  of 10 and 40. These values approximately represent the extremes of  $\frac{c}{r}$  used in the experiments.

It is observed from Fig. 20 that if the current  $I_d^{(2)}$  extends from the surface of the discharge point by as much as two tip radii (0.0763 cm), we could expect relative deviations from the curve of Fig. 18 by approximately 6%. The points appear to lie closer to the curve than this although the experimental accuracy is not sufficiently good to justify an assertion that such deviations do not occur. More exhaustive experiments, conducted along the lines suggested here but under even more carefully controlled conditions and for a wider range of all the variables, would be necessary to accurately determine the extent of the discharge. Assuming, however, that in the present experiments the discharge is confined to a space  $2r$  in length, the integral of Eq. (17) can be evaluated. The value obtained for the integral is approximately  $\frac{V_1^{(1)}}{10}$ , which means that the measured transient current,  $I_1^{(2)}$ , is less than one tenth of the actual discharge current  $I_2^{(2)}$ . If the spatial extent of the discharge is less than  $2r$ , as it may well be, then the ratio of measured current to discharge current is still less.

Although a more accurate determination of the extent of the discharge current than that given above is of some theoretical interest, it is not necessary in the present analysis. We are interested here only in the determination of an equivalent dipole moment of the discharge and for that purpose it is sufficient to know that the currents are confined to a space small enough so that the magnitude of the terminal current is accurately proportional to the surface field as is shown by Fig. 18. With that information we can assume that the discharge is confined to an infinitesimal region  $\delta$  in which the field is constant and has the value  $E_c^{(1)}$ . We then measure the strength of the discharge not in terms of the actual discharge current but in terms of a current moment  $M$  such that

s  $z'$  for  
 the ex  
  
 s from the  
 (3 cm) we  
 roxi  
 s although  
 assertion  
 conducted  
 rolled  
 necessary  
 owever,  
 ace  $2r$  in  
 ained for  
  
 d tran  
 ge current  
 it may  
 is still  
  
 ischarge  
 is not  
 the  
 for that  
 a space  
 rately  
 at infor  
 smal  
 e then  
 ischarge

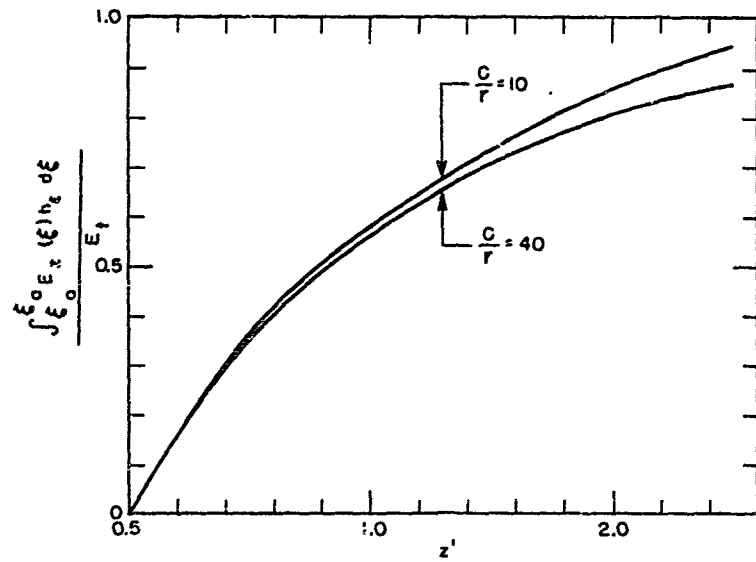
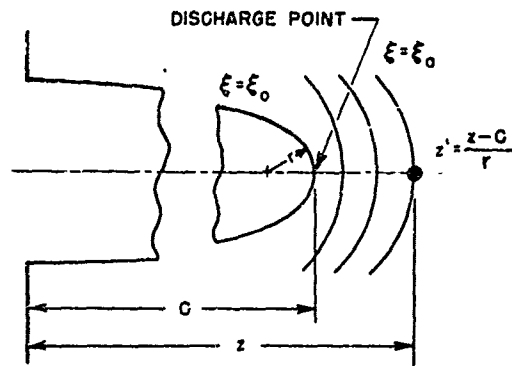


FIG. 20  
 COMPARISON OF FIELDS AT TIP  
 OF DISCHARGE POINT FOR TWO VALUES OF  $\frac{C}{r}$   
 A-591-TR37-233

$$E_t^{(1)} M = \int_{T_2} E^{(1)} \cdot J \, dv, \quad (18)$$

or from Eq. (8)

$$M = \frac{I_1^{(2)} V_1^{(1)}}{E_t^{(1)}}. \quad (19)$$

The quantity  $\frac{V_1^{(1)}}{E_t^{(1)}}$  for each value of  $\frac{C}{r}$  can be evaluated by means of a mathematical model discussed in Appendix A. Its value, for each of the discharge points used in obtaining the oscillograms of Fig. 4, is given with the oscillograms.

(18)

## CHAPTER IV

### RESPONSE OF THE RECEIVER TO CORONA PULSES

(19)

#### A. The Coupling Function

It was shown in Chapter II that the short circuit current at the antenna terminals can be computed when the distribution of the discharge currents and the field produced in the discharge region by a voltage applied to the antenna terminals is known. In Chapter III it was demonstrated that the character of the discharges is such that they can be defined by a current moment  $M$ , and considered as being confined to a region infinitesimally close to the surface of the discharge point. Because of this property, the problem of finding the short circuit response to the discharge is simply that of finding the coupling function  $\frac{E_t^{(1)}}{V_1^{(1)}}$ , which shall hereafter be designated  $\psi$ .

The results of the last chapter were simplified because, for the experimental electrode configurations used, all dimensions were small compared to the wavelengths of the highest frequencies in the discharge, and  $\psi$  could be determined by quasi-static analysis. In considering the response at the antenna terminals to a discharge from some remote point on the aircraft such a simplification is decidedly not possible. In such a situation  $\psi$  is a function of frequency and must be evaluated by the methods of electrodynamics.

For antenna configurations which form natural boundaries in certain simple coordinate systems, the function  $\psi$  can be found by direct solution of the wave equation. The problem is similar to that of finding the impedances of the antennas. Unfortunately, the number of antenna configurations which can be treated in this way is very small. Stratton and Chu<sup>22</sup> and others treat the case of a sphere split on the equatorial plane, and

Stratton and Chu<sup>23</sup> have treated the center driven prolate spheroid. The solution for even these simple cases is very tedious. The expressions for the electric field involve series of the appropriate wave functions which, because of the assumption of an infinitesimal driving gap, diverge. The series can be made to converge by assuming a finite gap and postulating a convenient form for the gap driving voltage. Even with these simplifications, however, computation of actual field values is difficult, and for the more interesting case of the spheroidal antenna the wave functions have not been tabulated. Nevertheless, enough can be learned from the study of the spheroid to justify its consideration, and it will be treated in a later section.

The foregoing discussion makes it clear, however, that a treatment of the problem as a boundary value problem is not promising, and that some other approach is necessary if significant answers are to be obtained. One approach which promises useful results is an experimental determination of  $\psi$  by means of measurements on scale models of actual aircraft. Model techniques are used in many investigations where the complicated boundary conditions render a theoretical treatment of the problem impossible. Examples of the fruitful use of such techniques occur in the determination of radiation patterns and impedances of aircraft antennas.<sup>24</sup> To determine  $\psi$ , models similar to those used for h f antenna impedance measurements could be excited at the antenna terminals and the electric fields at likely discharge points explored by probe measurements. Other methods might be devised which make use of a relationship between  $\psi$  and mutual impedance. This relationship will be discussed later. Since the present investigation is concerned more with outlining principles than with obtaining specific answers for specific aircraft, no such experimental measurements were undertaken.

Although an exact theoretical treatment of practical aircraft antennas is out of the question, approximate theories can be developed for two idealized antennas which correspond closely to antennas of practical

interest. The first of these is the unbalanced open wire transmission line which approximates the fixed wire antenna used in aircraft. The second is the asymmetric cylindrical dipole. This antenna embodies many of the characteristics of the wing-cap and tail-cap antennas which are rapidly becoming the standard high-frequency antennas for modern, high-speed aircraft.

B. The Fixed Wire Antenna

As indicated above, the fixed wire antenna can be closely approximated by a transmission line of the type shown in Fig. 21. Although in actual practice the far end of the antenna may be either shorted or open, we shall assume first that it is open as shown. To find the coupling function  $\psi$ , we make use of simple transmission line theory. The simple theory states that if a voltage  $V_1^{(1)}$  is applied to the antenna terminals the voltage  $V_x$  at point  $x$  is given by

$$V_x = V_1^{(1)} \frac{\cos k(l - x)}{\cos kl} \quad (20)$$

where  $k = \frac{\omega}{c}$  is the propagation constant. Applying elementary electric field theory, we find that the field  $E_x$  on the surface of the antenna wire at point  $x$  is given by

$$E_x = \frac{V_x}{a \ln \frac{2h}{a}} \quad (21)$$

If the discharge actually takes place from some protrusion or from the end of the antenna, the field given in Eq. (21) would be raised by some factor  $\alpha$  to account for field concentration on the discharge point. In this analysis, however, we will ignore any such effect.

The function  $\psi$ , which is the ratio of input voltage to electric field at the discharge point is expressed as

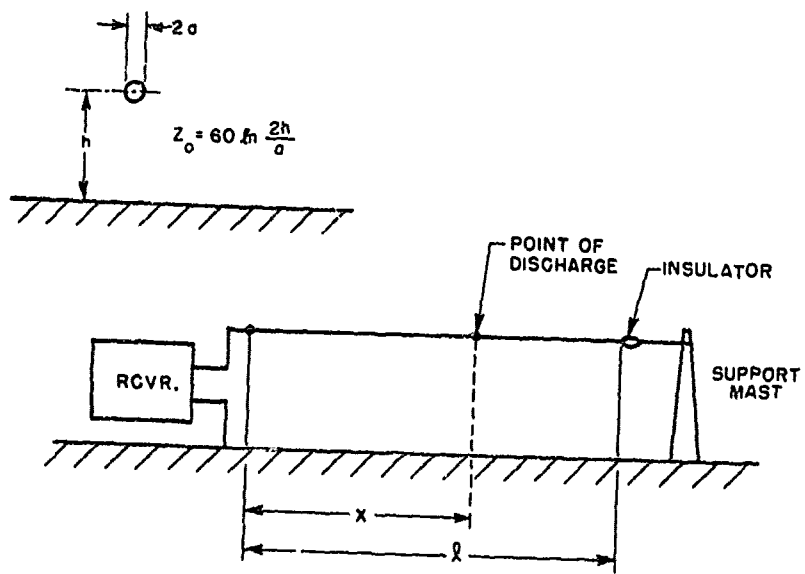


FIG. 21  
 MODEL FOR ANALYSIS OF FIXED WIRE ANTENNA  
 A-591-TR37-211

imated  
 ual  
 shall  
 $\psi$ , we  
 s that  
 at

(20)

ic  
 na wire

(21)

the end  
 factor  
 his  
 ic field

$$\psi = \frac{E_x}{V_1^{(1)}} = \frac{1}{a \ln \frac{2h}{a}} \frac{\cos k(l-x)}{\cos kl}, \quad (22)$$

and the short circuit current at the antenna terminals is

$$I_1^{(2)} = \frac{M}{a \ln \frac{2h}{a}} \frac{\cos k(l-x)}{\cos kl}, \quad (23)$$

where  $M$  is the discharge current moment discussed in Chapter III.

A study of Eq. (23) by means of transmission line theory reveals a significant fact. The expression given in that equation is precisely the expression for a transmission line fed at the point  $x$  by an infinite impedance generator furnishing a current  $I_s$ , where

$$I_s = \frac{M}{a \ln \frac{2h}{a}}. \quad (24)$$

It is therefore evident that the problem of the response of fixed wire antennas to corona pulses reduces to the problem of the transient response of transmission lines to current pulses from an infinite impedance generator. The transient response of transmission lines is treated elsewhere, and will not be discussed in detail here, although some discussion is in order.

The voltage developed at the terminals obviously depends upon the effective impedance connected across the terminals. It also depends upon the position on the antenna of the point at which the discharge takes place, and upon the termination at the far end of the line. If the input is terminated in the characteristic impedance of the line, the arriving current pulse is absorbed, producing a voltage pulse at the terminals of the same form as the discharge pulse. If the discharge occurs at a point other than the far end, the response is actually a pair of pulses. The

(22)

source current  $I_g$  divides to form two waves, one traveling toward the receiver, the other toward the far end where it is reflected and returns to the receiver with a time delay proportional to the additional distance it travels. If the receiver presents an impedance that is high compared to  $Z_0$ , the pulse is successively reflected from the receiver and the far end of the line, forming a sequence of pulses which is gradually damped by the attenuation of the line and the absorption of power in the receiver input impedance.

(23)

When the input is terminated in a reactive element, the picture is much more complicated. The arriving pulse is deformed by the reactance and reflected. Each successive reflection deforms the pulse further. In addition, damping due to line attenuation occurs.

(24)

A comment concerning the equivalent source current  $I_g$  is appropriate. It has been observed in practice that the use of large diameter conductors for fixed wire antennas results in considerable reduction of precipitation static noise. Although the large diameter wire probably results in some reduction of corona from the wire, it seems likely that a more probable explanation for this reduction lies in the expression of Eq. (24).

Equation (24) states that for a discharge of moment  $M$ ,  $I_g$  is inversely proportional to  $a \ln \frac{2h}{a}$ . Since  $\frac{h}{a}$  is large,  $\ln \frac{2h}{a}$  changes very slowly with  $a$ , and  $I_g$  is approximately inversely proportional to  $a$ . The noise power produced by a given discharge is therefore inversely proportional to  $a^2$ .

It is interesting to attempt a quantitative calculation using the formula of Eq. (24). A typical fixed wire installation might be approximated by the dimensions  $a = 1$  mm and  $h = 1$  m. For these dimensions,  $Z_0 \approx 460 \Omega$  and  $\ln \frac{2h}{a} = 7.6$ . From Fig. 4, we obtain for a 0.015 in. tip radius at atmospheric pressure,  $M_{max} = 0.74$  ma cm. Substituting the values into Eq. (24),  $I_{g, max} \approx 1$  ma. Thus, for an antenna with the receiver terminals terminated in  $Z_0$  and the discharge occurring near the center of the antenna, we would expect pulses of voltage having crest magnitudes of 0.23 v. For conditions similar to those hypothesized, Newman and others have

reported oscillographic measurements of pulses with crest magnitudes of 0.2 to 0.5 v.<sup>25</sup>

C. The Prolate Spheroidal Antenna

The previous discussion of the fixed wire antenna does not yield an insight into the nature of the coupling from other parts of the aircraft to the receiver terminals, or how this coupling is affected by the electromagnetic resonances of the aircraft as a whole. The present discussion, although severely limited by the difficulty of working with the prolate spheroidal wave functions, does yield some information on these questions.

In their treatment of the center-driven prolate spheroidal antenna, Chu and Stratton<sup>23</sup> have solved the Maxwell equations in spheroidal coordinates, assuming circular symmetry about the polar axis. They derive expressions for the three field components  $E_\xi$ ,  $E_\eta$  and  $H_\phi$ . The spheroidal coordinates  $\xi$  and  $\eta$  are the same as those defined in Appendix A. Since we are seeking the normal electric field on the surface of a spheroidal conducting body defined by  $\xi = \xi_0$ , we are interested in  $E_\xi$  at  $\xi = \xi_0$ . Due to the high concentration of static field at the tips of the spheroid, corona is much more likely to occur at the tips than elsewhere. We shall therefore consider only this case.

At the tips of the spheroid, where  $\xi = \xi_0$  and  $\eta = 1$ , the expression for  $E_\xi$  given by Chu and Stratton reduces to

$$E_{p.o.} = E_\xi = \frac{1}{j\omega\epsilon} \sum_{l=0}^{\infty} A_l \text{Re}_{1l}^{(4)}(g, \xi_0) \frac{d}{dn} [(1-n^2) \text{Se}_{1l}^{(1)}(g, \eta)]_{\eta=1}, \quad \eta=1 \quad (25)$$

where  $\text{Re}_{1l}^{(4)}(g, \xi)$  and  $\text{Se}_{1l}^{(1)}(g, \eta)$  are respectively the radial and angular spheroidal wave functions defined by Chu and Stratton in their paper. The variable  $g$  is equal to  $k \frac{d}{2}$ , where  $k$  is the propagation constant and  $d$  is the distance between foci of the spheroid. It can be shown that

$$\frac{d}{dn} [(1 - \eta^2) \text{Se}_{1i}^{(1)}(g, \eta)]_{\eta=1} = - [\text{Se}_{1i}^{(1)}(g, \eta)]_{\eta=1} .$$

The expression for the normal electric field at the tips of the spheroid therefore becomes

$$E_{\text{pole}} = \frac{-1}{j\omega\epsilon} \sum_{i=0}^{\infty} A_i \text{Re}_{1i}^{(4)}(g, \xi_0) \text{Se}_{1i}^{(1)}(g, 1) . \quad (26)$$

The coefficients  $A_i$  are determined by the boundary conditions on the driving field. We are applying a voltage  $V_1^{(1)}$  across a gap at the equator, which is the same boundary condition applied by Chu and Stratton, and the coefficients  $A_i$  are therefore identical to those of Chu and Stratton. Substituting these coefficients into Eq. (26), we have

$$\frac{E_{\text{pole}}}{V_1^{(1)}} = \frac{2}{d} \sum_{i=0}^{\infty} \frac{\text{Re}_{1i}^{(4)}(g, \xi_0) \text{Se}_{1i}^{(1)}(g, 1) \text{Se}_{1i}^{(1)}(g, 0)}{N_i \frac{d}{d\xi_0} (\xi_0^2 - 1) \text{Re}_{1i}^{(4)}(g, \xi_0)} , \quad (27)$$

where  $N_i$  is a normalizing coefficient defined by Chu and Stratton and the prime on the summation indicates a sum over even values of  $l$  only. The coupling function  $\psi$  is given by

$$\psi = \alpha \frac{E_{\text{pole}}}{V_1^{(1)}} \quad (28)$$

where  $\alpha$  is a concentration factor relating the field at the tip of the discharge point, which is probably a protrusion such as a rivet head, to the gross field  $E_{\text{pole}}$  at the pole of the spheroidal antenna. The expression for  $\psi$  is similar to the expression for input admittance found by Chu and Stratton. It is possible to define modes of coupling similar to their modes of admittance.

Comparing the function  $\psi$  to the input admittance functions  $Y_i$ , we find that for corresponding terms

$$\psi_{i+1} = \alpha \left\{ -j \frac{60}{k \frac{d^2}{4} (\xi_0^2 - 1)} \frac{Se_{1i}^{(1)}(g, 1)}{Se_{1i}^{(1)}(g, 0)} \right\} Y_{i+1} \quad (29)$$

In terms of the more commonly used wave functions discussed by Stratton, Morse, Chu and Hutner,<sup>26</sup> and by Flammer,<sup>27</sup> Eq. (29) becomes

$$\psi_{i+1} = \alpha \left\{ -j \frac{60}{k \frac{d^2}{4} (\xi_0^2 - 1)} \frac{[(1 - \eta^2)^{-\frac{1}{2}} S_{1i}^{(1)}(g, \eta)]_{\eta=1}}{S_{1i}^{(1)}(g, 0)} \right\} Y_{i+1} \quad (30)$$

The function

$$\gamma_{i+1} = \frac{[(1 - \eta^2)^{-\frac{1}{2}} S_{1i}^{(1)}(g, \eta)]_{\eta=1}}{S_{1i}^{(1)}(g, 0)} \quad (31)$$

which relates  $\psi_{i+1}$  to  $Y_{i+1}$  can be readily evaluated from coefficients tabulated by Flammer. For the first mode,  $\gamma_1$ , as a function of the electrical length of the spheroid, is given by the graph of Fig. 22. In terms of the geometrical quantities for the spheroid, shown in Fig. 22,  $\psi_1$  becomes

$$\psi_1 = -j \frac{\alpha}{L} \left(\frac{L}{D}\right)^2 \frac{60}{\pi \frac{L}{\lambda}} \gamma_1 Y_1 \quad (32)$$

Expressions similar to Eq. (32) can be written for the higher coupling modes. In this discussion, however, we will limit our attention to  $\psi_1$ .

Chu and Stratton show that the admittance near the frequency which makes  $\frac{L}{\lambda} = \frac{1}{2}$  is dominated by the mode admittance  $Y_1$ , while the admittance

we

(29)

ton,

(30)

(31)

s

In

22,

(32)

ig

b<sub>1</sub>.

ich

mce

11-37

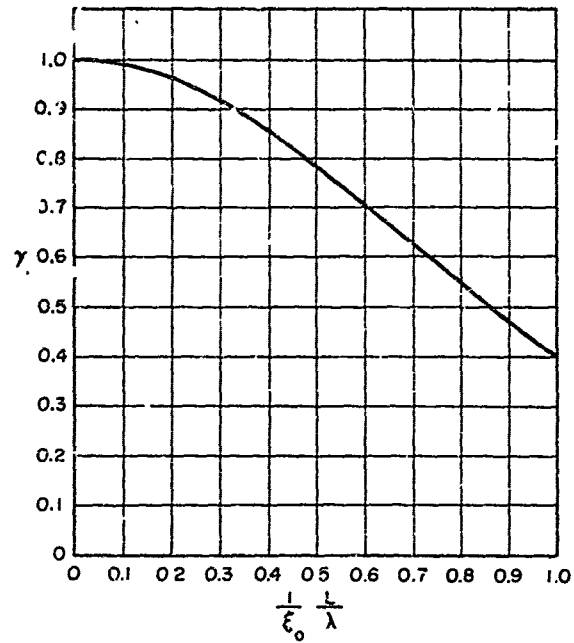
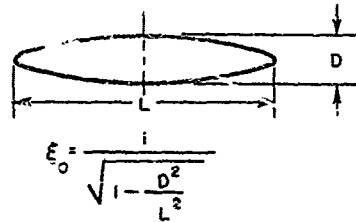


FIG. 22

THE FUNCTION  $\gamma$ , WHICH RELATES  $\psi_1$  AND  $\gamma_1$

A-591-TR37-234

near  $\frac{L}{\lambda} = \frac{z}{2}$  is dominated by  $Y_3$ , etc. This is particularly true for slender spheroids. The same can be said for the coupling function  $\psi$ . For the frequency components of the discharge near that frequency which makes the electrical length of the spheroid  $\frac{\lambda}{2}$ , the coupling is principally determined by  $\psi_1$ .

We can learn much concerning the effect of structure resonances on the coupling of noise from the discharge by examining  $\psi_1$  for a range of values of  $\frac{L}{\lambda}$  between zero and unity. Figures 23 and 24 show the components of the function  $\frac{L}{a} \psi_1$  versus electrical length for two values of  $\frac{L}{D}$ . These curves indicate a peak in the terminal short circuit current near the  $\frac{L}{2}$  point. The peak is more pronounced for the more slender antenna. A similar though less pronounced peak would occur near  $\frac{3\lambda}{2}$  point due to  $\psi_3$ .

Certain other aspects of the coupling function given by Eq. (30) are of interest. The equation indicates a general drop-off of coupling with increasing frequency. In addition, the curves of Fig. 10 showing typical pulse spectra indicate a pronounced drop in noise produced by the discharges at frequencies above the h-f range. The combination of these effects explains adequately why precipitation static is not troublesome at v h-f and u-h f frequencies.

Another effect that is apparent from a study of the ordinates of the curves of Figs. 23 and 24 is the increase of coupling from discharges at the extremities of slender bodies. A discharge pulse at the tip of the spheroid of  $\frac{L}{D} = 70.7$  produces a terminal current approximately 100 times as high as the same discharge pulse would produce at the terminals of the spheroid for which  $\frac{L}{D} = 7.07$ . Thus, we would expect the discharges from the end of a slender trailing wire to couple quite strongly into the receiver.

One further consequence of Eq. (32) is worthy of note. We observe that  $\psi$  is inversely proportional to  $L$ . Therefore, other things being equal, distant discharges couple less strongly into the receiver. However, this last conclusion must be considered in the light of the effects previously discussed.

slender  
the  
kes the  
deter.  
es on  
ge of  
ponents  
These  
the  $\frac{L}{2}$   
A  
to  $\psi_3$ .  
(0) are  
with  
ypical  
is-  
se ef-  
me at  
of the  
es at  
the  
times  
of the  
from  
erve  
ig  
however,  
previ  
91 37

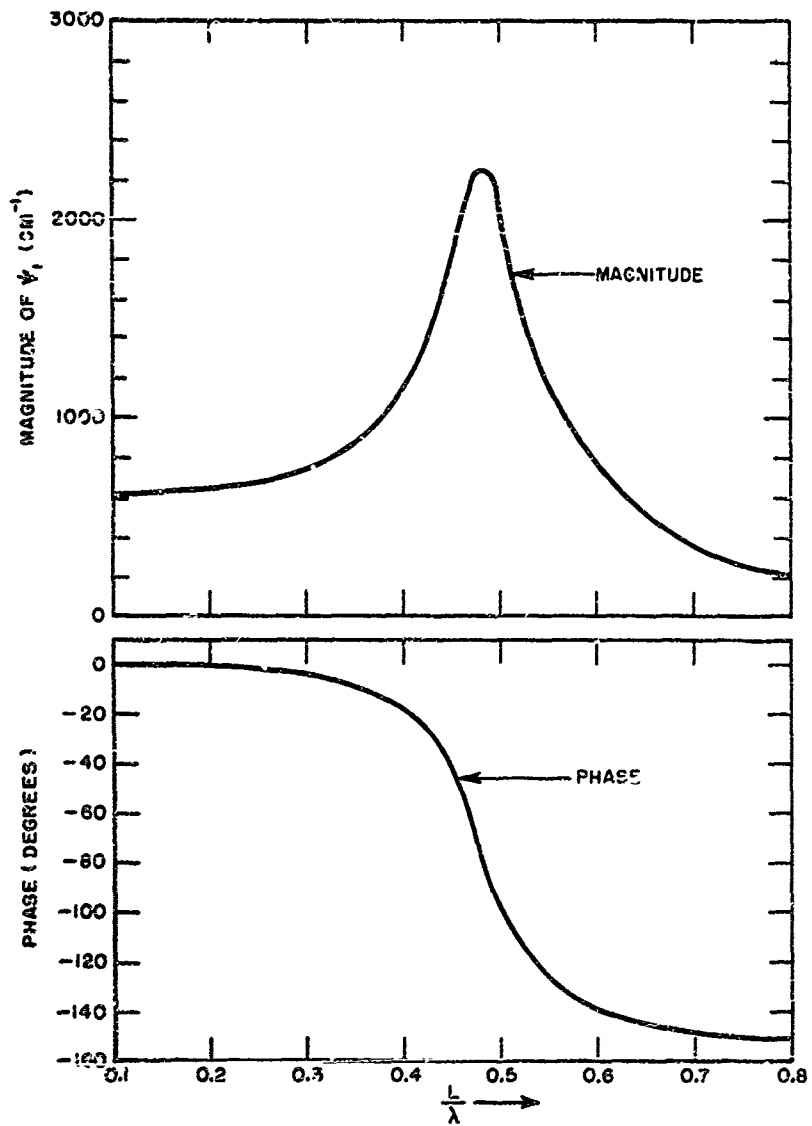


FIG. 23  
COUPLING FUNCTION  $\psi_1$  FOR SPHEROID OF  $\frac{L}{D} = 70.7$   
A-591-TR37-216

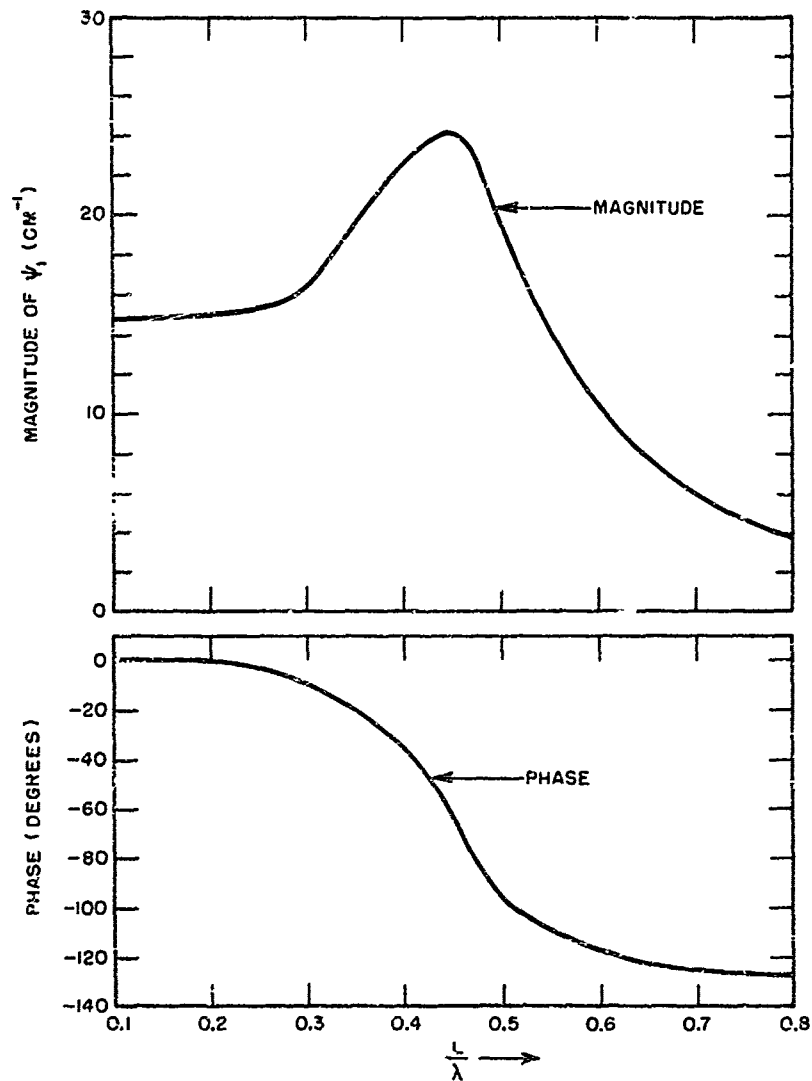


FIG. 24  
 COUPLING FUNCTION  $\psi_1$  FOR SPHEROID OF  $\frac{L}{D} = 7.05$   
 A-591-TR37-217

## CHAPTER V

### THE CYLINDRICAL DIPOLE ANTENNA

#### A. General Considerations

Cylindrical dipole antennas are of interest for several reasons. These antennas have been subjected to much analysis and as a consequence their impedance characteristics are well known. As we shall see later, the coupling function  $\psi$  can be derived from the antenna impedance, so an accurate knowledge of the impedance is of value. Furthermore, the results from the analysis of the cylindrical dipole can be used to corroborate and extend the conclusions reached in the treatment of the prolate spheroid.

Another consideration of some importance is that methods have been devised for treating the asymmetric cylindrical dipole. This configuration is the nearest approximation to wing-cap and tail-cap antennas, in common use on high speed aircraft, which can be handled with reasonable ease analytically.

#### B. Relation of Coupling Function to Antenna Impedance

Let us consider the case of coupling from a corona pulse at the tip of the antenna to the antenna terminals. This situation is illustrated by the diagram of Fig. 25 in which, for convenience of analysis the discharge is assumed to take place between the tip of the antenna itself and a very small electrode spaced a distance  $\delta$  from the tip. The entire configuration can be considered as a four terminal network in which the antenna terminals are terminal pair 1, and the tip of the antenna together with the small electrode is terminal pair 2.

Now let us apply voltage  $V_1^{(1)}$  to terminals 1. It is clear that the open circuit voltage at terminals 2 is given by

ons.  
quence  
later,  
so an  
results  
rate and  
eroid.  
been  
figuration  
n high

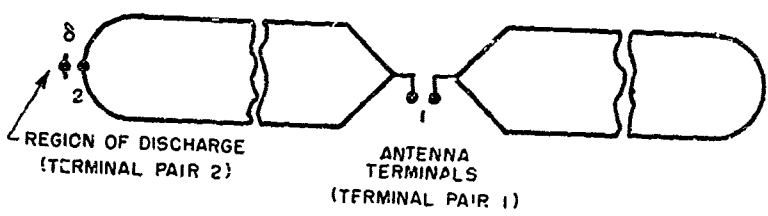


FIG. 25  
ILLUSTRATING APPLICATION OF IMPEDANCE  
ANALYSIS TO COUPLING FUNCTION  
FOR CYLINDRICAL DIPOLE

A-591-TR37-207

e tip  
ated by  
ischarge  
a very  
uration  
erminals  
all  
the

$$V_{20} = I_1^{(1)} Z_{12} = \frac{V_1^{(1)}}{Z_{11}} Z_{12} . \quad (33)$$

It is also clear that the voltage  $V_{20}$  can be expressed as

$$V_{20} = E_t \delta . \quad (34)$$

or

$$E_t \delta = V_1^{(1)} \frac{Z_{12}}{Z_{11}} . \quad (35)$$

Rearranging Eq. (35), we obtain

$$\psi = \frac{E_t}{V_1^{(1)}} = \frac{1}{\delta} \frac{Z_{12}}{Z_{11}} . \quad (36)$$

It is therefore possible to find the functional behavior of  $\psi$  by finding the functional behavior of  $\frac{Z_{12}}{Z_{11}}$ . In finding  $\frac{Z_{12}}{Z_{11}}$  we can make use of the methods of function theory and many of the general theorems of network analysis.

Knowing the functional behavior of  $\psi$  we can find its value everywhere by determining its value at one frequency. The value of  $\psi$  at zero frequency can be determined by simple experiments using electrolytic tank techniques or charge separation measurements, or it can be found analytically by means of simple mathematical models such as those discussed in Appendix A.

It is shown in the treatment of electrical networks<sup>28</sup> that physical impedances and admittances such as  $Z_{11}$  and  $Z_{12}$  are either rational algebraic or meromorphic functions with isolated singularities, all of which occur in the left half of the  $p$ -plane (where  $p$  is the complex frequency variable  $p = \sigma + j\omega$ ), at  $p = 0$  or at  $p = \infty$ . It is further shown that the functional behavior of such impedance functions is completely

(33) determined if we specify the positions of the singular points. Furthermore, it is demonstrated that all singularities which occur in the finite  $p$ -plane occur either as conjugate pairs or on the  $\sigma$  axis. Another fact which is demonstrated in network analysis is that the mutual impedance  $Z_{12}$  may have the same poles as the self impedance  $Z_{11}$ , but cannot have poles which  $Z_{11}$  does not have.

(34) Let us now examine the antenna impedances  $Z_{11}$  and  $Z_{12}$  in view of the foregoing facts. Because of the distributed character of antennas it is evident that their impedances must be represented by meromorphic rather than algebraic functions. As will be shown later, however, it is possible to find rational functions which approximate the antenna impedances very closely over the range of frequencies with which we are concerned. Another observation which can be made immediately is that  $Z_{11}$  has a pole at zero, since at very low frequencies the dipole antenna becomes a static capacitor. The self impedance  $Z_{11}$  can therefore be expressed as

$$Z_{11} = K_{11} \frac{(\text{zeros}_{11})}{p (\text{poles}_{11})} \quad (37)$$

where  $(\text{zeros}_{11})$  represents the product of all the factors  $(p - p_i)$  which indicate the zeros of the function, and  $(\text{poles}_{11})$  represents the product of similar factors which indicate the poles which occur at points other than zero.

Now let us consider the singularities of the mutual impedance  $Z_{12}$ . Physical reasoning can be used to demonstrate that for such a simple physical configuration as the linear dipole  $Z_{12}$  has exactly the same poles as  $Z_{11}$ . The impedance  $Z_{12}$  is given by the open circuit voltage at terminals 2 for unit current into terminals 1. Suppose now that unit current is injected into terminals 1 at a value of complex frequency for which a pole occurs. For such a condition infinite voltage is produced at the terminals, and therefore infinite fields must exist on the antenna in the vicinity of the terminals. The field equations for the antenna indicate

that an infinite field cannot exist at one point of the antenna without infinite fields at all points. Therefore, the field at the tip of the antenna where terminals 2 are located is infinite, and consequently  $Z_{12}$  is infinite. Similar reasoning suggests strongly that unit current flowing into terminals 1 at any frequency will produce a finite voltage at the tip. This means that all the zeros of  $Z_{12}$  occur at infinity.

The conception of the impedance functions suggested in the foregoing paragraphs is reinforced when we consider the antenna as a nonuniform dissipative transmission line. For a uniform, open-ended dissipative line of length  $l$ , it can easily be shown that

$$Z_{11} = Z_0 \coth_1 kl = Z_0 \frac{\cosh kl}{\sinh kl} \quad (38)$$

whereas

$$Z_{12} = \frac{2Z_0}{\sinh kl} \quad (39)$$

The poles of  $Z_{11}$  and  $Z_{12}$  are the same, and occur at the roots of  $\sinh kl$ . The zeros of  $Z_{11}$ , on the other hand, occur at the roots of  $\cosh kl$  while the zeros of  $Z_{12}$  all occur at infinity. We will therefore assume, as suggested, that for the cylindrical dipole  $Z_{12}$  is of the form

$$Z_{12} = K_{12} \frac{1}{p(\text{poles}_{11})} \quad (40)$$

Although we have not established this relationship with anything approaching mathematical rigor, it is undoubtedly true and could be established by a more thorough analysis.

Combining Eqs. (37) and (40), we obtain

$$\frac{Z_{12}}{Z_{11}} = \frac{K_{12} \frac{1}{p(\text{poles}_{11})}}{K_{11} \frac{1}{p(\text{poles}_{11})}} = \frac{K_{12}}{K_{11}} \frac{1}{(\text{zeros}_{11})} \quad (41)$$

urther  
finite  
fact  
ance  
have  
  
of the  
it is  
rather  
possible  
s very  
Another  
zero  
capacitor.  
  
(37)  
  
which  
oduct  
ther  
  
Z<sub>12</sub>  
e  
ne poles  
termi  
rrent  
ich a  
he  
n the  
cate  
  
91 37

hou  
the  
Z,  
ag  
go  
m  
e  
  
(  
  
1  
il  
  
(4  
  
ab  
  
(4

Equation (41) shows that the poles of  $\psi$  coincide with the zeros of the terminal impedance. They therefore coincide with the poles of the terminal admittance. The zeros of  $\psi$  all occur at infinity. Such a description of  $\psi$  is compatible with the behavior we found in the analysis of the prolate spheroid. There is was found that  $\psi$  had peaks corresponding to the peaks of the admittance function, that it had a finite value at zero frequency and that it dropped off with increasing frequency.

C. The Symmetric Dipole

The first specific case which we treat is the center-driven dipole. Perhaps the most accurate impedance data available is that derived by Tai using a variational method.<sup>29</sup> The thickest antenna treated by Tai is for a thickness factor  $\Omega = 10$ , which corresponds to a length to diameter ratio of approximately 75. The data we obtain for this antenna should therefore correspond quite closely to the data for the spheroid of  $\frac{L}{D} = 70.7$ .

The solid curves of Fig. 26 show the impedance calculated by Tai. From the pronounced resonances it is apparent that the poles and zeros of the impedance function lie quite close to the real frequency axis. For such a function it is known that the behavior on the real frequency axis is principally determined by the singularities near the frequency under consideration. The effect of distant singularities is small and can be neglected. We therefore should expect to approximate the impedance function quite closely in the frequency range of interest by a rational function which includes only the singularities lying in that range.

Ignoring the behavior of the function at values of  $\omega$  greater than those included in Fig. 26, it is apparent that the function is characterized by five poles and four zeros arranged approximately as shown in Fig. 27 where we have normalized the frequency variables as shown in the figure.

The coordinates of the poles in the  $p$  plane were found by considering the behavior of the resistance curve in the vicinity of the resistance

e  
 rmi  
 ption  
 pro  
 the  
 fre  
  
 le  
 Tai  
 for  
 ratio  
 efore  
  
 s of  
 or  
 xis  
 er  
 be  
  
 al  
  
 n  
 ter  
  
 the  
  
 ering  
 e  
 1 37

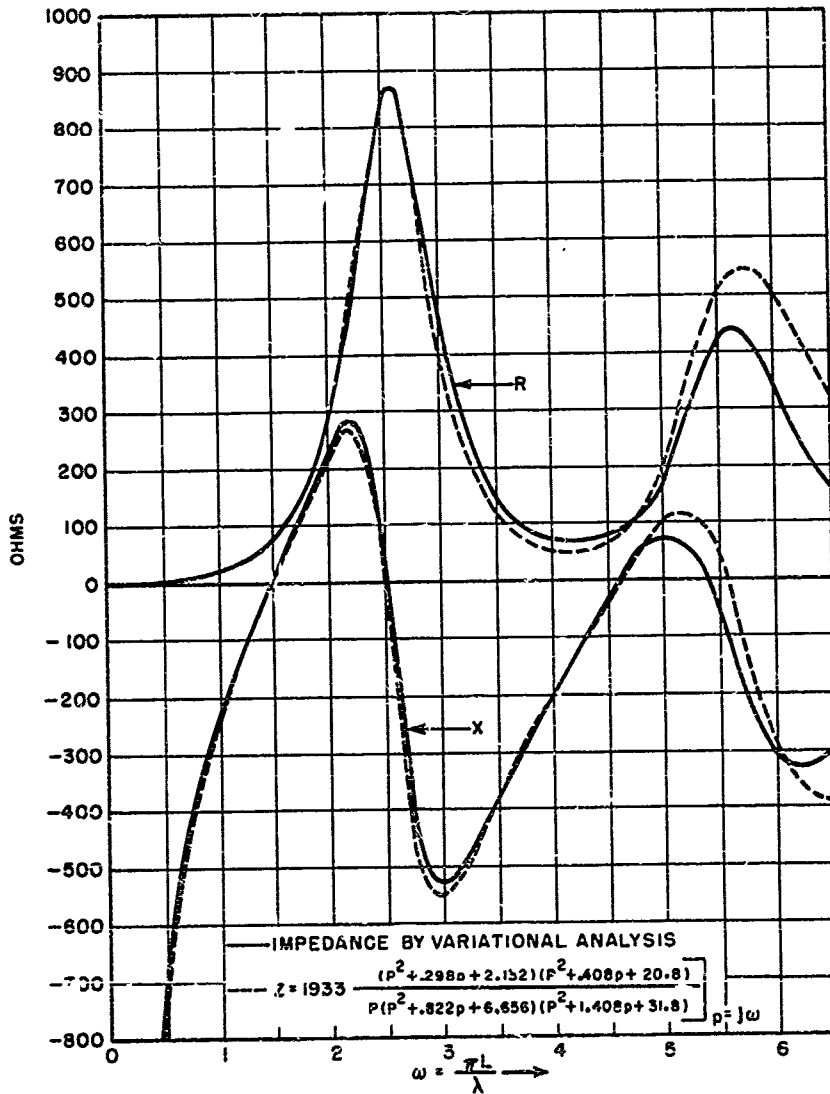


FIG. 26  
 IMPEDANCE OF CYLINDRICAL DIPOLE  
 FOR THICKNESS FACTOR  $\Omega=10$ , COMPARED  
 WITH RATIONAL FUNCTION APPROXIMATION

A-591-TR37-226

POLES:

$P_0 = 0$   
 $P_2 = -0.411 + j2.545$   
 $P_4 = -0.704 + j5.59$

ZEROS:

$P_1 = -0.149 + j1.453$   
 $P_3 = -0.203 + j4.56$

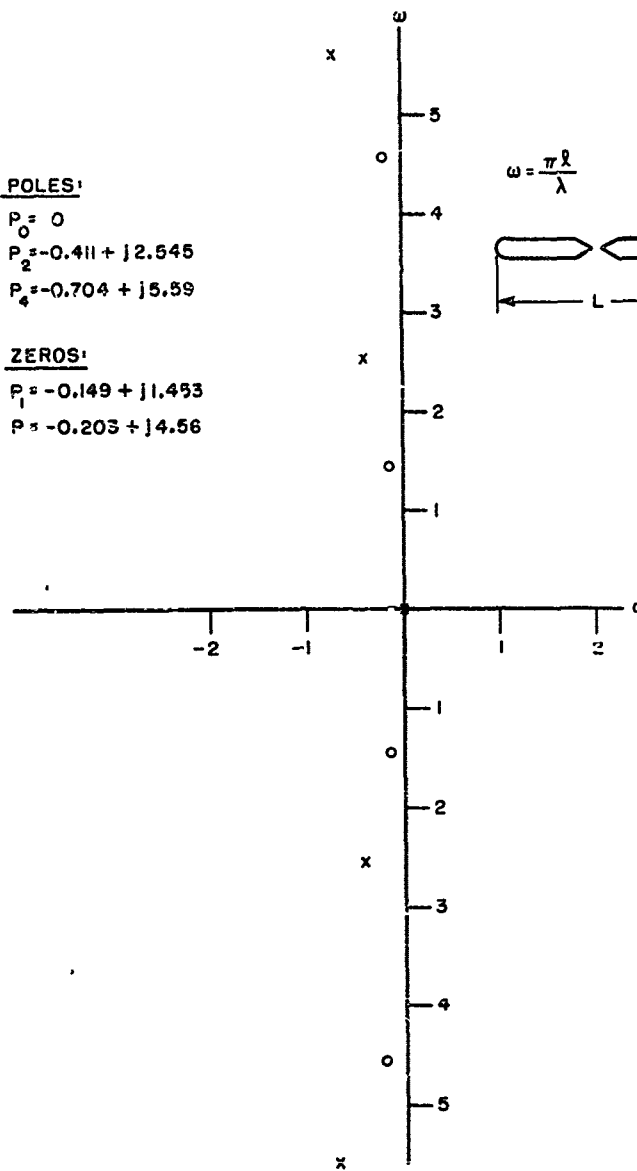


FIG. 27

POSITIONS OF SINGULARITIES CHARACTERIZING  $Z_{11}$

A-591-TR37-208

peaks and ignoring the effect of interaction between the poles. The coordinates of the zeros were found by a similar consideration of the conductance near the conductance peaks. It is evident from the close approximation obtained that the interaction between the singularities actually is small. A second approximation could be obtained by including interaction effects as determined from the first approximation. This is unnecessary, however, since we are not concerned here with a high order of numerical accuracy. Besides, the approximation at the higher frequencies could not be greatly improved without including higher order singularities.

As shown in the previous section, the response function of  $\psi$  can be expressed as

$$\psi = K_{\psi} \frac{1}{(\text{zeros}_{11})} \quad (42)$$

where  $K_{\psi}$  may be determined by static techniques. The functional behavior of the symmetric dipole can therefore be readily expressed as the reciprocal of the product of the zero factors shown in Fig. 27, that is,

$$\psi_{(j\omega)} = K_{\psi} \frac{1}{(j\omega - p_1)(j\omega - \bar{p}_1)(j\omega - p_3)(j\omega - \bar{p}_3)} \quad (43)$$

The function  $\frac{\psi(j\omega)}{K_{\psi}}$  thus obtained is plotted in Fig. 28. The similarity of this function to the coupling function obtained for the prolate spheroid is evident, and corroborates the conclusions reached in that discussion.

#### D. Effect of Terminating Impedance

The impedance in which the antenna is terminated has a pronounced effect upon the noise voltage at the receiver. We shall here consider two possible values of terminating impedance. These are: (1) a very small resistance, and (2) a very large resistance.

he  
 he con-  
 approxi-  
 ally is  
 action  
 ssary,  
 ical  
 ld not

in be

(42)

avior  
 cipro

(43)

ity of  
 roid  
 ion.

ed  
 er two  
 all

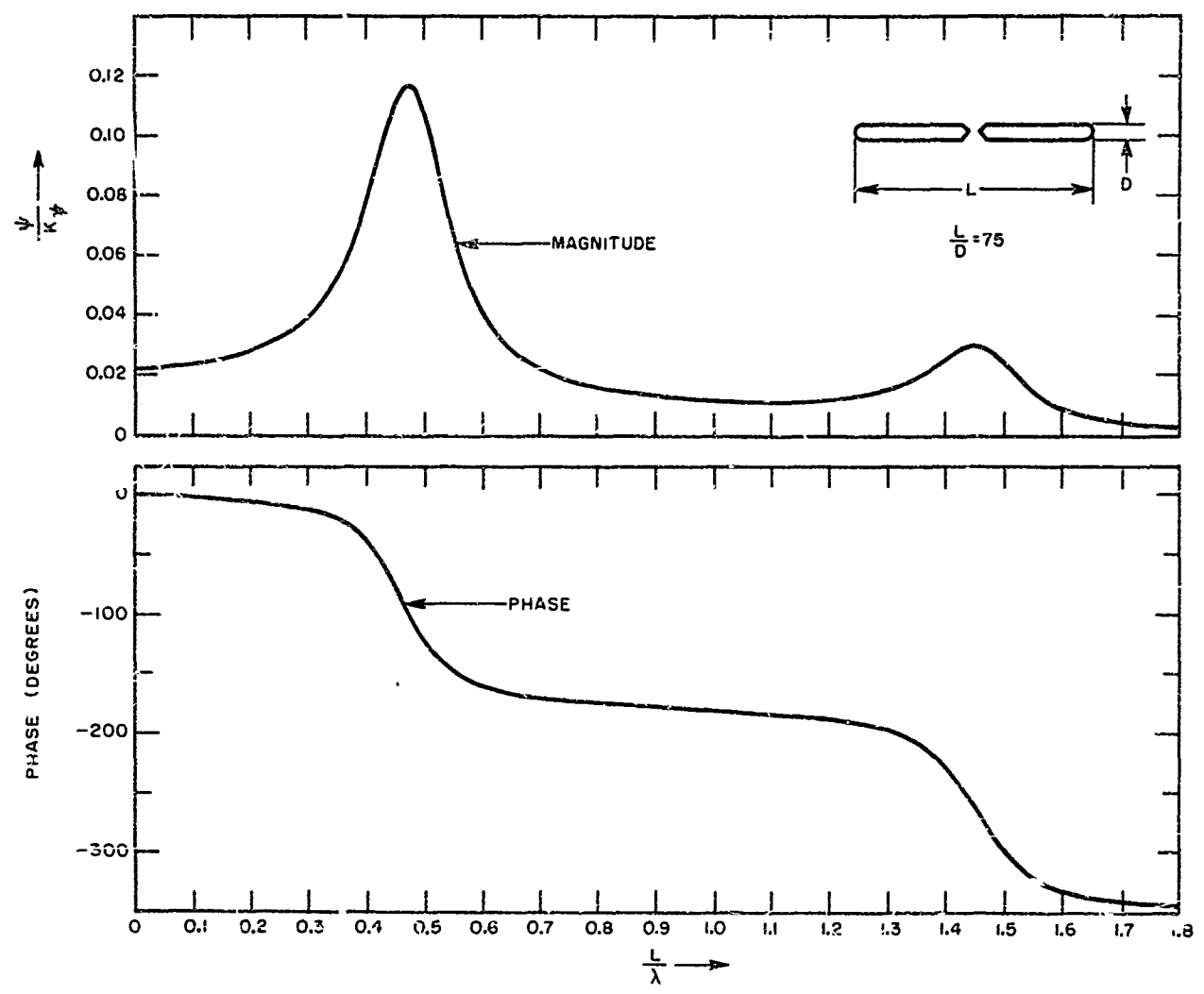


FIG. 28  
 BEHAVIOR OF COUPLING FUNCTION FOR SYMMETRIC DIPOLE

9-591-TR37-225

With a very small resistance as the terminating impedance, the load current and consequently the load voltage is inappreciably different from the short circuit current. If we designate the terminating resistor by  $R_t$ , then the terminal voltage, expressed as a function of  $p$ , is given by

$$V = R_t M(p) \psi(p) . \quad (44)$$

The magnitude of  $V$  is the product of the magnitudes of  $M$  and  $\psi$ . The magnitude of  $M$  as a function of frequency is given in Fig. 10, while the magnitude of  $\psi$  as a function of normalized frequency is given by Fig. 28. For an antenna 30 m long at sea level pressure the behavior of the terminal voltage as a function of frequency is given in Fig. 29.

If the impedance across the antenna terminals is very high, the terminal voltage is essentially the open-circuit terminal voltage. The behavior of the open-circuit voltage with frequency is also readily obtained. We know by Thevenin's theorem that the open-circuit voltage is given by the product of the short-circuit current and the impedance seen looking into the antenna terminals. That is,

$$V_{oc} = M(p) \psi(p) Z_{11}(p) . \quad (45)$$

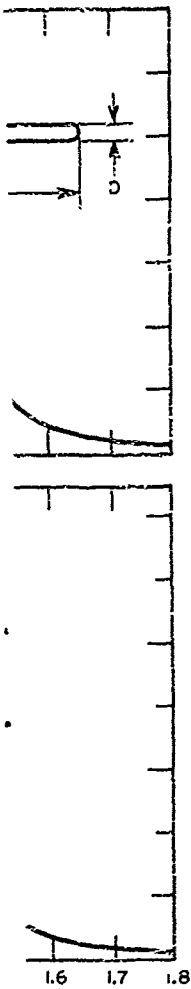
Replacing  $\psi(p)$  and  $Z_{11}(p)$  by their values as determined in the previous analysis we find that

$$V_{oc} = M(p) K_\psi \frac{1}{(\text{zeros}_{11})} K_{11} \frac{(\text{zeros}_{11})}{p (\text{poles}_{11})} . \quad (46)$$

or

$$V_{oc} = K_\psi K_{11} M(p) \frac{1}{p (\text{poles}_{11})} .$$

The functional behavior of the open circuit voltage can be computed from data previously given. For an antenna 30 m in length at sea level pressure the behavior of  $V_{oc}$  versus frequency is given in Fig. 30.



load  
nt from  
or by  
ven by  
(44)

the magni  
magni  
. For  
inal  
e termi-  
behavior  
. We  
y the  
into  
(45)

ous  
(46)

from  
essure  
1 37

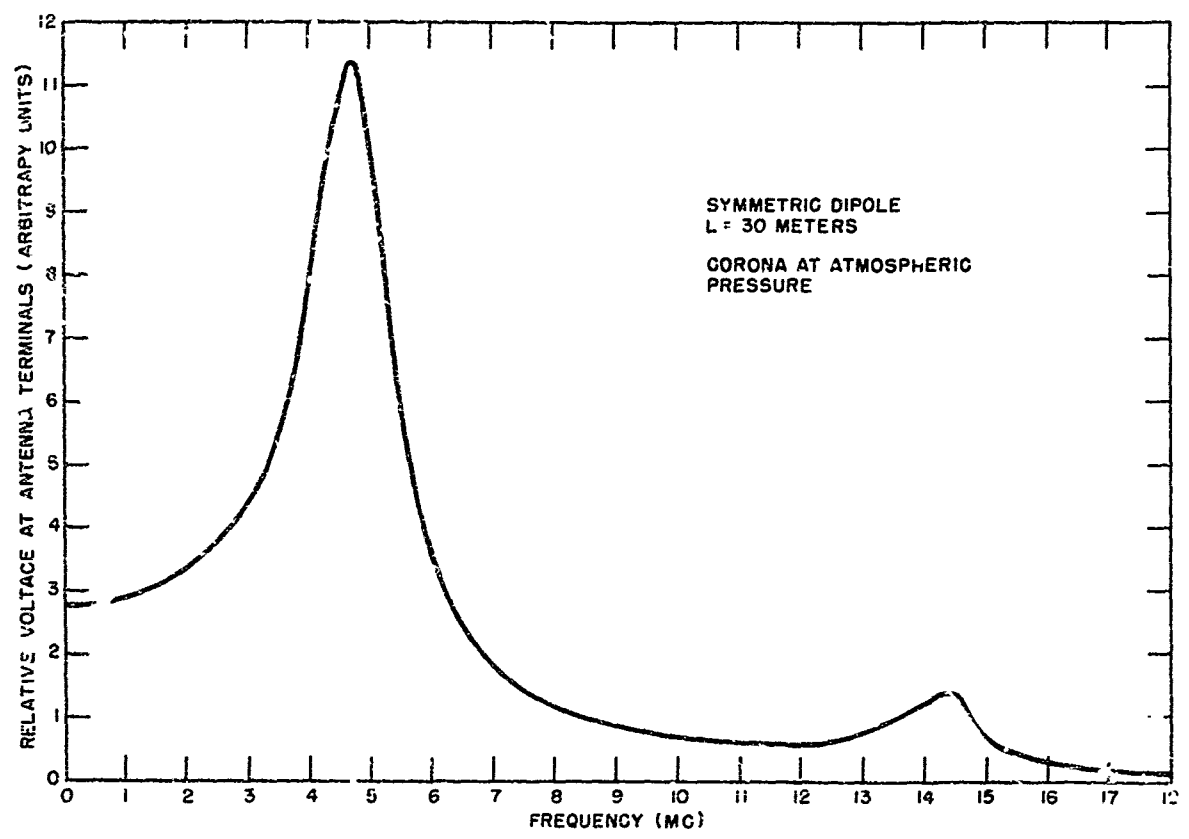


FIG. 29  
TERMINAL VOLTAGE VS FREQUENCY FOR SMALL RESISTANCE TERMINATION  
A-391-TR37-2.9

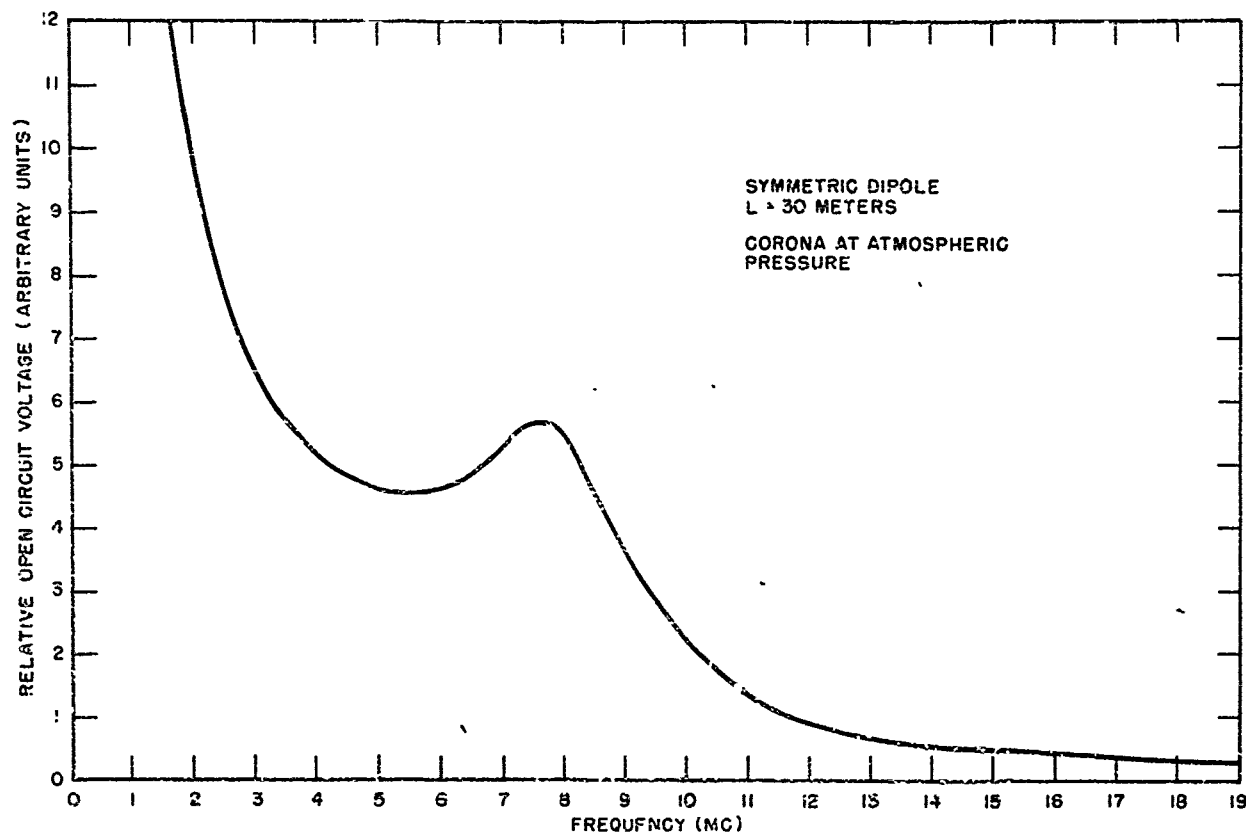


FIG. 30  
 OPEN CIRCUIT TERMINAL VOLTAGE VS. FREQUENCY

B-591-TR37-218

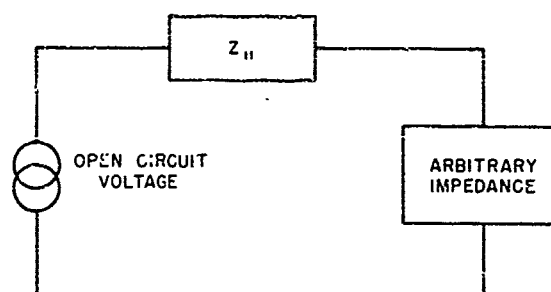
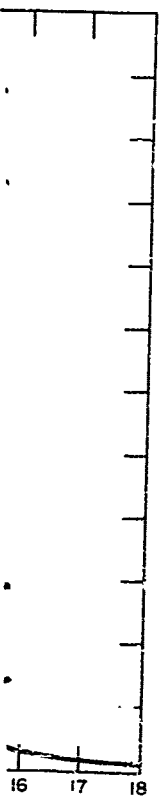


FIG. 31  
 THEVENIN'S EQUIVALENT CIRCUIT FOR  
 OBTAINING ANTENNA RESPONSE WITH  
 ARBITRARY TERMINATING IMPEDANCE

A-591-TR37-240



A-591-TR37-219

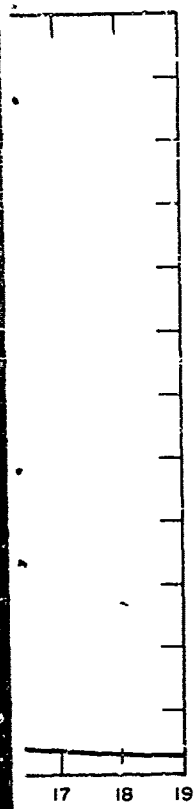
The noise at the receiver terminals for other types of terminating impedance can be readily computed from the data given by the use of a Thevenin's equivalent circuit as shown in Fig. 31.

#### E. The Asymmetric Dipole

The most interesting antenna configuration which can be discussed theoretically is the asymmetric dipole. It was pointed out earlier that this antenna is similar in several respects to the wing-cap and tail-cap antennas which are in common use.

As discussed by King<sup>30</sup> and others, the asymmetric dipole impedance is given approximately as the mean value of the impedances of two symmetric dipoles one of which corresponds to the short leg and the other to the long leg of the asymmetric antenna. Although this mean value formula is not correct to a high order of quantitative accuracy, it is sufficiently close for the purposes of the present discussion. We consider here an asymmetric antenna for which the low-frequency reactance of the short leg is 10 times that of the long leg. The ratio of the lengths of the legs will be approximately 10, although the thickness factor  $\Omega = 10$  used in computing the impedance of the long leg leads to a diameter which would make the short leg very stubby. Since none of the impedance formulas presently available give accurate answers for very thick antennas, it is impossible to compute with any accuracy the length of the short leg.

The impedance of the symmetric antenna corresponding to the long element is of the same form as the symmetric dipole discussed earlier. We will again assume for the purpose of discussion that the impedance is correctly given by the rational function approximation shown in Fig. 26. The short element of the asymmetric dipole will be short compared to the wavelength of the highest frequencies with which we are concerned. We can therefore to a good approximation represent the impedance of the short element as that of a lumped capacitance. It is clear from the foregoing



B-591-TR37-218

that if we denote the impedances of the corresponding long and short symmetric antennas by  $Z_\alpha$  and  $Z_\beta$  respectively, then

$$Z_\alpha = K_\alpha \frac{(\text{zeros}_\alpha)}{p (\text{poles}_\alpha)}, \tag{47}$$

$$Z_\beta = K_\beta \frac{1}{p}$$

where  $(\text{zeros}_\alpha)$  and  $(\text{poles}_\alpha)$  denote the singularities of  $Z_\alpha$ .

If we now let the terminal impedance of the asymmetric antenna be represented by  $Z_{11A}$ , then from the mean-value formula we have

$$Z_{11A} = \frac{1}{2} K_\beta \frac{1}{p} + K_\alpha \frac{(\text{zeros}_\alpha)}{p (\text{poles}_\alpha)}. \tag{48}$$

The asymmetric dipole impedance computed from Eq. (48) is shown in Fig.32. It is evident that for the asymmetric dipole we shall have different coupling functions  $\psi$  for discharges occurring at the different ends of the antenna.

F. Coupling from Discharge at End of Short Element

Let us consider first the case of a discharge at the end of the short element. The condition that the short element be of length small compared to the wavelength of the highest frequencies considered means that the mutual impedance between the antenna terminals and the end of the short element can be represented as simply a mutual capacitance. Thus,

$$Z_{12\beta} = \frac{K_{12\beta}}{p}. \tag{49}$$

The functional behavior of  $\psi_\beta$  is given by the ratio  $\frac{Z_{12\beta}}{Z_{11A}}$ . When this ratio is evaluated, it is apparent that the pole at  $p = 0$  is removed and  $\psi_\beta$  can be expressed as

sym.

(47)

be

(48)

ig. 32.

of the

short

mpared

he

ort

(49)

s ratio

g can

31 37

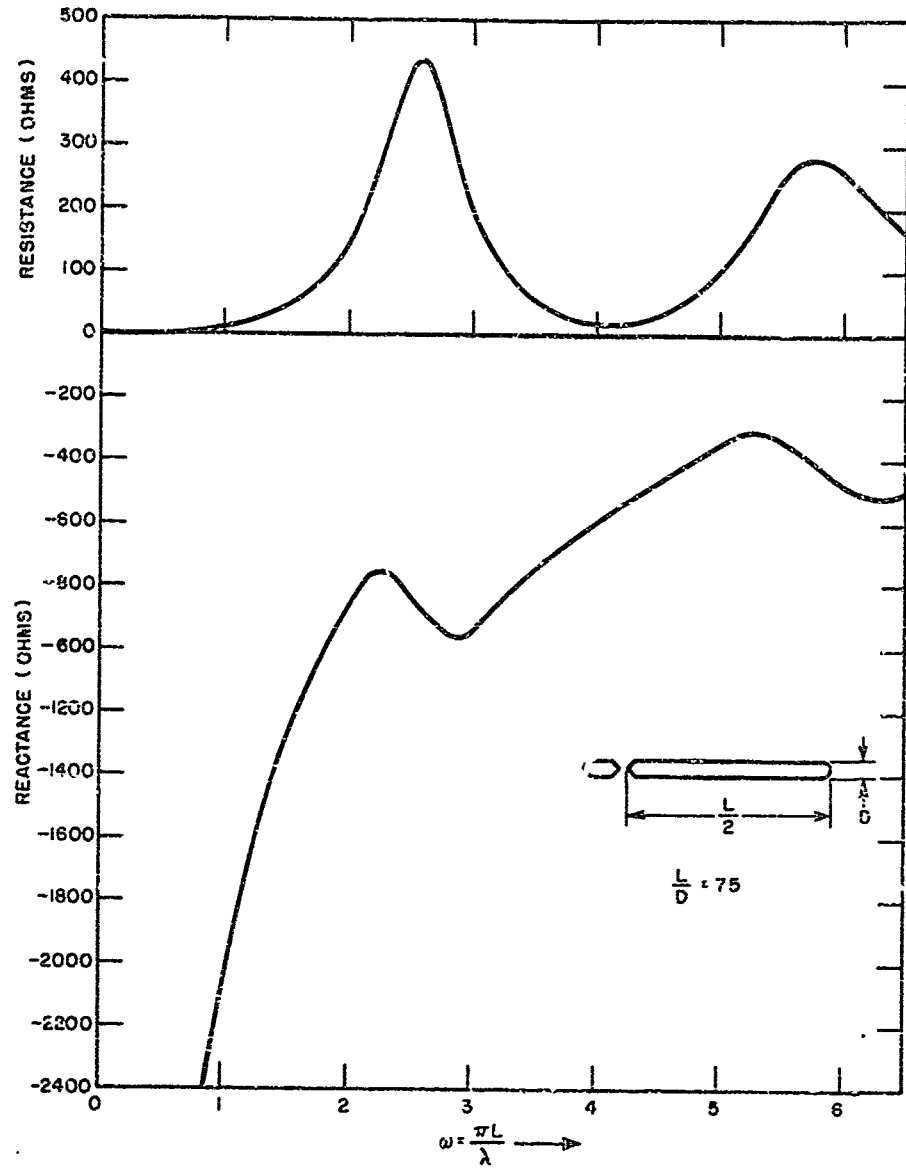


FIG. 32

ASYMMETRIC DIPOLE IMPEDANCE  
(FROM RATIONAL FUNCTION APPROX. AND MEAN VALUE FORMULA)

A-221-TR37-257

$$\psi_{\beta} = A_{\beta} \frac{1}{1 + \frac{K_{\alpha} \left( \frac{\text{zeros}_{\alpha}}{\text{poles}_{\alpha}} \right)}{K_{\beta}}} \quad (50)$$

where several constants have been absorbed into  $A_{\beta}$ . The constant  $A_{\beta}$  depends upon the local geometry of the discharge point as well as the overall antenna geometry. It can be evaluated by static measurements provided we know the values of  $\frac{K_{\alpha} \left( \frac{\text{zeros}_{\alpha}}{\text{poles}_{\alpha}} \right)_{p=0}}$ . It is apparent that this quantity is simply the ratio of the limiting values of the low frequency reactances of the two elements of the antenna. We assumed earlier that these reactances were in the ratio 1 to 10, so that

$$\frac{K_{\alpha} \left( \frac{\text{zeros}_{\alpha}}{\text{poles}_{\alpha}} \right)_{p=0}}{K_{\beta}} = \frac{1}{10} \quad (51)$$

Since we have agreed to accept the rational function approximation of  $Z_{\alpha}$  as a true representation of that impedance, it is possible to evaluate each of the constants specifically. From the rational function formula given in Fig. 26

$$K_{\alpha} = 1933 \quad (52)$$

$$\left( \frac{\text{zeros}_{\alpha}}{\text{poles}_{\alpha}} \right)_{p=0} = 0.202 \quad (53)$$

Therefore,

$$K_{\beta} = 10 K_{\alpha} 0.202 = 3905 \quad (54)$$

The functional behavior of the coupling from the short element of the asymmetric dipole can be obtained by plotting the function  $\frac{\psi_{\beta}}{A_{\beta}}$  as obtained from Eq. (50). This function is shown in Fig. 33. The feature most worthy of note in the curve of Fig. 33 is its relative smoothness compared to the

(50)

de-  
over  
ovided  
quantity  
stances  
eact

(51)

ion of  
luate  
ia

(52)

(53)

(54)

of the  
lined  
worthy  
o the

11 37

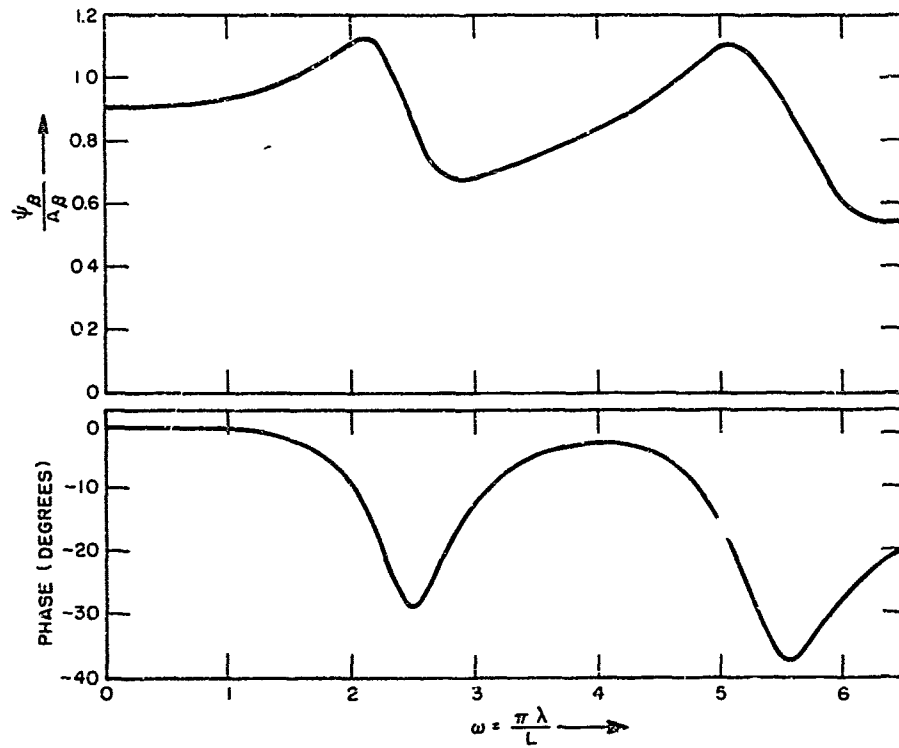
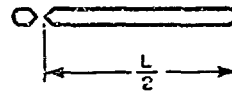


FIG. 33

FREQUENCY BEHAVIOR OF COUPLING  
FROM SHORT ELEMENT OF ASYMMETRIC DIPOLE

A-591-TR37-224

other response curves we have obtained. The singularities of the impedance function, representing electromagnetic resonances on the antenna, introduce irregularities in both real and imaginary components of the coupling function which are smaller than those in the other coupling functions studied. From a transient point of view this means that the short-circuit current at the antenna terminals is a pulse not greatly altered in form from the corona discharge pulse itself. The noise produced at any frequency for any type of load impedance can be calculated in the same manner as for the symmetric dipole. From the coupling function, the pulse spectrum and the terminal impedance, a Thevenin's or Norton's equivalent circuit can be set up and the computations made in a straightforward manner.

G. Coupling from Discharge at End of Long Element

For a discharge at the end of the long element of the antenna, which is characterized by the coupling function  $\psi_a$ , we are concerned with the ratio  $\frac{Z_{12a}}{Z_{11A}}$ , where  $Z_{12a}$  is the mutual impedance between the antenna terminals and the end of the long element. By the same argument which was applied to the symmetric dipole we recognize that  $Z_{12a}$  is given by

$$Z_{12a} = \frac{K_{12a}}{p \text{ (poles}_a\text{)}} \quad (55)$$

The coupling function  $\psi_a$  is therefore given by

$$\begin{aligned} \psi_a &= \frac{K_{12a} \frac{1}{p \text{ (poles}_a\text{)}}}{\sum \left( K_\beta \frac{1}{p} + \frac{\text{(zeros}_a\text{)}}{\text{(poles}_a\text{)}} \right)} \\ &= A_a \frac{1}{\text{(poles}_a\text{)} + \frac{K_a}{K_\beta} \text{(zeros}_a\text{)}} \end{aligned} \quad (56)$$

where miscellaneous constants have been absorbed in  $A_\alpha$ . The constant  $A_\alpha$  can be determined by static measurements in the same manner as was  $A_\beta$ .

The functional behavior of  $\psi_\alpha$  is readily computed from the rational function approximation of  $Z_\alpha$ . It is shown in the curve of Fig. 34. In contrast to the rather uniform curve of Fig. 33, the curve of Fig. 34 shows a marked peak corresponding roughly to the frequency which makes the antenna one-half wavelength long, with a lesser peak at the frequency corresponding to a length of one wavelength. Both of these peaks would be a great deal more pronounced for a more slender antenna. The curve of Fig. 34 indicates that the coupling from a discharge at the end of the long element is profoundly influenced by the electromagnetic resonances of the antenna structure and may be quite large. We therefore see that the conception previously held, that the discharges which occur at large distances from the antenna terminals do not contribute appreciably to the noise, may be quite mistaken.

An observation made by Huckle<sup>3</sup> in 1937 is very interesting in the light of the results just obtained. In the course of the investigation reported by Huckle the attractive but somewhat naive idea occurred to the investigators of forcing the discharge to occur at one particular frequency, thereby confining the noise produced to that frequency and eliminating noise at other frequencies. A mechanism was accordingly arranged by which a trailing wire could be let out, with the idea of tuning the entire aircraft, and thereby forcing the discharge to occur at the frequency to which the aircraft was tuned. Two radio receivers, one tuned to 5 Mc and the other to a range beacon at approximately 350 kc, were connected in the meantime to separate antennas. As 150 ft of trailing wire were reeled out, two noise maxima and two minima were observed on the receiver tuned to 5 Mc while no change was evident for the noise in the beacon receiver. The success with which the present theory explains these observations is quite striking. A large share of the noise was undoubtedly being produced by discharges from the end of the trailing wire. As the wire was reeled out, the total length of wire plus aircraft fuselage increased to more than one

ant  $A_a$   
 $A_\beta$   
 tional  
 In  
 34  
 kes the  
 y cor  
 d be a  
 licates  
 influ  
 e large.  
 occur  
 reci  
 e light  
 ported  
 sti  
 ng  
 which  
 air  
 o which  
 the  
 re  
 ed out  
 o  
 The  
 quite  
 by  
 out  
 n one

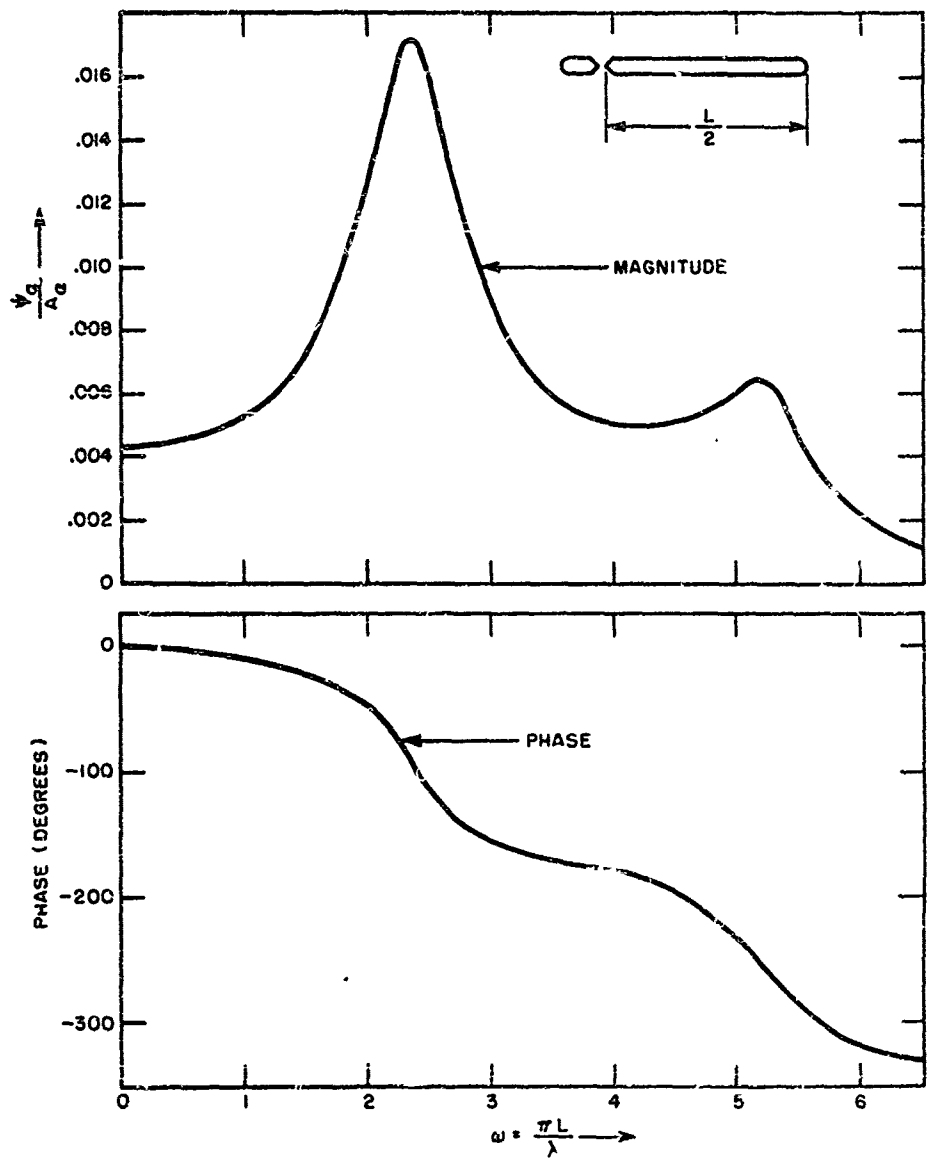


FIG. 34

FREQUENCY BEHAVIOR OF COUPLING FROM  
 LONG ELEMENT OF ASYMMETRIC DIPOLE

B-591-1R37-220

wavelength at 5 Mc, accounting for the noise maxima and minima on the basis of maxima and minima in  $\psi$ . For the beacon frequency the longest length of trailing wire was small compared to a wavelength. The coupling function at that frequency therefore did not pass through any peaks similar to those observed at the higher frequency.

the  
engt  
acti  
to

## CHAPTER VI

## CONCLUSIONS AND RECOMMENDATIONS

A. General Considerations for an Ideal Discharger

It is interesting to visualize, in the light of the foregoing analysis, the form which an ideal aircraft discharger would take. The function of the discharger is to relieve the aircraft of its accumulated static charge with the attendant production of r-f noise reduced to a minimum. It is apparent that the problem can be attacked in either or both of two possible ways (1) the r f noise generated by the discharge for a given d c current flow can be reduced, or (2) the coupling between the discharge and the receiver can be reduced.

Let us consider for a moment the first of these possibilities. Since the data of Chapter III indicate that the shapes of the corona pulses remain approximately the same, irrespective of size, it becomes clear that the simplest means of reducing generated noise is to reduce the magnitudes of the pulses. Although it is necessary to increase the pulse frequency in order to maintain the same d-c discharge current, we nevertheless obtain a net reduction of generated noise. This fact is illustrated by the diagram of Fig. 35. In this figure we have, for purposes of illustration, shown rectangular pulses. However, the same principle applies to pulses of any shape. We see from the figure that by halving the pulse magnitude but doubling the repetition frequency, the mean-square current and the noise power are halved.

The oscillograms of Fig. 4 indicate that the magnitude of the discharge pulses can be reduced by reducing the tip radius. Although the function  $\psi$  is increased by reducing the tip radius, the discharge moment is reduced more than enough to compensate. Furthermore, if we go to tip

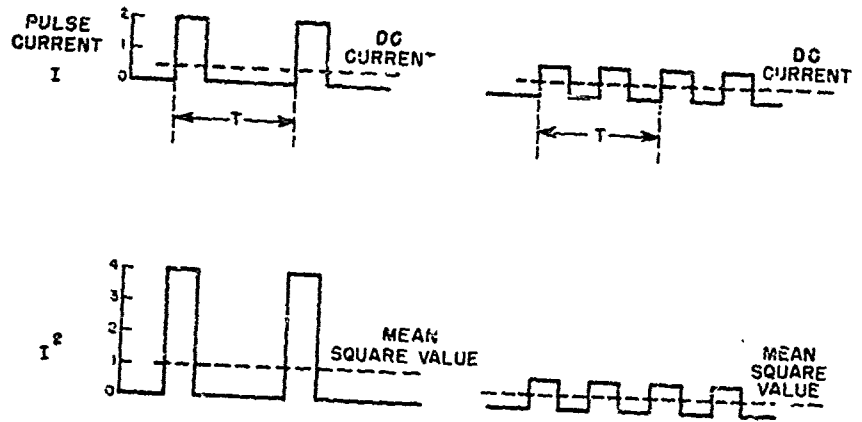


FIG. 35  
 ILLUSTRATING REDUCTION IN GENERATED  
 NOISE BY REDUCTION OF PULSE SIZE

radii which are extremely small, the supposition that the discharge takes place in a volume which is of the dimensions of the tip radius is manifestly impossible. Much of the discharge current flow occurs at distances which are considerably larger than the tip radii. The coupled noise as measured by Eq. (8) is therefore reduced from the value obtained assuming the flow to take place in the near vicinity of the tip. We therefore can expect to reduce very greatly the noise generated by the discharge of given value of d-c current if we force the discharge to occur at points of very small radius.

The second method of reducing the noise at the receiver is to reduce the coupling between the discharge and the receiver. We therefore look for ways in which such a reduction might be accomplished, and on first inspection the prospects do not appear to be good. The points of high d-c field concentration are in general the points at which a high field is produced by a voltage at the antenna terminals, so that discharges tend to occur naturally at points from which their effects are coupled strongly into the receiver. Two possible solutions suggest themselves, however. First, we might exploit the fact that the field which induces the discharge is a d-c field whereas the field defined by the coupling function  $\psi$  is an r-f field. An electrode arrangement might be conceived in which the discharge point is tied to the aircraft at d-c, but very well decoupled at r-f. An arrangement fulfilling these requirements is illustrated in Fig. 36. For maximum effectiveness the discharge electrode must be sufficiently far removed from the aircraft that the capacitance between the aircraft and the electrode is very small compared to the self capacitance of the electrode. The resistance of the connecting cable must likewise be high compared to the reactance of the self capacitance of the discharge electrode. If these conditions are fulfilled, the arrangement shown constitutes a resistance-capacitance filter which decouples the aircraft from the discharge point. Needless to say, the resistance of the connecting cable must be distributed throughout its length rather than concentrated at one point if minimum

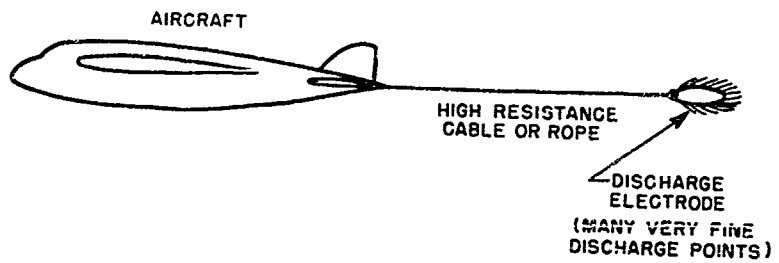


FIG. 36  
DISCHARGE SCHEME IN WHICH  
THE DISCHARGE POINTS ARE  
DECOUPLED FROM THE AIRCRAFT

A-591-TR37-230

capacitance between the discharge electrode and the aircraft is to be obtained.

The second possibility for reducing the coupling between the discharge and the receiver is to force the discharge to occur at a point on the aircraft which is naturally shielded electrically. The coupling from a discharge occurring in a shielded region is inherently poor, but could be reduced still further by the use of very fine discharge points and a high resistance connection. An arrangement utilizing this principle is shown in Fig. 37. A discharge is forced to occur from a series of points similar to standard discharge wicks by applying them to a high negative voltage. The wicks are situated in the shielded region at the base of the wing. The airstream at this point is moving rapidly and would carry away the ions formed in the discharge. Investigation would be needed, however, to determine whether such a system were capable of discharging sufficiently large d.c. currents.

#### B. Evaluation of Common Anti-Precipitation Static Devices

It is interesting to examine the anti-precipitation static devices commonly in use at the present time in the light of the theory just developed. When this is done, it becomes apparent that all of the devices which have achieved reasonably successful results embody one or more of the principles outlined in the discussion of an ideal discharger. Consider, for example the dielectric-coated wire antenna. It is obvious that discharges from the antenna itself couple very strongly into the receiver. By protecting the antenna and antenna fittings with a high strength dielectric the discharges are forced to occur at other points on the aircraft from which the coupling is weaker.

The wick discharger operates on a combination of effects. It reduces the noise generated by the discharge by providing extremely fine discharge points, and it also provides considerable decoupling. The resistance of

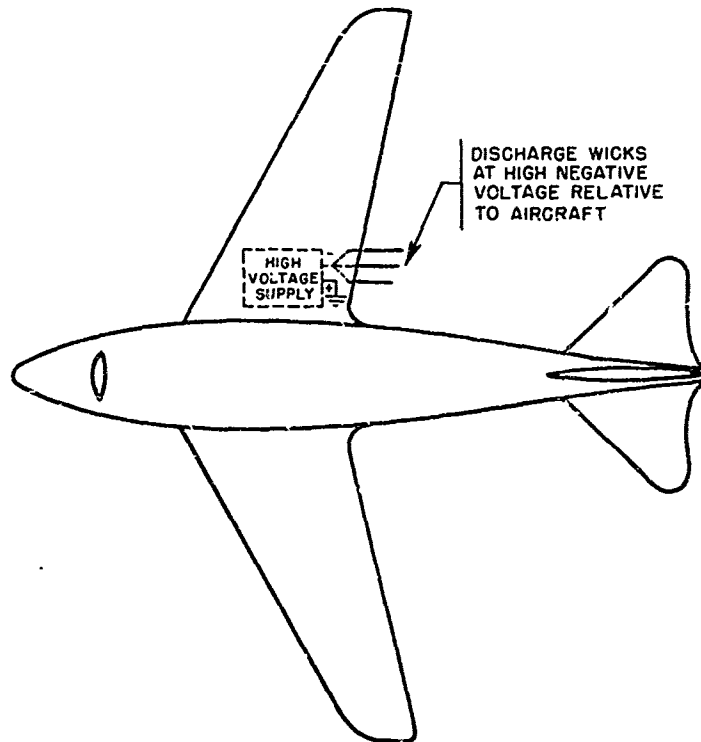


FIG. 37

LOW NOISE DISCHARGE SCHEME.  
DISCHARGE FORCED TO OCCUR AT REGION  
FROM WHICH COUPLING TO RECEIVER IS LOW.

A-591-TR37-228

the discharge wicks is very high, so high in fact that as far as the r f field in their vicinity is concerned their effect can be neglected. Thus the discharges which occur at the tips of the wicks are removed from the highly concentrated r-f fields which occur at the surfaces of sharp points on the metallic conductors. From the coupling principle given in Chapter II it is apparent that the coupling from the discharges is reduced in proportion to the reduction of the r-f fields in the region of the discharge.

By the same reasoning it is apparent that the discharge devices proposed by Beach<sup>31</sup> have little to commend them. These dischargers are simply brushes composed of bunches of fine wires. Since the discharge points are metallic, it is at once evident that no reduction of noise due to decoupling is experienced. The only benefit comes from a reduction of the generated noise due to a reduction in the size of the discharge points. Even in this respect, however, they would appear to be inferior to the wick discharger.

Another type of discharger which achieved some success is the trailing wire discharger growing out of the investigation reported by Hucke. This discharger achieved decoupling from the aircraft in a manner similar to that outlined in the discussion of an ideal discharger. A fine wire served as the discharge point. It was isolated from a supporting wire by means of a resistance. Although the decoupling achieved was less than could be obtained by the use of a distributed isolating resistor and a discharge electrode having greater self capacitance than the slender wire used it resulted in considerable reduction of noise.

### C. Suggestions for Additional Research

It is hoped that the investigation reported here will lead to a better understanding of the basic phenomena contributing to the production of radio noise by corona discharges, and that it will help to provide more successful solutions to the problem of precipitation static in aircraft. The investigations are not complete. The problem of the transient response

of antenna-receiver systems to corona discharges is not discussed at all. It is believed, however, that the transient problem can be attacked using many of the tools provided in this investigation. The investigation of the nature of corona discharges and how their character depends upon the possible variables is far from complete. We have, however, indicated the means by which a more exhaustive investigation can be undertaken. Another subject for investigation might be the experimental determination of the coupling function  $\psi$  for actual aircraft by means of model techniques. More effort might profitably be spent in developing new and more efficient discharge devices, or improving upon existing devices with the aid of the theory developed here.

### ACKNOWLEDGMENT

The author wishes to acknowledge his debt to his colleagues and advisors who have contributed greatly to whatever success may be claimed for this investigation. These include Dr. J. V. N. Granger who suggested the investigation and who provided incentive and encouragement to pursue it, Dr. J. T. Bolljahn, Dr. C. T. Tai, and Dr. Carson Flammner who contributed suggestions and much valuable discussion on different aspects of the problem. Many others, too numerous to mention individually, on the staff of the Stanford Research Institute have contributed in countless ways. The author is also greatly indebted to Professor W. G. Hoover of Stanford University for advice and assistance in carrying out the oscillographic investigations reported in Chapter III.

The investigation was supported by the U. S. Air Force under Contract No. AF 19(604)-266.

d at all.  
ked using  
tion of  
upon the  
cated the  
. Another  
of the  
ques.  
efficient  
d of the

### ACKNOWLEDGMENT

The author wishes to acknowledge his debt to his colleagues and advisors who have contributed greatly to whatever success may be claimed for this investigation. These include Dr. J. V. N. Granger who suggested the investigation and who provided incentive and encouragement to pursue it, Dr. J. T. Bolljahn, Dr. C. T. Tai, and Dr. Carson Flanger who contributed suggestions and much valuable discussion on different aspects of the problem. Many others, too numerous to mention individually, on the staff of the Stanford Research Institute have contributed in countless ways. The author is also greatly indebted to Professor W. G. Hoover of Stanford University for advice and assistance in carrying out the oscillographic investigations reported in Chapter III.

The investigation was supported by the U. S. Air Force under Contract No. AF 19(604)-266.

## APPENDIX A

Two configurations of discharge point geometry were used in obtaining the oscillographic data of Chapter III. In phase 1 of the study, the discharge point was a hemispherically capped cylindrical extension of the center conductor of a coaxial cable. It is illustrated schematically in Fig. Ala. As shown in Chapter II it is necessary, in order to compute the dipole moments of the discharges, to know the fields in the vicinity of the discharge when a voltage is applied at the base of the discharge point.

The actual discharge point does not conform to any simple coordinate system, and therefore is not amenable to an exact analysis. Electrolytic tank investigations provide some data on the fields, but results obtained in this way are not highly accurate and are also not amenable to analytical manipulations. Such investigations indicate, however, that the geometrical quantity of importance in the point configuration is the ratio of tip radius to point height, and that a mathematical model such as a prolate spheroid which has the same ratio of these dimensions as the actual discharge point will have very nearly the same fields in the vicinity of the tip.

The spheroidal model is shown in Fig. Alb. The field expressions for such a geometry are readily obtained in terms of spheroidal harmonics. We recognize by use of the image theorem that the potential expression for the configuration shown is the same as for a spheroid bisected on the equatorial plane with the top section held at potential  $V_1^{(1)}$  and the bottom section at  $-V_1^{(1)}$ . Since such an electrode configuration has axial symmetry, we know that the external potential is given by<sup>21</sup>

$$V_e = \sum_n [M_n P_n(\xi) + N_n Q_n'(\xi)] P_n(\eta) \quad (A1)$$

where the prolate spheroidal coordinates are illustrated in Fig. A2. The boundary conditions are such that  $V_e \rightarrow 0$  as  $\xi \rightarrow \infty$ , which requires that

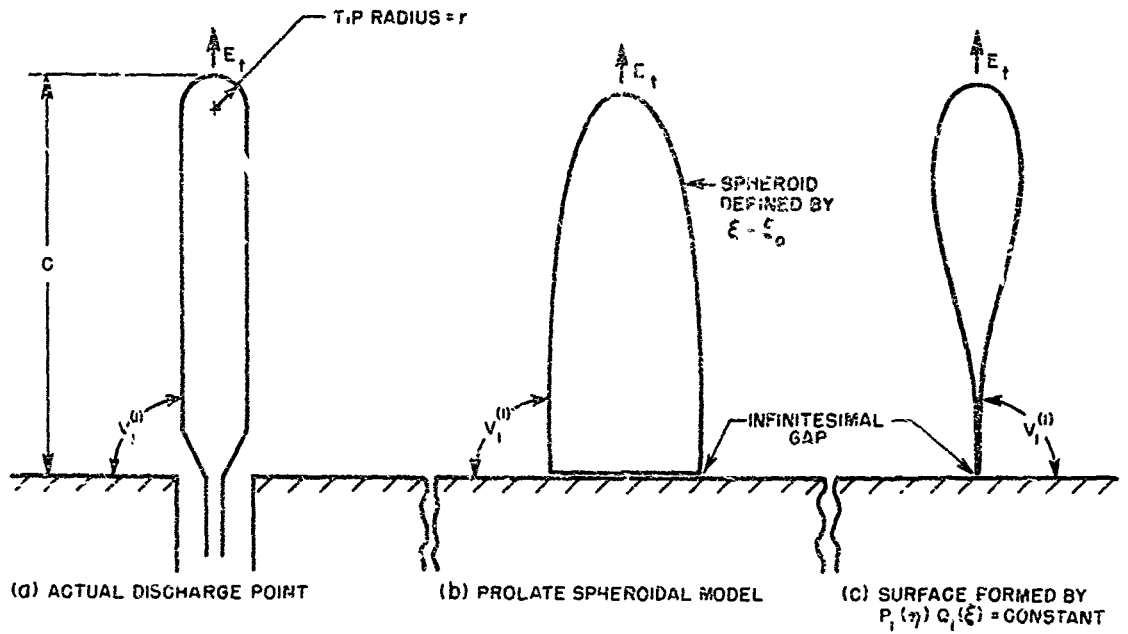


FIG. A-i

COMPARISON OF ACTUAL DISCHARGE POINT  
 WITH TWO POSSIBLE MATHEMATICAL MODELS  
 FOR WHICH THE RATIO  $\frac{c}{r}$  HAS THE SAME VALUE

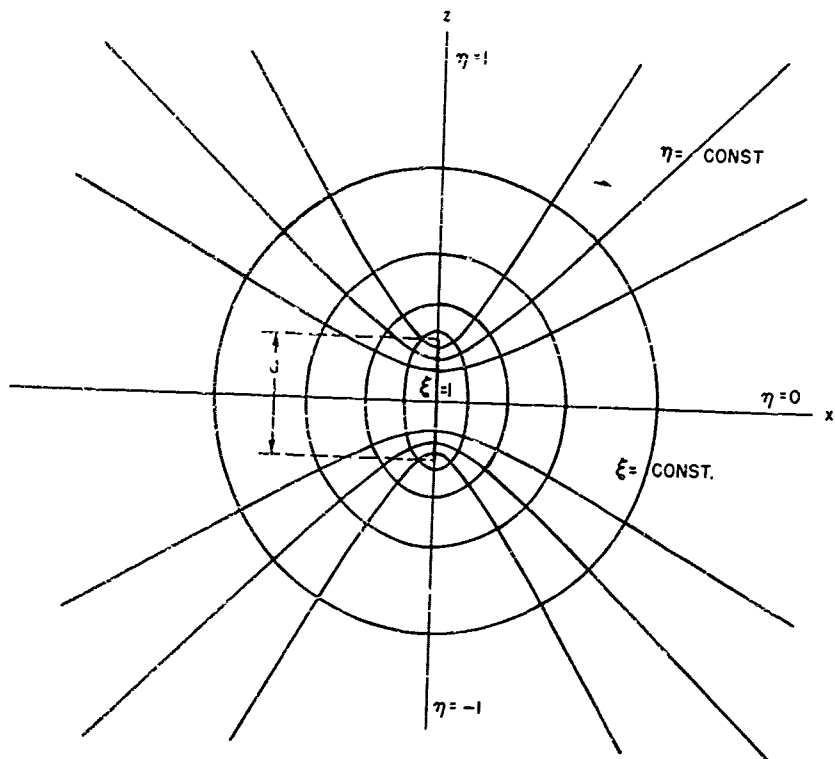


FIG. A-2  
 THE PROLATE SPHEROIDAL COORDINATE SYSTEM

A-591-TR37-242

$M_n = 0$ . The coefficients  $N_n$  are found from the boundary condition on the metallic surface. This condition can be stated as follows.

$$V_0(\xi_0) = \sum_n N_n Q_n(\xi_0) P_n(\eta) \begin{cases} = -V_1^{(1)} & -1 \leq \eta < 0 \\ = +V_1^{(1)} & 0 < \eta \leq +1 \end{cases} \quad (A2)$$

$N_n$  is evaluated by multiplying both sides of Eq. (A2) by  $P_n(\eta)$  and integrating over  $\eta$ . Because of the orthogonality of the Legendre polynomials the terms for which  $n \neq m$  vanish and we are left finally with the expression for  $N_n$ ,

$$N_n = \frac{V_1^{(1)}}{Q_n(\xi_0)} [P_{n-1}(0) - P_{n+1}(0)] \quad (A3)$$

The symmetry about the equatorial plane requires that  $N_n = 0$  for even values of  $n$ .

The electric field can be derived from the potential expression of Eq. (A2) by taking the gradient. The field actually has both a  $\xi$  component and an  $\eta$ -component, but for values of  $\eta$  differing only slightly from  $\eta = 1$  (Fig. 19), the  $\eta$ -component of field is negligibly small compared with the  $\xi$ -component. In other words, near the tip the field is normal to the spheroidal surfaces defined by  $\xi = \text{constant}$ . Expressed analytically,  $E_\xi$  is given by

$$E_\xi = \frac{\eta_0}{C} \frac{1}{\sqrt{(\xi^2 - \eta^2)(\xi^2 - 1)}} \sum_{\substack{n \\ n \text{ odd}}} N_n (n+1) P_n(\eta) [Q_n(\eta) - Q_{n+1}(\eta)] \quad (A4)$$

where  $N_n$  are the coefficients given by Eq. (A3), and  $C$  is the height of the spheroid. It can be shown that the series of Eq. (A4) diverges. The divergence is caused by the assumption of an infinitesimal gap which does

$M_n = 0$ . The coefficients  $N_n$  are found from the boundary condition on the metallic surface. This condition can be stated as follows.

$$V_0(\xi_0) = \sum_n N_n Q_n(\xi_0) P_n(\eta) \begin{cases} = -V_1^{(1)} & -1 \leq \eta < 0 \\ = +V_1^{(1)} & 0 < \eta \leq +1 \end{cases} \quad (A2)$$

$N_n$  is evaluated by multiplying both sides of Eq. (A2) by  $P_n(\eta)$  and integrating over  $\eta$ . Because of the orthogonality of the Legendre polynomials the terms for which  $n \neq m$  vanish and we are left finally with the expression for  $N_n$ ,

$$N_n = \frac{V_1^{(1)}}{Q_n(\xi_0)} [P_{n-1}(0) - P_{n+1}(0)] \quad (A3)$$

The symmetry about the equatorial plane requires that  $N_n = 0$  for even values of  $n$ .

The electric field can be derived from the potential expression of Eq. (A2) by taking the gradient. The field actually has both a  $\xi$ -component and an  $\eta$ -component, but for values of  $\eta$  differing only slightly from  $\eta = 1$  (Fig. 19), the  $\eta$ -component of field is negligibly small compared with the  $\xi$ -component. In other words, near the tip the field is normal to the spheroidal surfaces defined by  $\xi = \text{constant}$ . Expressed analytically,  $E_\xi$  is given by

$$E_\xi = \frac{\eta_0}{C} \frac{1}{\sqrt{(\xi^2 - \eta^2)(\xi^2 - 1)}} \sum_{n \text{ odd}} N_n (n+1) P_n(\eta) [Q_n(\eta) - Q_{n+1}(\eta)] \quad (A4)$$

where  $N_n$  are the coefficients given by Eq. (A3), and  $C$  is the height of the spheroid. It can be shown that the series of Eq. (A4) diverges. The divergence is caused by the assumption of an infinitesimal gap which does

not correspond to physical reality. The series could be made to converge by assuming a different type of gap but even if this were done, convergence would be so slow that the resulting field expression would be very cumbersome to work with analytically.

An alternative analytical model is shown in Fig. A1c. Here we have defined the surface by the equation

$$P_1(\eta) Q_1(\xi) = \text{Constant} \quad (A5)$$

and chosen the value of the constant to make the ratio  $\frac{c}{r}$  equal to that of the actual point. This model circumvents the problem of the infinitesimal gap since it reduces to a point of infinitesimal diameter as it approaches the ground plane. The fields about an electrode of the shape thus defined differ considerably from those of the spheroid or the cylindrical discharge point in the region near the base. In the vicinity of the tip, however, the fields are very similar to those of the actual discharge point. Inasmuch as the fields of the model are described by a single harmonic, they are simple to work with mathematically. For this reason we choose the model of Fig. A1c to represent the actual discharge point.

It is easily verified that for the electrode configuration of Fig. A1c the external potential is given by

$$V_e = V_1^{(1)} \eta \frac{Q_1(\xi)}{Q_1(\xi_0)} \quad (A6)$$

where  $\xi_0$  is the value of  $\xi$  on the tip of the electrode ( $\eta = 1$ ) and is defined in terms of the  $\frac{c}{r}$  ratio of the electrode by the relation

$$\xi_0 = \frac{1}{\sqrt{1 - \frac{r}{c}}} \quad (A7)$$

We again take the gradient of the potential expression to find the field, and as with the spheroidal model we find that the  $\eta$  component of

field is negligibly small for values of  $\eta$  differing only slightly from unity. The  $\xi$ -component of the field is found to be

$$E_{\xi} = \frac{V_1^{(1)} \xi_0}{c \left( \frac{\xi^2 - \eta^2}{\xi^2 - 1} \right)^{1/2}} \frac{Q_1'(\xi)}{Q_1(\xi_0)}. \quad (\text{A8})$$

It is shown in Smythe<sup>21</sup> that  $Q_1(\xi)$  is given by

$$Q_1(\xi) = \xi \operatorname{coth}^{-1} \xi - 1. \quad (\text{A9})$$

From Eq. (A9) it is easily found that

$$Q_1'(\xi) = \operatorname{coth}^{-1} \xi - \frac{\xi}{\xi^2 - 1}. \quad (\text{A10})$$

In the present investigation we are interested in the value of the field at the surface of tip, where  $\xi = \xi_0$  and  $\eta = 1$ . When these values, together with the expressions of Eqs. (A9) and (A10) are substituted into Eq. (A8) we obtain

$$\frac{rE_t}{V_1^{(1)}} = \frac{r}{c} \frac{\operatorname{coth}^{-1} \xi_0 - \frac{\xi_0}{\xi_0^2 - 1}}{\operatorname{coth}^{-1} \xi_0 - \frac{1}{\xi_0}}. \quad (\text{A11})$$

We have expressed the field relation in the dimensionless form shown in order to make it more generally applicable. From Eqs. (A11) and (A7) it is possible to obtain the value of  $\frac{rE_t}{V_1^{(1)}}$  as a function of the ratio  $\frac{c}{r}$ .

This quantity has been computed and is shown in the graph of Fig. A3.

In phase 2 of the oscillographic study the discharge electrode is a hemispherically capped cylinder situated in the uniform field between two discs. Such a configuration is closely approximated by a prolate

field is negligibly small for values of  $\eta$  differing only slightly from unity. The  $\xi$ -component of the field is found to be

$$E_{\xi} = \frac{V_1^{(1)} \xi_0}{c \left( \frac{\xi^2 - \eta^2}{\xi^2 - 1} \right)^{\frac{1}{2}}} \frac{Q_1'(\xi)}{Q_1(\xi_0)} \quad (A8)$$

It is shown in Smythe<sup>21</sup> that  $Q_1(\xi)$  is given by

$$Q_1(\xi) = \xi \coth^{-1} \xi - 1 \quad (A9)$$

From Eq. (A9) it is easily found that

$$Q_1'(\xi) = \coth^{-1} \xi - \frac{\xi}{\xi^2 - 1} \quad (A10)$$

In the present investigation we are interested in the value of the field at the surface of tip, where  $\xi = \xi_0$  and  $\eta = 1$ . When these values, together with the expressions of Eqs. (A9) and (A10) are substituted into Eq. (A8) we obtain

$$\frac{rE_t}{V_1^{(1)}} = \frac{r}{c} \frac{\coth^{-1} \xi_0 - \frac{\xi_0}{\xi_0^2 - 1}}{\coth^{-1} \xi_0 - \frac{1}{\xi_0}} \quad (A11)$$

We have expressed the field relation in the dimensionless form shown in order to make it more generally applicable. From Eqs. (A11) and (A7) it is possible to obtain the value of  $\frac{rE_t}{V_1^{(1)}}$  as a function of the ratio  $\frac{c}{r}$ .

This quantity has been computed and is shown in the graph of Fig. A3.

In phase 2 of the oscillographic study the discharge electrode is a hemispherically capped cylinder situated in the uniform field between two discs. Such a configuration is closely approximated by a prolate

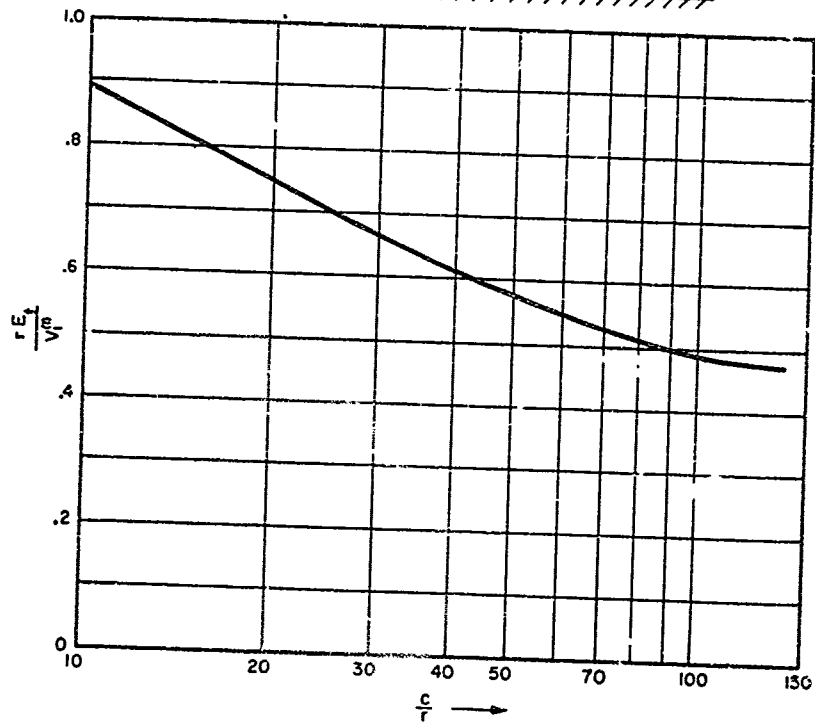
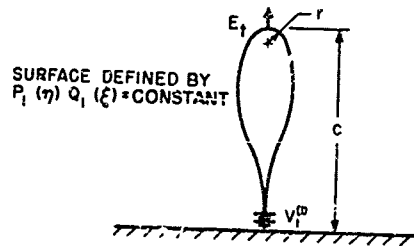


FIG. A-3  
 RATIO OF TIP FIELD TO BASE VOLTAGE FOR  
 IDEALIZED DISCHARGE ELECTRODE

A-591-TR37-231

spheroidal projection from a conducting plane which forms one boundary of a uniform field. Smythe shows that the potential in the latter case is given by

$$V_0 = E_0^{(1)} c\eta \frac{\xi}{\xi_0} \left( 1 - \frac{\coth^{-1} \xi - \frac{1}{\xi}}{\coth^{-1} \xi_0 - \frac{1}{\xi_0}} \right), \quad (A12)$$

where  $E_0^{(1)}$  is the uniform field which exists at large distances from the spheroidal projection, whose surface is defined by  $\xi = \xi_0$ . The ratio  $\frac{c}{r}$  of the projecting spheroid is related to  $\xi_0$  by Eq. (A7).

The field is found by taking the gradient of  $V_0$  and again we find that near the axis ( $\eta$  near 1) only the  $\xi$ -component of the field is important. On the axis the field is given by

$$E_x = E_0^{(1)} \left( 1 - \frac{\coth^{-1} \xi - \frac{\xi}{\xi^2 - 1}}{\coth^{-1} \xi_0 - \frac{1}{\xi_0}} \right). \quad (A13)$$

The concentration of field at the tip of the discharge point is equal to  $\frac{E_x(\xi_0)}{E_0^{(1)}}$ . The numerical value of this factor is easily found from Eq. (A13) and is the curve plotted in Fig. 18 in Chapter III.

It is interesting to determine the decay of the field as we move away from the tip of the discharge point. In this way we can find whether the proximity of the upper disc appreciably interferes with our assumption of unbounded uniform field above the lower disc. From Eq. (A13) we find that for a point with a  $\frac{c}{r}$  ratio of 40, which corresponds roughly to the maximum point height for which oscillograms were taken, the field has dropped to a value exceeding  $E_0^{(1)}$  by only 7% at a distance from the tip which is equal to  $c$ . The actual modification of the field at the tip due to the upper disc would be much less than this. Since the minimum spacing between the discs was more than 2½ times greater than the height of the point, we can safely conclude that the field at the tip is correctly given by Eq. (A13)

APPENDIX B

In the analysis of Appendix A we derive an expression giving the field at the tip of the discharge point as a function of the  $\frac{c}{r}$  ratio of the point and the uniform field which exists near the axis of the electrode configuration shown in Fig. 14. To determine the tip field as a function of the terminal voltage  $V_1^{(1)}$ , however, we must find an expression for the field  $V_0^{(1)}$  as a function of that voltage. To a first approximation the field  $E_0^{(1)}$  is given by

$$E_0^{(1)} = \frac{V_1^{(1)}}{S},$$

where  $S$  is the spacing between the discs. It is obvious, however, that this expression breaks down for large values of  $S$ , since it predicts zero field for very large  $S$ , while we know from physical reasoning that a finite field will exist for this condition. Since the diameter of electrode B in Fig. 14 is considerably larger than that of electrode A, and also much larger than the maximum value of  $S$ , while the spacing between A and the ground plane is small compared to the radius of A (which we shall designate in the following analysis by  $b$ ) the actual electrode geometry is closely approximated by the idealized geometry shown in Fig. B1.

It is known from potential theory that one set of harmonic potential functions from which solution to the Laplace equation in cylindrical coordinates with axial symmetry can be constructed, have the form shown in Eq. (B1).

$$V = \sum_n [A_n e^{\mu_n z} + B_n e^{-\mu_n z}] [C_n J_0(\mu_n \rho) + D_n N_0(\mu_n \rho)] \quad (B1)$$

The potential on the axis is finite, which requires that  $D_n = 0$ ; the constants  $C_n$  can be absorbed in  $A_n$  and  $B_n$ .

the  
tio of  
elec  
as a  
xpression  
roximation

that  
ts zero  
a finite  
ode B in  
much  
d the  
desig.  
is

ential  
d co-  
own in

(B1)

e

591 37

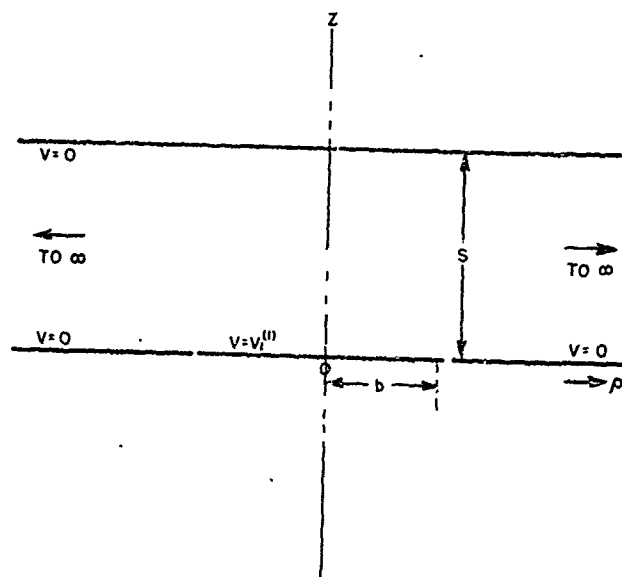


FIG. B-1  
IDEALIZED ELECTRODE GEOMETRY APPROXIMATING  
THE GEOMETRY OF FIG. 14

A-591-TR37-206

Because the region of interest extends to infinity in the radial direction, the sum indicated in Eq. (B1) becomes an integral or Hankel transform.<sup>32</sup> The potential expression therefore becomes

$$V(\rho z) = \int_0^{\infty} \mu [A(\mu) e^{-\mu z} + B(\mu) e^{\mu z}] J_0(\mu \rho) d\mu . \quad (B2)$$

The boundary conditions shown in Fig. B1 require that

$$(1) \quad V(\rho, 0) = \begin{cases} V_1^{(1)} & , \quad 0 \leq \rho < a \\ 0 & , \quad a < \rho < \infty \end{cases} \quad (B3)$$

$$(2) \quad V(\rho, s) = 0 . \quad (B4)$$

Applying the Hankel inversion theorem to Eq. (B3) and evaluating the integral which arises, we find that

$$\mu [A(\mu) + B(\mu)] = V_1^{(1)} b J_1(\mu b) . \quad (B5)$$

From Eq. (B4) we easily determine that

$$A(\mu) e^{-\mu s} + B(\mu) e^{\mu s} = 0 ,$$

or

$$B(\mu) = -A(\mu) e^{-2\mu s} . \quad (B6)$$

Substitution of Eq. (B6) into Eq. (B5) shows that

$$\mu A(\mu) = \frac{V_1^{(1)} b}{1 - e^{-2\mu s}} J_1(\mu b) , \quad (B7)$$

and the coefficient  $B(\mu)$  is found by substituting Eq. (B7) into Eq. (B6).

When the coefficients  $A(\mu)$  and  $B(\mu)$  thus determined are substituted into Eq. (B2), the expression for the potential becomes

$$V(\rho, z) = \int_0^{\infty} \frac{V_1^{(1)} b}{1 - e^{-2\mu s}} [e^{-\mu z} - e^{\mu(z-2s)}] J_1(\mu b) J_0(\mu \rho) d\mu. \quad (B8)$$

Since we are concerned only with the field on the axis, the expression of Eq. (B8) simplifies to

$$V(0, z) = V_1^{(1)} b \int_0^{\infty} \frac{e^{-\mu z} - e^{\mu(z-2s)}}{1 - e^{-2\mu s}} J_1(\mu b) d\mu. \quad (B9)$$

The axial electric field is given by

$$E_z = - \frac{\partial V}{\partial z}.$$

We are here interested in the field in the vicinity of the discharge point which is evidently given by

$$E_0^{(1)} = - \frac{\partial V}{\partial z} \Big|_{\substack{\rho=0 \\ z=0}}. \quad (B10)$$

When the derivative indicated in Eq. (B10) is taken, we find that

$$E_0^{(1)} = \frac{V_1^{(1)}}{b} \int_0^{\infty} \nu \frac{1 + e^{-2\zeta}}{1 - e^{-2\zeta}} J_1(\nu) d\nu, \quad (B11)$$

where we have set  $\nu = \mu b$  and  $\zeta = \frac{s}{b}$ .

The integral of Eq. (B11) cannot be evaluated in closed form. If the denominator of the integrand is expanded in a series, however, the result is the integral of Eq. (B12):

$$E_0^{(1)} = \frac{V_1^{(1)}}{b} \int_0^\infty \nu (1 + 2e^{-2\nu\zeta} + 2e^{-4\nu\zeta} + 2e^{-6\nu\zeta} + \dots) d\nu. \quad (B12)$$

This integral can be evaluated term by term to form the rapidly converging series of Eq. (B13):

$$E_0^{(1)} = \frac{V_1^{(1)}}{b} \left\{ 1 + \frac{2}{[1 + (2\zeta)^2]^{\frac{3}{2}}} + \frac{2}{[1 + (4\zeta)^2]^{\frac{3}{2}}} + \frac{2}{[1 + (6\zeta)^2]^{\frac{3}{2}}} + \dots \right\} \quad (B13)$$

from which numerical values of  $\frac{E_0^{(1)}}{V_1^{(1)}}$  can be computed.

It is apparent that the idealized geometry of Fig. B1 does not correspond exactly to the true physical geometry. The difference lies chiefly in the fact that there is a finite separation between the disc of electrode A and the surrounding grounded surface. We expect on physical grounds that this difference might be accounted for by giving  $b$  an effective value which is larger than the actual radius of electrode A. We can find what numerical value to give  $b$  by determining what value of  $b$  causes the field  $E_0^{(1)}$  to reduce to  $\frac{V_1^{(1)}}{S}$  for small  $S$ , as we know it must. The numerical value of  $b$  which fulfills this requirement is  $b = 4$  cm, whereas the actual radius of disc A was 3.8 cm.

Values of  $\frac{E_r^{(1)}}{V_1^{(1)}}$  have been computed from Eq. (B13) and are plotted in Fig. 15.

LIST OF REFERENCES

1. R. H. Marriot, 'Radio Range Variation.' Proc. IRE, Vol. 2, No. 3, March 1914.
2. H. W. Morgan, 'Rain Static,' Proc. IRE, Vol. 24, No. 7, July 1937.
3. H. M. Hucke, "Precipitation Static Interference," Proc. IRE, Vol. 27, No. 5. May 1939
4. Austin Curtis, Discussion on 'Radio Range Variation' by R. H. Marriot," Proc. IRE, Vol. 2, No. 3, March 1914
5. Ross Gunn, et al. 'Army-Navy Precipitation Static Project," Proc. IRE, Vol. 34, Nos. 4 and 5, April-May 1946.
  - Pt. I The precipitation-static interference problem and methods for its investigation.
  - Pt. II Aircraft instrumentation for precipitation static research.
  - Pt. III Electrification of aircraft flying in precipitation areas.
  - Pt. IV Investigation of methods for reducing precipitation-static radio interference.
  - Pt. V The high-voltage characteristics of aircraft in flight.
  - Pt. VI High-voltage installation of the precipitation-static project.
6. H. J. Dana, "Block and Squirter for Reduction of Precipitation Static," Second Air Force Operations Analysis Report No. 15, February 1945.
7. M. M. Newman and J. R. Stahmann, "Radio Interference Rejection at Antenna," Tech. Report No. 12, Lightning and Transients Research Institute, Minneapolis, 1949.
8. W. H. Huggins, "Final Report on Precipitation Static Reduction Research, June 15, 1941 - March 31, 1943," Oregon State College.

9. I. Langmuir and H. E. Tanis, "The Electrical Charging of Surfaces Produced by the Impact of High Velocity Solid Particles." Report on Contract No. W 33 106 sc 65, General Electric Co., May 1945
10. I. Langmuir "Final Report on Investigation of Fundamental Phenomena of Precipitation Static" Report on Contract No. W-33 106 sc 65 General Electric Co. May 1945.
11. G. W. Trichel, Phys. Rev., Vol. 54, p. 1078, 1938.
12. L. B. Loeb Fundamental Processes of Electrical Discharges in Gases John Wiley and Sons, Inc. New York, 1939.
13. L. B. Loeb, A. F. Kip, G. G. Hudson, W. N. Bennett, Phys. Rev., Vol. 60, p. 714, 1941.
14. W. N. English "Positive and Negative Point to-Plane Corona in Air" Phys. Rev. Vol. 74 No. 2, July 15, 1948.
15. L. B. Loeb, "Recent Developments in Analysis of the Mechanisms of Positive and Negative Coronas in Air," J. A. P. Vol. 19 No. 10, October 1948
16. E. E. Stickley, J. D. Robb, and M. M. Newman. "Radio Interference Associated with Precipitation Charging of Aircraft Windshields" Tech. Paper No. 17 Lightning and Transients Research Laboratory, Minneapolis, December 1949.
17. C. A. Bartlett "Reduction of Precipitation Static on Aircraft Canopies." Abstracts of papers delivered at 1952 Conference on Airborne Electronics.
18. M. M. Newman, and J. L. Rondeau, "Radio Interference from Charged Rain Drops." Abstracts of papers delivered at 1952 Conference on Airborne Electronics.
19. J. A. Stratton, Electromagnetic Theory, pp. 485-6, McGraw Hill Book Co. Inc., New York, 1941.
20. E. J. Lawton, "A Study of High Voltage Corona Discharge from Points at Atmospheric Pressure as a Cause of Radio Interference." Report on Contract No. W 33 106-sc-65 General Electric Co. July 1944.
21. W. R. Smythe, Static and Dynamic Electricity, McGraw Hill Book Co. Inc. New York 1939

faces  
port on

phenomena  
65

Gases

in Air

s of  
0.

ence  
s  
ory

ged  
on

Book

oints  
ort on

Co.

591 37

22. J. A. Stratton and L. J. Chu, "Forced Oscillations of a Conducting Sphere," J.A.P., Vol. 12, No. 3, March 1941
23. L. J. Chu and J. A. Stratton, "Forced Oscillations of a Prolate Spheroid," J.A.P., Vol. 12, No. 3, March 1941
24. C. Steele, J. Shimizu, and J. Taylor, "Model Impedance Measurements for H F Antennas," Tech. Report No. 40 Contract No. AF 19(504) 266. SRI Project 591, Stanford Research Institute, Stanford California. (To be published)
25. M. M. Newman, "Corona Interference with Radio Reception in Aircraft," Proc. National Electronics Conference, Chicago, 1948.
26. J. A. Stratton, P. M. Morse, L. J. Chu and R. A. Hutner, Elliptic Cylinder and Spheroidal Wave Functions, John Wiley and Sons, Inc., New York 1941.
27. C. Flammer, "Prolate Spheroidal Wave Functions," Tech. Report No. 16, SRI Project No. 188 Stanford Research Institute, Stanford, California February 1951.
28. D. F. Tuttle, Network Synthesis, Stanford University Electrical Engineering Department, Stanford, California, 1951.
29. C. T. Tai, "A Variational Solution to the Problem of Cylindrical Antennas," Tech. Report No. 12, SRI Project No. 188, Contract No. AF 19(122) 78. Stanford Research Institute, August 1950
30. R. King, "Asymmetrically Driven Antennas and the Sleeve Dipole," Tech. Report No. 93. Cruft Laboratory, Harvard University, 1949.
31. R. Beach, "What of Air Safety?" Elec. Eng. Vol. 67, No. 5, May 1948.
32. I. N. Sneddon, Fourier Transforms McGraw-Hill Book Co. Inc. New York 1951.

## TECHNICAL REPORTS IN THIS SERIES

Reports Issued on Contract AF 19(122)-78

1. "Electric Dipoles in the Presence of Elliptic and Circular Cylinders" by W. S. Lucke, September 1949.
2. "Asymmetrically Fed Antennas," by C. T. Tai, November 1949.
3. "Double-Fed and Coupled-Antennas," by C. T. Tai, February 1949.
4. "Equivalent Radii of Thin Cylindrical Antennas with Arbitrary Cross Sections," by Carson Flammer, March 1950.
5. "Use of Complementary Slots in Aircraft Antenna Impedance Measurements," by J. T. Bolljahn, February 1950.
6. "Wing-Cap and Tail Cap Aircraft Antennas," by J. V. N. Granger, March 1950.
7. "Investigation of Current Distribution on Asymmetrically-Fed Antennas by Means of Complementary Slots," by R. M. Hatch, Jr., February 1950.
8. "Electromagnetic Resonance Phenomena in Aircraft Structures," by A. S. Dunbar, May 1950.
9. "The Effect of a Grounded Slab on the Radiation from a Line Source," by C. T. Tai, June 1950.
10. "A Method for the Calculation of Progressive-Phase Antennas for Shaped Beams," by A. S. Dunbar, June 1950.
11. "Admittance of an Open-Ended Coaxial Line in an Infinite Grounded Plane," by W. J. Lucke, June 1950.
12. "A Variational Solution to the Problem of Cylindrical Antennas," by C. T. Tai, August 1950.
13. "Uniform Progressive-Phase Antennas Having Asymmetrical Amplitude Distributions," by A. S. Dunbar, September 1950.
14. "Small Dipole-Type Antennas," by J. T. Bolljahn, September 1950.
15. "Tables of Modified Cosine Integrals," January 1951.
16. "Prolate Spheroidal Wave Functions," by Carson Flammer, February 1951.
17. "An Antenna Evaluation Method," by W. S. Lucke, April 1951.

18. "Radar Response from Thin Wires," by C. T. Tai, March 1951.
19. "The Measurement of Low-Frequency Aircraft Antenna Properties Using Electrostatic Methods," by J. T. Bolljahn, September 1951.
- 20 (dropped)
21. "A Method for the Calculation of Progressive-Phase Antennas for Shaped Beams," Part II, by A. S. Dunbar, May 1951.
22. "The Prolate Spheroidal Monopole Antenna," by Carson Flammer [pending, issued on contract AF 19(604) 266].
- 23 "Variational Solution for the Problem of the Asymmetric Dipole," by I. Reese, August 1951
- 24 "Quasi Static Solution for Diffraction of a Plane Electromagnetic Wave by a Small Oblate Spheroid," by C. T. Tai, September 1952 [issued on contract AF 19(604)-266].
- 25 "Transmission Through a Rectangular Aperture in an Infinite Screen," by W. S. Lucke, September 1951

Reports Issued on Contract AF 19(604)-266

26. "Improvements in Instrumentation for the Investigation of Aircraft Antenna Radiation Patterns by Means of Scale Models," by R. M. Hatch, Jr., August 1952.
27. "The Vector Wave Solution of the Diffraction of Electromagnetic Waves by Circular Disks and Apertures." by Carson Flammer, September 1952.
28. "An Investigation of the Distribution of Current on Collinear Parasitic Antenna Elements, by R. M. Hatch, Jr., August 1952.
29. "On the Theory of Diffraction of Electromagnetic Waves by a Sphere," by C. T. Tai, October 1952
30. "High-Frequency Airborne Direction Finding," by P. S. Carter, Jr., December 1952
31. "An Electrolytic Tank Method for Low-Frequency Loop Antenna Studies," by R. F. Reese (pending)
32. "Radiation From a Uniform Circular Loop Antenna in the Presence of a Sphere," by C. T. Tai, December 1952.

33. "A Computer for Use with Antenna Model Ranges," by C. E. Fisher, February, 1953.
34. "Tail-Cap Antenna Radiation Pattern Studies," by J. H. Bryan, January, 1953.
35. "Methods of Improving Tail-Cap Antenna Patterns," by A. R. Ellis (pending).
36. "Mutual Admittance of Slots in Cylinders," by W. S. Lucke, February, 1953.
37. "Radio Interference from Corona Discharges," by N. L. Tanner, April, 1953.
38. "Effects of Airframe Configuration on Low-Frequency Antenna Characteristics," by C. M. Hoblitzell (pending).
39. "Reference Antenna for Use with Model Pattern Ranges," by A. R. Ellis, (pending).
40. "Model Impedance Measurements for H-F Antennas," by J. Taylor, J. Shimizu, C. Steele (pending).
41. "Some Electromagnetic Problems Involving a Sphere," by C. T. Tai (pending).
42. "Radiation Pattern Measurements of Stub and Slot Antennas on Spheres and Cylinders," by J. Bain (pending).

Using

r Shaped

pending,

," by

ic Wave

ried on

een,"

aft

Hatch,

Waves

195 .

arasitic

ere,"

lies,"

of a